Study of Hot Post-AGB Stars

A Thesis in Physics

Submitted For The Degree of

Doctor of Philosophy in the Faculty of Science

BANGALORE UNIVERSITY

By

GEETANJALI GAUBA

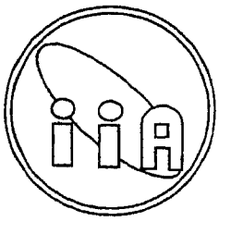

INDIAN INSTITUTE OF ASTROPHYSICS

Koramangala, Bangalore 560034, INDIA

August 2003

DECLARATION

I hereby declare that this thesis submitted to Bangalore University for the award of the degree of Doctor of Philosophy, is a result of the investigations carried out by me at the Indian Institute of Astrophysics, Bangalore, under the supervision of Prof. M. Parthasarathy. The results presented herein have not been subject to scrutiny by any university or institute for the award of any Degree, Diploma, Associateship or Fellowship whatsoever

Geetanjali Gauba
(Ph.D. Candidate)

Indian Institute of Astrophysics
Koramangala, Bangalore 560034, INDIA

August 2003

INDIAN INSTITUTE OF ASTROPHYSICS

Koramangala, Bangalore 560034, INDIA

CERTIFICATE

This is to certify that the thesis titled 'Study of Hot Post-AGB Stars' submitted by **Geetanjali Gauba** in the Faculty of Science, Bangalore University for the degree of Doctor of Philosophy, is based on the results of the investigations carried out by her under my supervision and guidance at the Indian Institute of Astrophysics. This thesis has not been submitted for the award of any Degree, Diploma, Associateship, Fellowship, etc. of any university or institute.

Prof. M. Parthasarathy

(Thesis Supervisor)

August 2003

Acknowledgements

I wish to sincerely thank my supervisor, Prof. M. Parthasarathy, for introducing me to the subject of post-AGB stars. He gave me a broad perspective of the field of observational astronomy, post-AGB stars and stellar evolution. His constant advice, push and the many discussions that I had with him were invaluable.

I owe this thesis to my parents under whose training I inculcated discipline, patience and the love for science and scientific pursuit. That I was able to do research work, is largely due to their influence. The love of my family - my sisters, parents in-law, sister in-law and brothers in-law gave me the strength during the course of my thesis.

Words are not enough to express the love, support and constant advice that I received from my husband, Tapobrata, during difficult times. I consider myself immensely lucky to have had him by my side since the time I first entered a research institute.

I would like to thank the Director, IIA and the Board of Graduate Studies for giving me an opportunity to do research work. The Chairman, Physics Department, Bangalore University, Prof. Puttaraju, the former Chairmen of the Department and the staff at the Ph.D. section of Central College are sincerely thanked for all their help in the smooth processing of thesis related formalities.

My sincere thanks to Prof. Ram Sagar, Mr. Brijesh Kumar and Dr. R.K.S. Yadav, for obtaining photometric data of a few stars at my request with the 1.04m telescope of the State Observatory, Uttaranchal.

Dr. B. Eswar Reddy is sincerely thanked for obtaining high resolution spectra of two stars at my request with the CTIO, 4m. telescope.

I would like to thank Dr. T. Sivarani for introducing me to observation techniques and to some data reduction softwares during the beginning of my thesis work.

I wish to sincerely thank Ambika, for her friendship which made life easier for me away from home and family, in the hostel. The scientific discussions that I had with her proved to be very fruitful. I would also like to thank Raji for her friendship, for being a wonderful room-mate and for her advice and help on several issues.

My sincere thanks to the staff at the Vainu Bappu Observatory (VBO), Kavalur, in particular to the observing assistants for all their help during observations.

I would like to thank Mr. A. Elangovan for the time and effort spent in xeroxing this thesis. My sincere thanks to Mr. D. Kanagaraj and Mr. D. Thyagarajan for the care taken in binding this thesis.

Last but not the least, I would like to thank all the technical and non-technical staff at IIA for providing an environment in which research work could be carried out easily and smoothly.

Abstract

This thesis is a study of the observational properties of 25 hot post-AGB stars. These stars were selected on the basis of their IRAS data, high galactic latitudes and OB-giant or supergiant spectra in the optical. 9 hot post-AGB candidates were imaged in U,B,V,R,I and H_α. The H_α images revealed nebulosity around 4 of these stars. From their low resolution spectra, two new hot post-AGB candidates at high galactic latitudes, LSE 163 and LSE 45 were identified. 15 hot post-AGB stars were studied in the UV (1150Å to 3200Å). NV(1240Å), CII(1335Å), SiIV(1394, 1403Å), CIV(1550Å), NIV(1718Å), FeII(2586-2631Å) and MgII(2800Å) lines typical of hot stars and the central stars of planetary nebulae (PNe) were identified in the International Ultraviolet Explorer (IUE) satellite spectra of these stars. We derived stellar wind velocities > 1000 kms^{-1} from the violet shifted NV (1250Å) and CIV (1550Å) resonance lines. We found that due to circumstellar dust, 10 hot post-AGB stars are partially obscured in the UV. The circumstellar extinction law was found to be proportional to λ^{-1} in these 10 cases. We estimated the temperatures and gravities of these stars. On the log g − log T_{eff} diagram of Schönberner they were found to be evolving into PNe with core masses in the range 0.546 $M_\odot$ to 0.644 $M_\odot$. We also studied the dust shell characteristics of 23 hot post-AGB stars. Using a radiative transfer code, DUSTY, we derived the dust temperatures, mass loss rates, expansion velocities, angular radii of the inner boundary of the dust envelopes, dynamical ages from the tip of the AGB and the distances to these stars. Study of the Infrared Space Observatory (ISO) spectra of 7 hot post-AGB stars revealed emissions due to amorphous and crystalline silicates, polyaromatic hydrocarbons (PAH's), silicon carbide etc. in the circumstellar environment of these stars. From the grain-types used to model the SEDs and from the ISO spectra we may infer the carbon-rich

or oxygen-rich nature of the circumstellar dust shells. High resolution spectra from 4900Å to 8250Å of two stars from this sample, IRAS13266-5551 (CPD-55 5588) and IRAS17311-4924 (Hen3-1428) were analysed. Absorption lines of C II, N II, O II, Al III, Si III and Fe III and emission lines of H I, He I, C II, N I, [N II], O I, [O I], Mg II, Al II, Si II, V I, Mn II, Fe II, Fe III, [Fe II] and [Cr II] were identified in the spectra of these stars. We derived the radial velocities from the absorption and the emission lines. Atmospheric parameters and chemical compositions under the LTE approximation were obtained for IRAS13266-5551 (CPD-55 5588). Since, the hot post-AGB stars evolve into low excitation PNe, we also studied the UV(IUE) spectra of two PNe, IRAS18523-3219 (Hb7) and IRAS18033-5101 (Sp3). The IUE spectra showed violet shifted P-Cygni profiles of CIV (1550Å) and NV (1240Å) indicating stellar wind and post-AGB mass loss.

LIST of PUBLICATIONS

Accepted, Submitted, and in Preparation

---

1. *UV(IUE) spectra of the central stars of high latitude planetary nebulae Hb7 and Sp3*

Gauba, G., Parthasarathy, M., Nakada, Y., Fujii, T., **2001, A&A 373, 572**

2. *IUE and ISO observations of the bipolar proto-planetary nebula Hen401 (IRAS 10178-5958)*

Parthasarathy, M., García-Lario, P., Gauba, G., et al., **2001, A&A, 376, 941**

3. *Hot Post-AGB Stars*

Parthasarathy, M., Gauba, G., Fujii, T., Nakada, Y.

in Post-AGB Objects as a Phase of Stellar Evolution, Proceedings of the Torun Workshop held July 5-7, 2000. Edited by R. Szczerba and S. K. Górny. Astrophysics and Space Science Library Vol. 265, ISBN 07923-71453. Publisher: Kluwer Academic Publishers, Boston/Dordrecht/London, 2001.

4. *Photometry and low resolution spectroscopy of hot post-AGB candidates*

Gauba, G., Parthasarathy, M., Kumar, Brijesh, Yadav, R.K.S., Sagar, R.,

2003, A&A, 404, 305

5. *UV(IUE) spectra of hot post-AGB candidates*

Gauba, G. and Parthasarathy, M., **A&A (in press)**

6. *Circumstellar dust shells of hot post-AGB stars*

Gauba, G. and Parthasarathy, M., **submitted to A&A**

7. *High resolution spectroscopy of the hot post-AGB stars : IRAS13266-5551 (CPD-55 5588) and IRAS17311-4924 (Hen3-1428)*

Gauba, G., Parthasarathy, M., Reddy, B.E., **(in preparation)**

Contents

Chapter 1

Introduction

Low and intermediate mass stars ($0.8 - 8$ $M_\odot$) pass through the post-asymptotic giant branch (post-AGB) phase of evolution. Iben and Renzini (1983) define low mass stars as those that develop an electron degenerate helium core immediately following the main sequence phase. This places an upper limit of about $2 - 2.3$ $M_\odot$ and a lower limit of $0.8 - 1.0$ $M_\odot$ on the initial main sequence mass of such stars (the precise limits being a function of initial composition). Intermediate mass stars are those that ignite helium "non-degenerately" but develop an electron degenerate carbon-oxygen (C-O) core following the exhaustion of helium at the center. This places an upper limit of about $8 - 9$ $M_\odot$ on the initial mass of such stars, with the precise value again a function of composition.

1.1 Evolution of low and intermediate mass stars

Fig. 1.1 shows the evolutionary tracks of model low (1 $M_\odot$) and intermediate (5 $M_\odot$) mass stars in the H-R diagram (adapted from Iben, 1985). The heavy portions along the tracks indicate where nuclear burning in the interior takes place on a long timescale. On the main sequence hydrogen is being converted into helium in the core, "H $\rightarrow$ He". The main sequence lifetime of a 1 $M_\odot$ star is $\sim 10^{10}$ yrs. and 10^8 yrs. for a 5 $M_\odot$ star. After hydrogen disappears at the centre, the hydrogen-exhausted core of

the star contracts rapidly and driven by energy produced in a thin hydrogen-burning shell, the envelope expands. The star becomes a red giant. Stars less massive than about 2.3 $M_{\odot}$ develop a hydrogen-exhausted core in which electrons are degenerate. As a consequence of hydrogen burning in a thin shell, this core grows in mass until a helium-burning thermonuclear runaway also referred to as a "helium core flash" lifts the degeneracy. Heavier intermediate mass stars do not experience the core helium flash but ignite helium relatively quiescently. Low-mass, low-metallicity (low Z) core helium-burning stars, such as those found in Galactic globular clusters, populate a "horizontal branch", whereas high-metallicity counterparts of these stars in the Galactic disk are compressed into a "clump" near the giant branch. After exhausting helium at their centres, low and intermediate mass stars develop an electron-degenerate C-O core with hydrogen and helium burning in shells around the core. The star is now in the double shell burning phase or the AGB phase of evolution. Fig. 1.2 is a schematic of the interior of an AGB star. The dredge up processes on the AGB are discussed in Sec. 1.1.3 below

1.1.1 The AGB phase

The AGB phase may be divided into the **early-AGB (E-AGB)** and the **thermally pulsing AGB (TP-AGB)** phase. In the E-AGB phase the star has a helium burning shell which narrows and strengthens forcing the material above it to expand and cool. The result is a temporary turn off of the hydrogen burning shell. Towards the end of the E-AGB phase, the dormant hydrogen burning shell is reignited and the narrowing helium burning shell below it begins to turn on and off periodically. The star is now in the TP-AGB phase. As the hydrogen burning shell dumps helium onto the helium layer below, the mass of the helium layer increases and it becomes slightly degenerate. When the temperature of the helium layer increases sufficiently, a helium shell flash occurs. This drives the hydrogen burning shell outward causing it to cool and turn off for a time. Eventually, the burning in the helium shell diminishes, the hydrogen burning shell recovers and the process repeats. The period between pulses is a function of the mass of the star, ranging from thousands of years for stars near 5

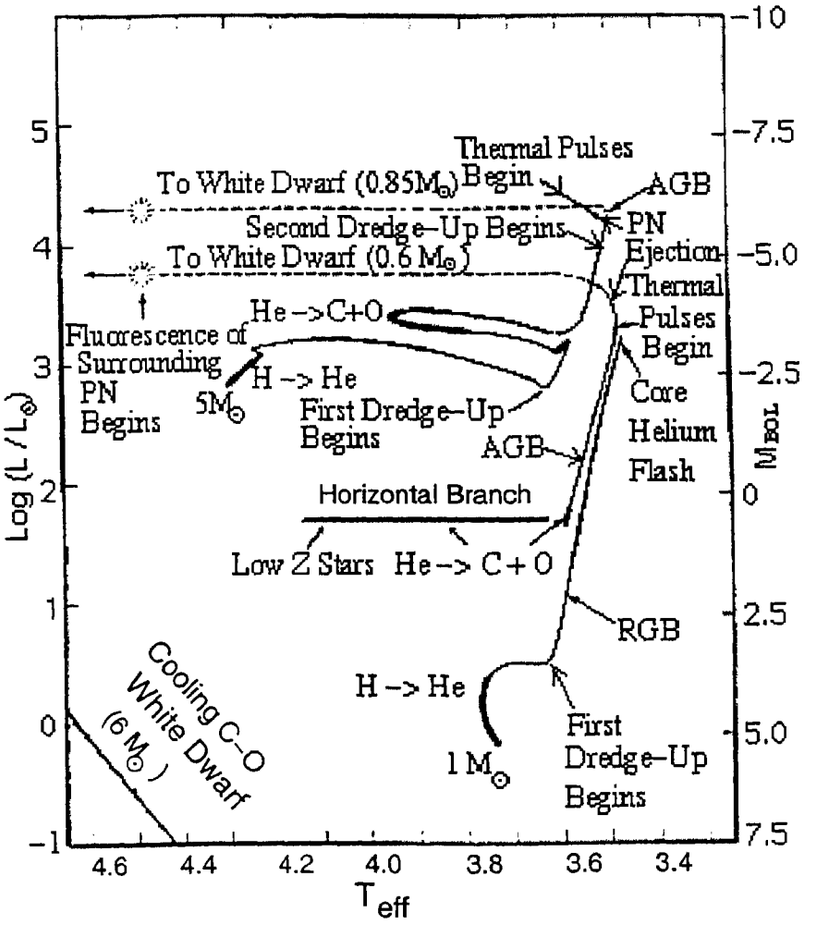

Figure 1.1: Tracks showing the evolution of theoretical model stars of low ($1M_{\odot}$) and intermediate ($5M_{\odot}$) mass in the H-R diagram (adapted from Iben, 1985). The heavy portions of each curve define locations where the major core nuclear burning phases occur.

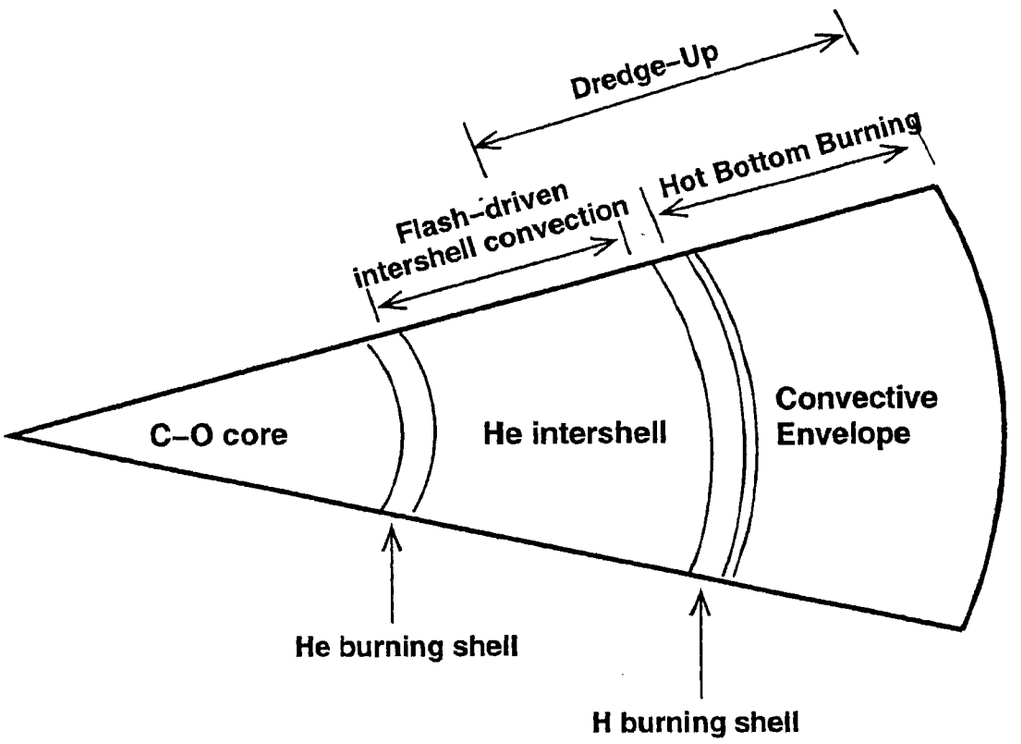

Figure 1.2: Schematic of the interior of an AGB star (adapted from Lattanzio and Forestini, 1999)

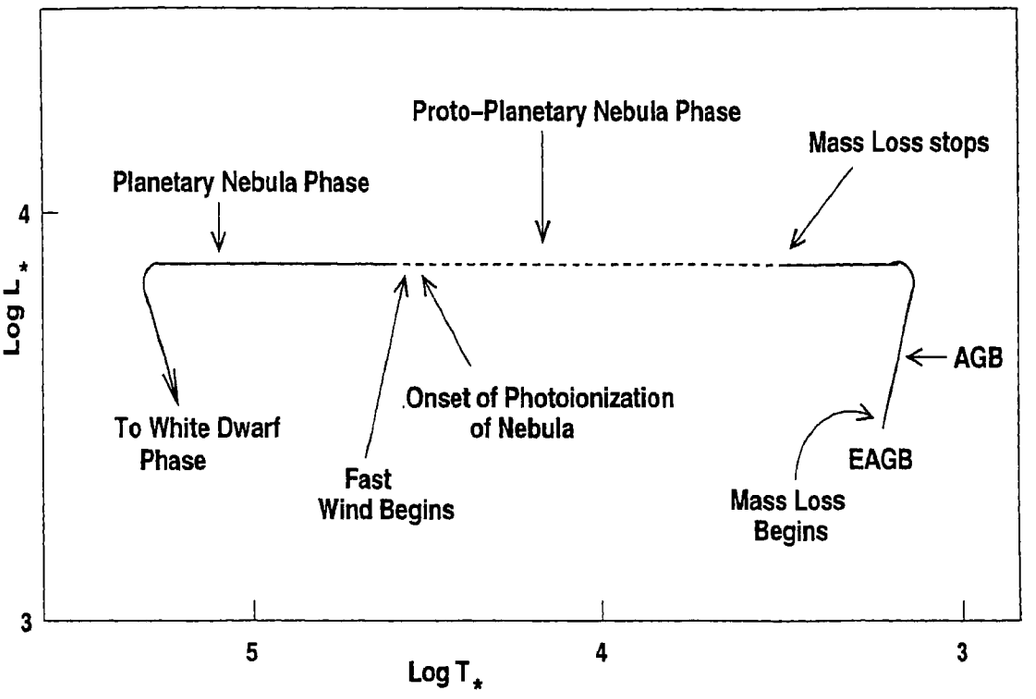

Figure 1.3: Schematic of the evolutionary path from AGB to PN in the H-R diagram (adapted from Kwok, 1987)

$M_\odot$ to hundreds of thousands of years for low mass stars, with the pulse amplitude growing with each successive event.

1.1.2 Mass loss and the termination of the AGB phase

Fig. 1.3 is a schematic of the evolution from the tip of the AGB to the PN stage. Low and intermediate mass stars ascend the AGB losing mass according to the Reimers mass loss rate. However, towards the end of the AGB phase, when a critical luminosity is reached, the stars eject most of their residual H-rich envelope by a superwind-type of mass loss process, on a time scale very short compared with the previous AGB lifetime. The final mass loss rates at the tip of the AGB range from $\sim 10^{-5}$ to $\sim 10^{-3}$ $M_\odot$ yr^{-1}, depending on the initial stellar mass. As a result of the superwind-type of mass loss, the star is embedded in an optically thick circumstellar dust shell, appears as a powerful IR source and is temporarily obscured from the optical. As the mass of the H-rich envelope (M_e) decreases, the star departs from the AGB at a rate that increases

with decreasing M_e. In turn, the movement of the star to higher effective temperatures (smaller radii, but nearly constant luminosity) affects the superwind process which eventually ceases when M_e falls below a critical value. After the superwind ceases, the ejected matter keeps expanding, while the remnant star continues its evolution towards higher temperatures. When the temperature reaches $\sim$ 30,000 K, the central star becomes hot enough to photoionise the surrounding nebula. Recombination lines of hydrogen and and forbidden lines of metals make the nebula easily observable in the optical. A new high-speed wind from the central star then compresses and shapes the AGB wind into a planetary nebula (PN).

1.1.3 Dredge-up processes in low and intermediate mass stars

First dredge-up: The first dredge-up occurs just before the star ascends the red giant branch (RGB). Evolutionary models predict a substantial reduction of the abundances of Li, Be and B, a decrease of the C abundance by $\sim$ 30%; a decrease in the $^{12}C/^{13}C$ ratio from $\sim$ 90 to $\sim$ 20 $-$ 30; an increase of the N abundance by a factor $\sim$ 0.44 $(C/N)_o$ where $(C/N)_o$ is the initial C to N ratio by number; and very little variation in the O abundance.

Second dredge-up: The second dredge-up phase accompanies the formation of an electron-degenerate C-O core, following the exhaustion of central helium. In intermediate mass stars of mass greater than $\sim$ 5 $M_\odot$, the convective envelope on the surface deepens and extends downwards to the chemical discontinuity between the hydrogen-rich outer layers and the helium-rich region above the helium burning shell. The mixing that results during the second dredge-up phase increases the helium and ^{14}N content of the envelope. The increase in ^{14}N is due to the previous conversion of ^{12}C and ^{16}O into ^{14}N in the intershell region.

Third dredge-up: In an AGB star, because of the sudden increase in energy flux from the helium burning shell during a flash episode, a convection zone is established between it and the hydrogen burning shell. At the same time, the depth of the envelope convection zone increses with pulse strength. For intermediate mass stars, the convection zones will merge and eventually extend down into regions where carbon

has been synthesised, carrying freshly processed material to the surface. The third dredge-up phase appears to explain the difference between oxygen-rich giants and carbon-rich giants called carbon stars that have been observed spectroscopically.

Hot bottom burning : For stars above about 5 $M_{\odot}$ an important phenomenon is the occurence of hot bottom burning (HBB) (Lattanzio and Forestini, 1999 and references therein). Here, the convective envelope is so deep that it penetrates into the top of the hydrogen burning shell so that nucleosynthesis actually occurs in the envelope of the star. Temperatures can reach as high as 10^8 K. This results in the activation of the CN-cycle within the envelope and the consequent processing of ^{12}C into ^{13}C and ^{14}N. This prevents the star from becoming a carbon star, because the primary carbon dredged up to the envelope is transmuted into nitrogen (Boothroyd et al., 1993). A consequence of HBB is that ^{7}Li can be produced by the Cameron-Fowler (1971) mechanism. Another consequence of HBB is the substantial production of ^{26}Al by the Mg-Al cycle (see eg. Mowlavi and Meynet, 2000).

1.1.4 Nucleosynthesis in TP-AGB stars

TP-AGB stars with small core mass are believed to be the major suppliers of Galactic s-process (slow neutron capture) isotopes. In these stars, the neutrons are most probably supplied by the reaction :

$^{13}C + \alpha \rightarrow {}^{16}O + n$

After the shell convective zone which is driven by the helium shell flash dies away, matter which was once in this zone is propelled to low densities and temperatures. This matter contains the products of partial helium burning, namely ^{12}C ($\sim$ 20% by mass), ^{4}He ($\sim$ 80% by mass) and s-process isotopes. When the temperature drops to about 10^6 K, a small pocket containing ^{12}C and ^{1}H at comparable abundances by number is formed. When the helium burning dies down, the region containing ^{12}C and ^{1}H contracts and heats until the reactions :

$^{12}C(p,\gamma)^{13}N(\beta^+,\nu)^{13}C(p,\gamma)^{14}N$

convert all of the ^{12}C and ^{1}H in the region into ^{13}C and ^{14}N. In the inner half of the region, ^{13}C is the major product and in the outer half, ^{14}N is the major product. At

the end of the quiescent hydrogen burning phase, when the next helium shell flast occurs, the outer edge of the convective zone driven by the flash sweeps through the ^{13}C layer. ^{13}C is convected downward and when it encounters temperatures of $150X10^6$ K, the reaction $^{13}C(\alpha,n)^{16}O$ takes place.

The other reactions that occur during a helium shell flash are :

$^{14}N + {}^4He \rightarrow {}^{18}F + \gamma$

$^{18}F \rightarrow {}^{18}O + e^+ + \nu$

and

$^{18}O + {}^4He \rightarrow {}^{22}Ne + \gamma$

In intermediate mass stars more massive than $\sim 6M_\odot$, the reaction :

$^{22}Ne + {}^4He \rightarrow {}^{25}Mg + n$

produces neutrons which, after a series of neutron-capture events result in the build-up of several hundred heavy neutron-rich isotopes in the so-called s-process distribution. Details of nucleosynthesis in TP-AGB stars and the synthesis of s-process and other neutron rich isotopes may be found in Iben and Renzini (1983).

1.2 Post-AGB stars

Severe mass loss terminates the AGB phase of evolution and the central star evolves rapidly towards the left in the H-R diagram at constant luminosity. The post-AGB phase is the evolution of the star from the tip of the AGB to the young PN stage. The transition times from the tip of the AGB to the PN stage vary with the remnant (core) masses. For a 0.6 $M_\odot$ remnant the transition time is a few thousand years while a remnant of 0.85 $M_\odot$ may evolve into a PN in a few hundred years (Schönberner and Blöcker, 1993). After the Infrared Astronomical Satellite (IRAS) mission in the 1980's it became clear that post-AGB stars emit a significant part of their energy in the mid- and far-infrared (Parthasarathy and Pottasch, 1986). Pottasch et al. (1988a) and van der Veen and Habing (1988) identified a region of the IRAS color-color diagram which was mainly populated by stars in transition from the tip of the AGB to the PN stage. Since then the investigation of this phase of evolution has

developed rapidly. Based on their far-IR colors, several cooler (G, F, A) and hotter (O-B) post-AGB stars have been discovered (Parthasarathy, 1993a; García-Lario et al., 1997a and references therein; Parthasarathy et al., 2000a and references therein). Parthasarathy (1993b) suggested that there is an evolutionary sequence from the cooler, G,F,A supergiant post-AGB stars to hotter O-B types evolving from the tip of the AGB towards young PNe.

Abundance anomalies were observed between the cooler post-AGB stars and some high galactic latitude hot post-AGB stars (Mc Causland et al. 1992, Conlon et al., 1993, 1994). Some of the high galactic latitude hot post-AGB stars were found to show severe carbon deficiency. It is possible that these stars evolved from the AGB before the occurence of the third dredge-up. The rapid evolution of the hot post-AGB stars, IRAS17119-5926 (Hen3-1357 = Stingray Nebula) and IRAS18062+2410 (SAO85766) from the post-AGB stage into young PNe (Parthasarathy et al., 1993c, 1995, 2000b; Feibelman, 1995; Bobrowsky et al., 1998) indicated the need to study a significant sample of hot post-AGB stars inorder to further understand the post-AGB evolution and PN formation (Schönberner, 1986 and Vassiliadis and Wood, 1994). The 21μ emission feature observed in several cooler carbon-rich post-AGB stars with overabundance of s-process elements (Parthasarathy et al., 1992; Reddy et al., 1997; Van Winckel and Reyniers, 2000; Hrivnak et al., 2000) is not seen in the infrared spectra of PNe. However, the carbon-rich PNe with [WC] central stars may have evolved from carbon-rich post-AGB A and F stars (Parthasarathy, 1999). Thus, it is important to study hot post-AGB stars inorder to further understand the evolution of cooler post-AGB stars into young central stars of PNe. In particular, we need to understand the characteristics of their central stars (such as temperatures, gravities, luminosities etc.) and of their circumstellar dust shells, the mass loss mechanisms, mixing and nucleosynthesis in these stars and the influence of these processes on the formation, shaping and early evolution of PNe.

In this thesis we have studied some of the observational characteristics of hot post-AGB stars. We have studied the hot central stars in the UV and optical and looked at their circumstellar dust shells in the infrared.

In **chapter 2** of the thesis we have obtained the U,B,V,R,I magnitudes of a small sample of hot post-AGB stars. These stars were also imaged through a narrow band H_α filter to search for nebulosity around the central stars. The U,B,V,R,I and H_α observations of the stars were made with the 104 cm. Sampurnanand Carl-Zeiss telescope of the State Observatory, Uttaranchal, India. We also present the low resolution optical spectra of a few hot post-AGB candidates obtained with the 102 cm. telescope of the Vainu Bappu Observatory, Kavalur, India. Our optical photometry was combined with near- and far-infrared data on the stars from literature to reconstruct their complete spectral energy distributions (SEDs).

In **chapter 3** of the thesis we have studied the International Ultraviolet Explorer (IUE) spectra of 15 hot post-AGB candidates. In 11 cases, the UV(IUE) spectra suggested partial obscuration of the central stars due to circumstellar dust. We modelled the circumstellar extinction law in these cases and found it to be linear in λ^{-1}. The effective temperatures and gravities of the stars were estimated and they were placed on the log g−log T_{eff} diagram showing the post-AGB evolutionary tracks of Schönberner (1983, 1987). Terminal wind velocities of the stars were estimated from the CIV and NV resonance lines.

In **chapter 4** of the thesis we have used a radiative transfer code (DUSTY) to derive the stellar and dust envelope parameters for 15 hot post-AGB stars. The optical, near- and far-infrared data on the stars were combined to reconstruct their SEDs. We estimated the dust temperatures, mass loss rates, expansion velocities, angular radii of the inner boundary of the dust envelopes, dynamical ages from the tip of the AGB and the distances to these stars. We also studied the Infrared Space Observatory (ISO) spectra of 7 of these stars and identified spectral features typical of carbon-rich and/or oxygen-rich circumstellar dust shells.

In **chapter 5** of the thesis we have analysed the high resolution spectra of two hot post-AGB stars, IRAS13266-5551 (CPD-55 5588) and IRAS17311-4924 (Hen3-1428) from 4900Å to 8250Å . These spectra were obtained with the Victor M. Blanco 4 m. telescope of the Cerro Tololo Inter-American Observatory (CTIO), Chile. Absorption and emission lines typical of hot post-AGB stars were identified in the spectra of

these stars. The H_α P-Cygni profiles indicated ongoing post-AGB mass loss. We derived heliocentric radial velocities to be $67.55 \pm 1.26\ \mathrm{kms}^{-1}$ and $26.09 \pm 1.88\ \mathrm{kms}^{-1}$ for IRAS13266-5551 (CPD-55 5588) and IRAS17311-4924 (Hen3-1428) respectively. Preliminary estimates for the CNO abundances in IRAS13266-5551 (CPD-55 5588) were obtained.

Finally, in **chapter 6** of the thesis we take a look at the evolutionary stage which succeeds the hot post-AGB phase. In this chapter, we have analysed the UV(IUE) spectra of the central stars of two high galactic latitude PNe, Hb7 (IRAS18523-3219) and Sp3 (IRAS18033-5101). From the CIV P-Cygni profiles we derived the stellar wind velocities and mass loss rates. The available data was used to reconstruct the SEDs of these two stars.

Chapter 2

Photometry and low resolution spectroscopy of hot post-AGB candidates

Abstract

We have obtained Johnson U, B, V and Cousins R, I photometry and low resolution spectra of a small sample of hot post-AGB candidates. Using the present data in combination with JHK data from 2MASS, infrared data from the MSX catalog and the IRAS fluxes, we have studied the spectral energy distribution (SED) of these stars. Using the DUSTY code we have estimated the dust temperatures, the distances to the stars, the mass-loss rates, angular radii of the inner boundary of the dust envelopes and dynamical ages from the tip of the AGB. These candidates have also been imaged through a narrow band Hα filter, to search for nebulosity around the central stars. Our Hα images revealed the bipolar morphology of the low excitation PN IRAS 17395-0841 with an angular extent of 2.8″. The bipolar lobes of IRAS 17423-1755 in Hα were found to have an angular extent of 3.5″(south-east lobe) and 2.2″(north-west lobe). The dust envelope characteristics, low resolution spectrum and IRAS colors suggest that IRAS 18313-1738 is similar to the proto-planetary nebula (PPN) HD

51585. The SED of IRAS 17423-1755, IRAS 18313-1738 and IRAS 19127+1717 show a warm dust component (in addition to the cold dust) which may be due to recent and ongoing mass-loss.

2.1 Introduction

Stars having initial mass between 0.8 and 8 $M_{\odot}$ pass through the asymptotic giant branch (AGB) phase of evolution (Iben & Renzini, 1983). These low and intermediate mass stars, undergo severe mass-loss (10^{-7} - 10^{-4} $M_{\odot}$ yr^{-1}) on the AGB. The post-AGB phase is the rapid evolution of the star from the tip of the AGB to the planetary nebula (PN) stage. During the post-AGB phase the circumstellar dust shell moves away from the star and decreases in temperature from $\sim$ 400 to 100K (Bedijn, 1987; Zijlstra et al., 1992). The rapidly evolving, hotter analogues (OB spectral types) of the cooler (G,F,A) post-AGB stars (Parthasarathy & Pottasch 1986, 1989) are interesting to study in order to understand the mass-loss mechanisms, dust envelope characteristics and dynamical time scales responsible for the evolution of low and intermediate mass stars to PNe of varied morphologies. In this chapter, we analyse the complete spectral energy distribution of a small sample of hot post-AGB candidates. We have also searched for nebulosity around these stars. As part of our search for new hot post-AGB candidates, we also present the spectra of two high galactic latitude early B-type supergiants.

2.2 Target Selection

Hot post-AGB stars may be identified on the basis of their high temperature, low surface gravity, evidence of remnant AGB envelope (infrared excess), detached dust envelope, double peaked spectral energy distribution and nebulosity due to scattered light (Parthasarathy et al., 2000a, Kwok, 2001). Pottasch et al. (1988a) and van der Veen & Habing (1988) identified a region of the IRAS color-color diagram ($F(12\mu)/F(25\mu) < 0.35$ and $F(25\mu)/F(60\mu) > 0.3$) which was mainly populated by stars in transition from the AGB to the PN phase. An occasional HII region, Seyfert galaxy, or T-Tau

Table 2.1: List of hot post-AGB candidates selected for photometry

IRAS	Name	l	b	Sp.Type	IRAS Fluxes (Jansky)			
					12μ	25μ	60μ	100μ
17074-1845	Hen 3-1347	4.1	+12.3	B3IIIe	0.50	12.20	5.66	3.47:
17395-0841	SS 318	17.0	+11.1	PN	0.31	4.18	8.43	6.38
17423-1755	Hen 3-1475	9.4	+5.8	Be	7.05	28.31	63.68	33.43
18237-0715	MWC 930	23.6	+2.2	Be	1.84	4.01	38.24	35.13
18313-1738	MWC 939	15.3	-4.3	Be	9.41	7.28	1.00:	68.70L
19127+1717	SS 438	51.0	+2.8	B9V	12.15	18.79	8.50	7.37L
19157-0247	LS IV -0229	33.6	-7.2	B1III	8.88	7.16	2.45	11.05L
19200+3457	StHA161	67.6	+9.5	B	0.25L	2.12	1.45	1.41L
19399+2312	LS II +2317	59.3	+0.1	B1III	1.13	2.27:	23.31L	80.20L

A colon : indicates moderate quality IRAS flux, **L** is for an upper limit

star is not excluded from this range (Pottasch et al., 1988a, Szczerba et al., 2001). But in the case of post-AGB stars, the circumstellar dust temperatures are in the range of 100 - 200K (Kwok, 2001). In addition to the cold dust, warm dust indicative of recent or ongoing post-AGB mass loss may also be present in the circumstellar envelopes of these stars (eg. Hen401, Parthasarathy et al., 2001a). Young massive OB supergiants are not expected at high galactic latitudes. Also young massive OB supergiants do not have detached cold circumstellar dust shells. High galactic latitude OB supergiants with detached dust shells and far-infrared colors similar to PNe were indeed found to be in the post-AGB stage of evolution (Parthasarathy, 1993b, Parthasarathy et al., 2000a). To firmly establish the evolutionary status it is important to obtain high resolution optical spectra of the candidate stars for determination of their chemical abundances and to look for signatures of AGB nucleosynthesis.

The targets selected for photometry (Table 2.1) were IRAS sources with OB spectral types having $F(12\mu)/F(25\mu) < 0.35$ and $F(25\mu)/F(60\mu) > 0.3$. Based on their low resolution spectra and spectral type, many of these targets had been classified as post-AGB stars by Parthasarathy et al. (2000a). Drilling & Bergeron (1995) ex-

Table 2.2: Characteristics of the hot post-AGB candidates selected spectroscopically

Object	R.A. (2000)	DEC (2000)	Sp. Type	V	E(B−V)	l	b	d (kpc)
LSE 163= CD -42 8141	13:08:46	-43:27:51	B2 I	10.4	0.1	306.3	+19.3	4.3
LSE 45= CD -49 8217	13:49:18	-50:22:46	B2 I	11.0	0.2	312.3	+11.4	4.8

tended the survey of luminous stars in the Milky Way to galactic latitude b = ± 30° for l = ± 60°. They designated this as the LSE survey. We have also selected few LSE stars at high galactic latitudes with OB-spectral types (Table 2.2). The optical counterparts of the IRAS sources were carefully identified using the Digitised Sky Survey and NASA's Sky View Java interface. The targets were searched within the IRAS error boxes. Besides most of the targets are in scarcely populated regions at high galactic latitudes.

2.3 Observations

U,B,V,R,I images of the hot post-AGB candidates were obtained on 10 April, 2000 at the State Observatory (SO) with the f/13 Cassegrain 104 cm. Sampurnanand Carl-Zeiss telescope. The central 1280X1280 pixels of a 2KX2K CCD were used for the purpose, in 2X2 binning mode, resulting in 680X680 pixels image frames. The PG 1323-086 standard stars field (Landolt, 1992) was observed several times during the night for calibration and extinction measurements.

The narrow band images of the stars were obtained with the same telescope on 11 April, 2000 with a 1KX1K CCD having plate scale of 0.37″pixel^{-1}. An Hα filter centered at 6565Å with a bandwith of 80Å and a continuum filter centered at 6650Å with a bandwith of 80Å were used for the purpose.

Optical spectra of the hot post-AGB candidates were obtained with the 1.02m telescope at the Vainu Bappu Observatory (VBO) on 20 January, 2000 with a res-

olution of 1.1Å pixel^{-1}. Appropriate number of flat fields and bias frames were observed on each night. Following each observation of a program star, we obtained a comparison lamp spectra and the spectra of a bright star close to the RA & DEC of the object.

2.4 Analysis of photometric and spectroscopic data

The DAOPHOT package in IRAF was used for the reduction and analysis of the photometric data (Massey & Davis, 1992). Bias subtraction and flat fielding was performed on the individual image frames. The extinction coefficient for each filter was determined from the standard star observations. The observed photometric magnitudes of the objects are listed in Table 2.3a. The 2MASS (2Micron All Sky Survey) Catalog was searched within 15″of each object for their JHK magnitudes. Whenever possible, the JHK magnitudes have been taken from García-Lario et al. (1997a). We also searched the MSX (Midcourse Space Experiment) catalog within 3″of the objects. The MSX fluxes are listed in Table 2.3b. The spectral types of the objects have been taken from literature.

The objects were imaged through the Hα and continuum filters. To detect Hα emission, we followed the procedure outlined by Beaulieu et al. (1999). The continuum images were scaled to match the total star signal above the sky in their corresponding Hα images. An appropriate offset was then applied to each continuum image to equate the sky level to that of the Hα image. To find the Hα emitting objects, we then divided the Hα image by the continuum image for each field. We detected Hα emission in four of the objects. Fig. 2.1 shows the continuum and resultant Hα images of the objects.

The optical spectra were bias subtracted, flat field corrected, wavelength calibrated and continuum normalised using the IRAF package. Fig. 2.2 shows the continuum normalised spectra from 4250Å to 5500Å . Spectral classification was performed using the spectra of standard stars from Jacoby et al. (1984).

Table 2.3 a: Photometry of hot post-AGB candidates

IRAS name	U mag	B mag	V mag	R mag	I mag	J mag	H mag	K mag	H_α emission
17074-1845	–	11.92[1]	11.55	11.25	11.07	11.33[2]± 0.13	12.06[2]± 0.16	11.02[2]± 0.11	NO
17395-0841	15.37	15.04	13.74	12.79	11.94	10.59[2]± 0.06	9.76[2]± 0.03	9.21[2]± 0.04	YES
17423-1755	13.57	13.3[3]	12.64	11.75	10.91	9.61[2]± 0.05	8.32[2]± 0.02	6.80[2]± 0.02	YES
18237-0715	15.48	14.88	12.37	10.51	8.78	–	–	–	YES
18313-1738	12.36	12.88	12.37	11.60	11.37	9.995± 0.027	8.374± 0.045	6.785± 0.019	YES
19127+1717	14.70	14.20	13.13	12.38	8.65	11.07[4]	9.94[4]	8.65[4]	NO
19157-0247	11.62	11.31	10.55	10.04	9.48	–	–	–	NO
19200+3457	10.59	11.35	11.25	11.14	11.09	11.008± 0.024	10.883± 0.025	10.739± 0.032	NO
19399+2312	–	10.90	10.05	9.46	8.85	8.573± 0.022	8.388± 0.003	8.331± 0.033	NO

[1] The B magnitude of IRAS17074-1845 is from the Tycho-2 Catalog (Hog et al., 2000)

[2] From Garcia-Lario, Manchado, Pych, & Pottasch (1997a)

[3] The B magnitude of IRAS17423-1755 is from the USNO-A2.0 Catalog (Monet et al., 1998)

[4] From Whitelock & Menzies (1986)

[5] The rms errors in U,B,V,R,I obtained from fitting the transformation equations to the standard stars are ± 0.05, ± 0.05, ± 0.05, ± 0.09, ± 0.07 respectively

Table 2.3 b: MSX data

IRAS	MSX Fluxes (Jansky)			
	Band A 8.28μ	Band C 12.13μ	Band D 14.65μ	Band E 21.34μ
18313-1738	8.9623	7.5263	6.0883	8.3414
19127+1717	8.332	11.737	12.577	16.636

Table 2.4: Input physical parameters for DUSTY and the adopted reddening values

IRAS	dust type	E(B−V) C.S.+I.S.	E(B−V) I.S.	T_* (K)	grain type	Optical depth (τ)
17074-1845	cold	0.66	0.28	17100	Sil-DL	0.105
17395-0841	cold	1.60	1.23	35000	amC-Hn	0.002
17423-1755	warm	0.86	0.67	20000	amC-Hn	0.16
	cold	0.86	0.67	20000	SiC-Pg	0.35
18237-0715	cold	2.71	-	20000	SiC-Pg	0.004
18313-1738	warm	0.71	-	20000	grf-DL	0.2
	cold	0.71	-	20000	Sil-DL	0.16
19127+1717	warm	1.14	-	10500	grf-DL	0.07
	cold	1.14	-	10500	Sil-DL, grf-DL & amC-Hn	0.7
19157-0247	cold	1.02	0.65	24000	SiC-Pg	0.004
19200+3457	cold	0.30	0.14	20000	Sil-Ow	0.04
19399+2312	cold	1.11	-	24000	SiC-Pg	0.006

Table 2.5 a: Derived stellar and dust envelope parameters for M_c=0.565

IRAS	T_d (K)	r1 (cm)	r0 (cm)	d (kpc)	θ ($''$)	$\dot{M}$ $M_\odot yr^{-1}$	V_e kms^{-1}	Δt yr.
17074-1845	122	$3.9X10^{16}$	$1.1X10^{14}$	3.1	0.8	$1.0X10^{-5}$	17.4	743
17395-0841	110	$1.7X10^{17}$	$1.4X10^{14}$	1.0	11.7	$1.1X10^{-6}$	7.7	7344
17423-1755	100	$2.9X10^{17}$	$1.5X10^{14}$	3.1	6.3	$5.3X10^{-5}$	23.3	4154
18237-0715	100	$1.4X10^{17}$	-	0.2	45.0	-	-	-
18313-1738	450	$2.3X10^{15}$	$1.1X10^{14}$	3.6	0.04	$3.6X10^{-6}$	18.9	39
19127+1717	300	$6.2X10^{15}$	$1.4X10^{14}$	4.0	0.1	$9.0X10^{-6}$	25.9	78
19157-0247	135	$1.1X10^{17}$	$1.4X10^{14}$	0.8	9.1	$1.4X10^{-6}$	8.8	4180
19200+3457	140	$3.1X10^{16}$	$1.5X10^{14}$	3.8	0.5	$4.0X10^{-6}$	12.8	805
19399+2312	127	$1.3X10^{17}$	-	0.6	16.0	-	-	-

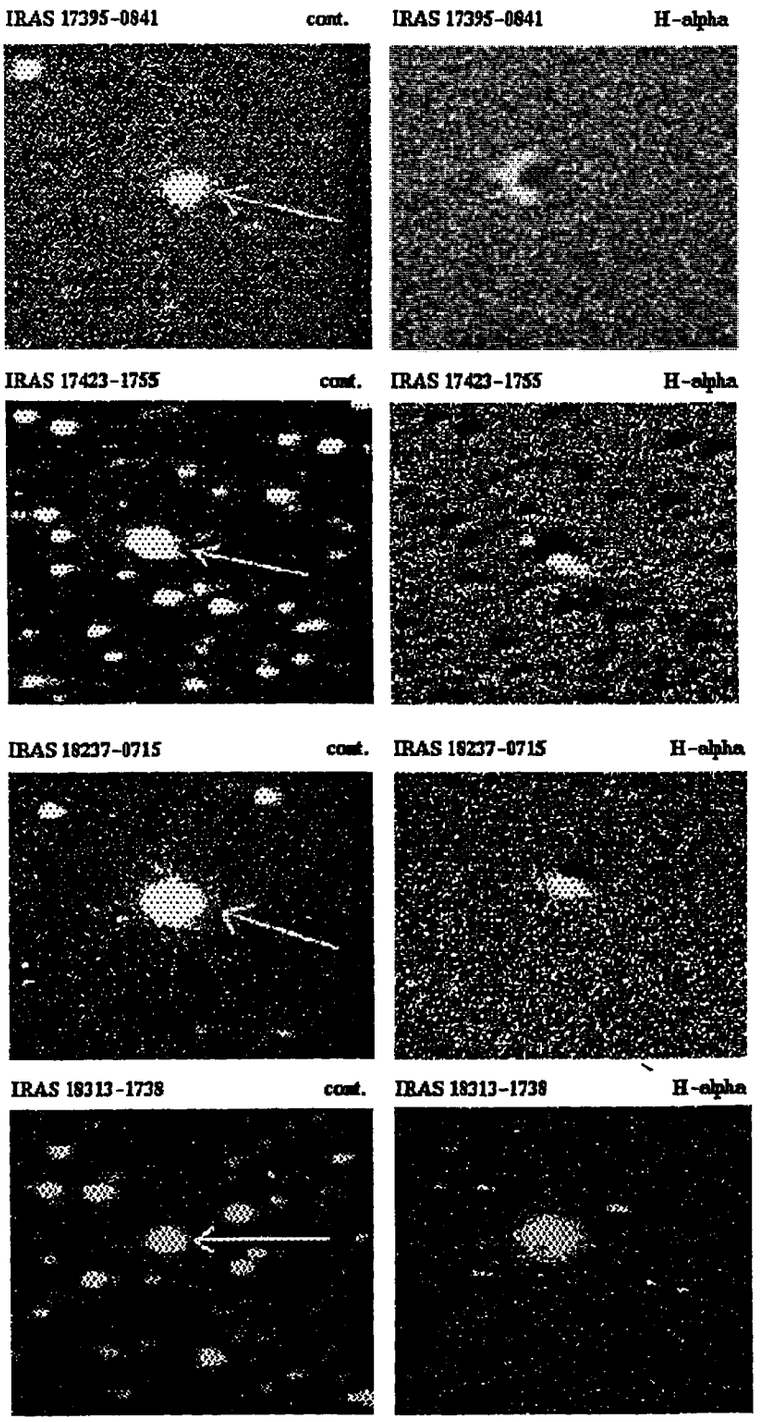

Figure 2.1: Continuum (λ=6650Å , $\Delta\lambda$=80Å) and Hα (λ=6565Å , $\Delta\lambda$=80Å) images of the selected hot post-AGB stars

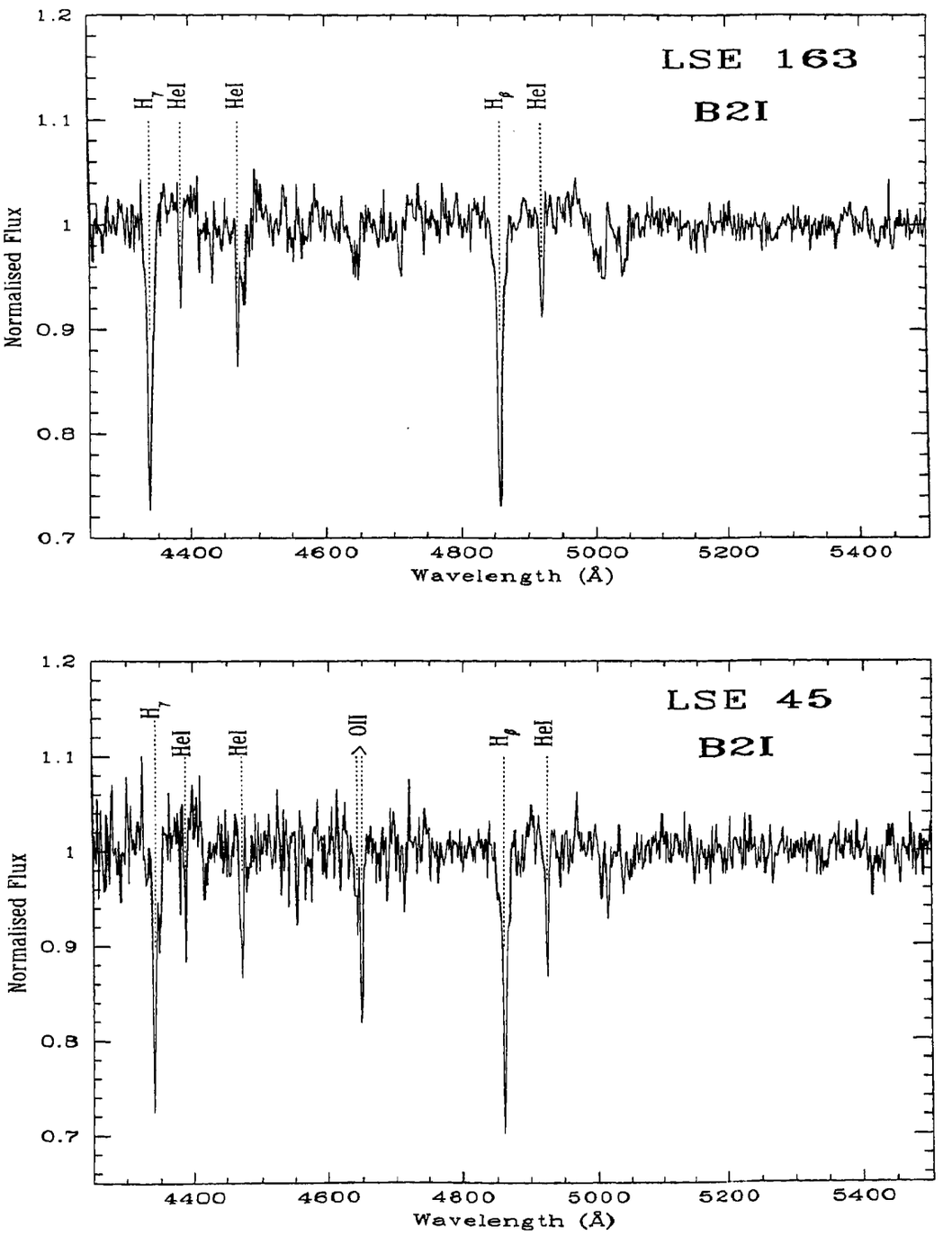

Figure 2.2: Low resolution spectra of LSE 163 and LSE 45

Table 2.5 b: Derived stellar and dust envelope parameters for M_c=0.605

IRAS	T_d (K)	r1 (cm)	r0 (cm)	d (kpc)	θ ($''$)	$\dot{M}$ $M_\odot yr^{-1}$	V_e kms^{-1}	Δt yr.
17074-1845	122	$4.6X10^{16}$	$1.8X10^{14}$	3.7	0.8	$1.3X10^{-5}$	20.6	743
17395-0841	110	$2.0X10^{17}$	$2.3X10^{14}$	1.1	11.8	$1.5X10^{-6}$	8.8	7543
17423-1755	100	$3.5X10^{17}$	$2.06X10^{14}$	3.7	6.3	$6.8X10^{-5}$	26.0	4481
18237-0715	100	$1.7X10^{17}$	-	0.2	45.0	-	-	-
18313-1738	450	$2.7X10^{15}$	$1.9X10^{14}$	4.2	0.04	$4.7X10^{-6}$	22.3	38
19127+1717	300	$7.4X10^{15}$	$2.3X10^{14}$	4.7	0.1	$1.2X10^{-5}$	28.7	84
19157-0247	135	$1.3X10^{17}$	$2.4X10^{14}$	0.9	9.2	$1.8X10^{-6}$	9.9	4336
19200+3457	140	$3.7X10^{16}$	$2.5X10^{14}$	4.6	0.5	$5.1X10^{-6}$	14.7	834
19399+2312	127	$1.6X10^{17}$	-	0.7	16.0	-	-	-

2.4.1 Central star temperatures and reddening

Whenever, the spectral type and luminosity class of the star was known, the effective temperature of the central star, was taken from Lang(1992). For Be stars and for the bipolar PPN Hen3-1475, we assumed a central star temperature of 20000K. The total extinction (I.S.+C.S.) towards the stars due to interstellar and circumstellar dust grains was estimated from the difference between the observed and intrinsic (B-V) values. For Be stars, we assumed intrinsic (B−V) = −0.20 corresponding to an effective temperature of 20000K and for the low excitation PN IRAS 17395-0841 we assumed intrinsic (B−V) = −0.3 corresponding to an effective temperature of 35000 K for the hot central star. Since the distances to the stars were not known, the interstellar extinction (I.S.) in the direction of the stars was estimated using the Diffuse Infrared Background Experiment (DIRBE)/IRAS dust maps (Schlegel et al., 1998). The DIRBE/IRAS reddening estimates have an accuracy of 16%. The difference between the two sets of values would give an estimate of the extinction due to circumstellar dust. The DIRBE/IRAS dust maps do not give reliable estimates of the interstellar extinction for $|b| < 5°$. The U,B,V,R,I and near infrared magnitudes

of the stars were corrected for the total extinction (E(B−V) I.S.+C.S.) assuming R_v = 3.1.

2.4.2 Modelling of the circumstellar dust envelopes with DUSTY code

To derive physical parameters from the spectral energy distribution of the stars, we solved the problem of radiation transfer through a dust envelope using the DUSTY code (Ivezić et al., 1999) developed at the University of Kentucky assuming centrally-heated spherical density distributions. The central stars were assumed to be point sources, at the center of the spherical density distributions and their spectral energy distributions were taken to be Planckian. For modelling, we chose from six different grain types : 'warm' (Sil-Ow) and 'cold' (Sil-Oc) silicates from Ossenkopf et al. (1992), silicates and graphites (Sil-Dl and grf-DL) from Draine and Lee (1984), amorphous carbon (amC-Hn) from Hanner (1988) and SiC (SiC-Pg) from Pégourié (1988). DUSTY contains data for the optical properties of these six grain types. For all stars except IRAS17395-0841 and MWC930 the standard Mathis, Rumpl, Nordsieck (MRN) (Mathis et al., 1977) power-law was used for the grain size (n(a)) distributions, i.e. $n(a) \propto a^{-q}$ for $a_{min} \leq a \leq a_{max}$ with q=3.5, a(min)=0.005μ and a(max)=0.25μ. For IRAS17395-0841 and MWC930, we used the MRN distribution with q=4.3, a(min)=0.005μ, a(max)=0.25μ and q=3.7, a(min)=0.10μ and a(max)=0.25μ respectively. The dust temperature (T_d) on the inner shell boundary and the optical depth (τ) at 0.55μ were varied assuming an inverse square law (y^{-2}) for the spherical density distribution. The shell was assumed to extend to 1000 times its inner radius. For MWC930 and LSII+2317, we had to adopt a different power law (y^{-p}) for the density distribution in the shell with p=1.3 and 0.55 respectively inorder to obtain a good fit. DUSTY does not allow simultaneous modelling of warm and cold dust shells. Hence, the cold dust in the case of Hen3-1475, MWC939 and SS438 had to be modelled and treated independent of the warm dust in these stars. We adopted the fits for which the sum of squares of the deviations between the observed and modelled fluxes (after scaling) were a minimum. Table 2.4 lists the adopted input

parameters. Fig. 2.3 shows the spectral energy distribution of the stars.

Having fixed T_d and τ, we then used the gas-dynamical mode of the DUSTY code, to derive the mass-loss rate for a given model. However, in the case of MWC930 and LSII+2317 where the density distribution follows a different law, a hydrodynamics calculation and hence the determination of mass-loss rate was not possible. The output of the code gives the shell inner radius, r1(cm) where the dust temperature (T_d) is specified. The radius scales in proportion to $L^{1/2}$ where L is the luminosity and the output value corresponds to $L=10^4 L_\odot$. The mass-loss rate ($\dot{M}$) scales in proportion to $L^{3/4}(r_{gd}\rho_s)^{1/2}$ where, the gas-to-dust mass ratio, r_{gd}=200 and the dust grain density, ρ_s=3 g cm^{-3}. We carried out calculations for hot post-AGB stars with core masses of $0.565 M_\odot$ and $0.605 M_\odot$ corresponding to luminosities of $4500 L_\odot$ (Schönberner, 1983) and $6300 L_\odot$ (Blöcker, 1995) respectively. The distances (d) were derived using r1 and the ratio of the observed and modelled fluxes at 0.55μ.

θ (=r1/d) is the angular radii of the inner boundary of the cold circumstellar dust envelopes. In some cases eg. IRAS19399+2312, θ is very large (16″) but the nebula is not detected in the optical and in the case of IRAS18237-0715, θ = 45″ but the detected nebulosity is less than 2″. In these cases, the scattered light radiated by the dust shells in the optical may be too faint to be seen by our observations. In the V-band, some of our stars have a flux of the order of $6.9X10^{-11}$ erg s^{-1} cm^{-2}, eg. IRAS 17395-0841 (V=13.74). The reflection nebular (scattered light) flux per pixel on the CCD frames will be several orders of magnitude fainter. Our maximum exposure in Hα was 5 minutes which is not sufficient enough to reach our telescope's detection limit in Hα. As we move away from the central star, the scattered light flux drops down rapidly (see eg. the radial intensity profile of AFGL 2688 in Kwok et al., 2001). Longer exposures would be required to detect the fainter reflection nebulae. High resolution HST images (eg. Su et al., 2001) and subarcsecond mid-infrared imaging (Kwok et al., 2002) have been used to resolve PPNe.

The time when the star leaves the AGB can be assumed to coincide with the ejection of its dust envelope. For post-AGB stars with core masses of 0.565 $M_\odot$ and 0.605 $M_\odot$ the effective temperatures at the tip of the AGB are 5000K (Schönberner,

1983) and 6000K (Blöcker, 1995) respectively. The dust condensation temperature is taken to be 1200K (Whittet, 2003). Using the hydrodynamic mode of the DUSTY code, we then obtained the terminal outflow velocities (V_e) and the distances (r0) at which the dust grains reached the condensation temperature. Ve scales in proportion to $L^{1/4}(r_{gd}\rho_s)^{-1/2}$. The present inner boundary of the dust envelopes is at r1. Thus, the dynamical age from the tip of the AGB is given by $(r1-r0)/V_e$. The V_e values are in good agreement with the expansion velocity of 10 kms^{-1} assumed by Volk and Kwok (1989) for models of PPNe and the expansion velocities for PPNe estimated from CO measurements by Loup et al. (1990). There is an inherent uncertainity of 30 % in the ($\dot{M}$) and V_e values obtained with the DUSTY code (Ivezić et al., 1999).

Tables 2.5 a and b list the respective values for T_d, r1, r0, d, θ, $\dot{M}$, V_e and Δt. All calculations were carried out using the best fit parameters for the cold circumstellar dust shells.

2.4.3 The LSE stars

On comparing the low resolution spectra of the high galactic latitude stars, LSE163 and LSE45 with that of standard stars from Jacoby et al. (1984) we classified them as B2I. They may be similar to PG 1323-086 and PG 1704+222, two high galactic latitude B-type post-AGB stars (Moehler & Heber, 1998). Using the relation between core-mass and quiescent luminosity maximum for AGB stars (Wood & Zaro, 1981), with a typical core-mass of 0.6 $M_\odot$, we estimated a value of $10^{3.79}$ $L_\odot$ for the luminosity of the central stars. Since, $M_{bol}(Sun) = 4.75$, we obtained an absolute bolometric magnitude of -4.73 for the stars. Applying the bolometric correction for the spectral type of the star (Lang,1992), and using the distance modulus method, we obtained distance estimates of 4.3 and 4.8 kpc respectively to these stars. If on the other hand, we adopt the absolute visual magnitude (M_v) of -6.4 for a normal Population I B-type supergiant we obtain distance estimates of 19.3 and 21.7 kpc respectively. Such large distance estimates, suggesting that these objects lie at the outer edge of our galaxy appear to be unphysical. Abundance analysis from the high resolution spectra of these objects may confirm their evolutionary status as evolved low mass post-AGB

stars.

2.5 Notes on individual objects

#IRAS 17074-1845 (= Hen3-1347)

Henize (1976) had identified it as an Hα emission line object. It was classified as a hot post-AGB star on the basis of its high galactic latitude, far-infrared colors similar to PNe and Be spectral type (Parthasarathy, 1993a). Based on near-IR observations, García-Lario et al. (1997a) also classified it as a post-AGB star. Parthasarathy et al. (2000a) classified it as a B3IIIe post-AGB star. They found Hβ and Hγ in emission. From our Hα image of this object, we did not detect nebulosity around the central star. The angular radius of the envelope inner boundary indicates a compact nebula ($< 2''$). The spectral type, dust temperature, double peaked spectral energy distribution and mass-loss rate indicate that it may be a post-AGB star evolving into the PN stage.

#IRAS 17395-0841 (= SS 318)

It was discovered as a young low excitation planetary nebula by Vijapurkar et al. (1997). The Hα image (300 s exposure) of the PN is clearly extended. Fig. 2.4 shows a contour plot of the object in Hα. The angular extent of the nebula at the FWHM of the Hα image is $2.8''$. It appears that bipolar outflows are just beginning to form in this nebula, similar to the case of Hen3-1357 (Bobrowsky et al., 1998). High resolution Hα images with longer exposure times may reveal the true morphology of this young PN.

#IRAS17423-1755 (= Hen3-1475)

On the basis of IRAS data, Parthasarathy and Pottasch (1989) first classified it as a hot post-AGB star. It is a bipolar proto-planetary nebula (PPN) (Bobrowsky et al., 1995, Riera et al., 1995). The collimated bipolar outflows, seen in our Hα image have been studied by Borkowski et al. (1997) and Bobrowsky et al. (1995). Wind velocities greater than 1000 km s^{-1} have been observed in this PPN (Sanchez Contreras & Sahai, 2001, Borkowski & Harrington, 2001). From our Hα image, the

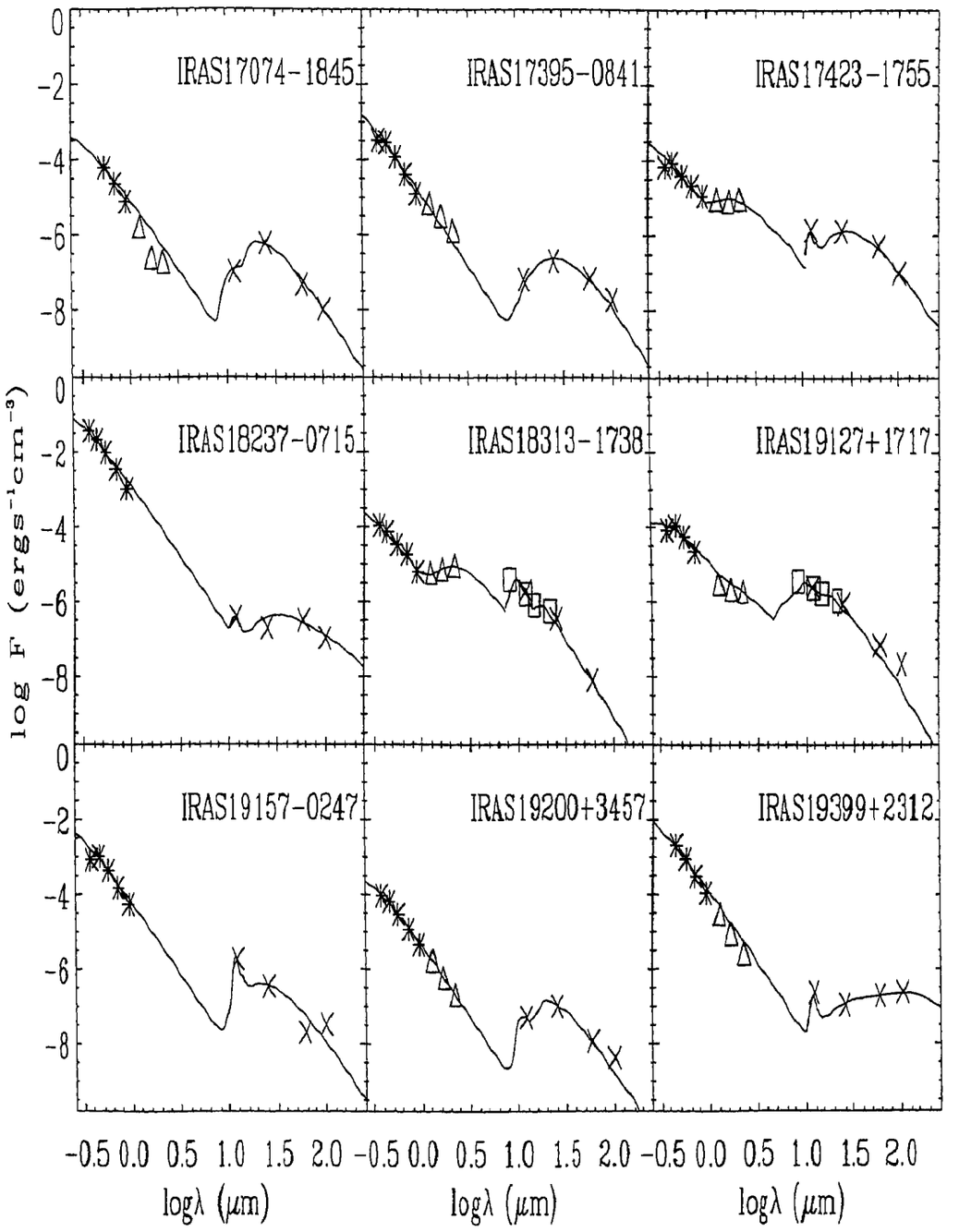

Figure 2.3: Spectral energy distributions (SEDs) of the hot post-AGB candidates. UBVRI data (asterisk) are plotted alongwith JHK (triangle), MSX (square) and IRAS data (cross). DUSTY model fits are shown by solid lines.

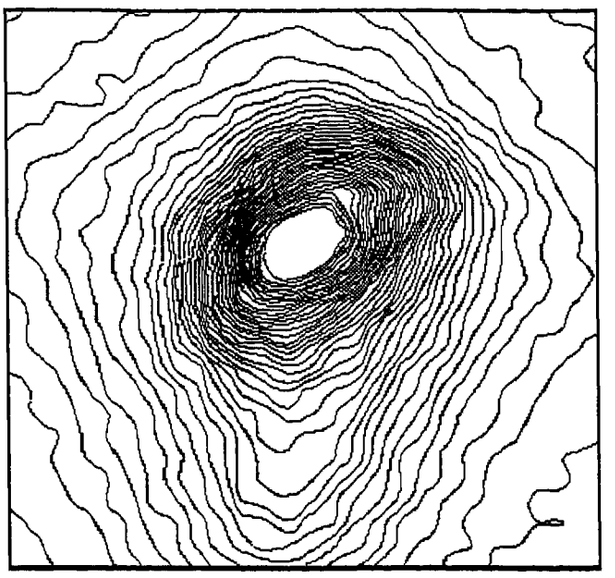

Figure 2.4: Contour plot of the low excitation PN IRAS 17395-0841 in Hα

south-east lobe appears to be more extended with an angular extent of 3.5″. The north-west lobe has an angular extent of only 2.2″. Based on [NII] HST images of the object, Borkowski et al. (1997) concluded that Hen3-1475 is a point symmetric nebula. They found emission knots in the outflows perpendicular to the dusty torus surrounding the central star with the outermost pair of knots at 7.82″and 7.57″from the star. From the spectral energy distribution, we detected a warm dust component at 1500K indicating cirumstellar dust close to the central star as a result of ongoing post-AGB mass-loss. The dynamical age from the tip of the AGB was estimated to be $\sim$ 4000 yrs. This value is uncertain due to the limitations of the DUSTY code and its inability to simultaneously model the warm and cold circumstellar dust (see Discussion below).

#IRAS 18237-0715(= MWC930)

Its spectra (Parthasarathy et al., 2000a, Vijapurkar et al., 1998) showed Balmer lines and several permitted and forbidden lines of [FeII] in emission. We found strong Hα emission in this star indicating the presence of a low excitation PN with an angular extent of less than 2″. Our seeing ($\sim$ 2arcsec) limited images could not resolve the nebula. There is considerable extinction (E(B$-$V)=2.1) towards the star. At a

distance of only 0.2 kpc, the heavy obscuration due to dust may be responsible for our inability to resolve the nebula. The effective temperature of the central star, spectral energy distribution and Hα emission suggest that it may be a hot post-AGB star. High resolution spectra and images of this object may help in understanding its true nature.

#IRAS 18313-1738(= MWC939)

Based on strong FeII and [FeII] emission lines Allen and Swings (1976) classified it as a Be star. In the spectrum taken in April, 1994 with the 1m CTIO telescope, covering the wavelength range from 3800Å to 5020Å at a resolution of 2Å , Vijapurkar et al.(1998), found Hβ, Hγ and several FeII and [FeII] lines in emission. Parthasarathy et al. (2000a) also classified it as a Be star. We have obtained the spectrum of this star from 5300 to 8800 Åwith 5Å pixel^{-1} resolution at the 1.02m VBO telescope (Fig. 2.5a). We find strong Hα emission alongwith [OI], FeII, [FeII], TiII and [TiII]. The spectral features observed appear to be very similar to the hot central star of the proto-planetary nebula HD51585(Klutz & Swings, 1977, Jascheck et al., 1996). The spectral energy distribution reveals the presence of warm dust at a temperature of 1200K. The warm dust may be a signature of ongoing post-AGB mass-loss in this star. This object was also detected in the A,C,D and E MSX bands. The narrow band CCD images also revealed Hα emission in this object. Owing to the limitations of the DUSTY code, the warm and cold dust shells were modelled independent of each other and hence the derived values of r1, θ and Δt may not be too appropriate.

We examined the IRAS low-resolution spectrum (LRS) of the object (Fig. 2.5b) retrieved from http://www.iras.ucalgary.ca/iras.html (cf. Kwok et al., 1997). The correction of the absolute calibration as in Volk and Cohen (1989) and Cohen et al.(1992) has not been applied to the data values. While the relative shape of the LRS spectrum is OK, the absolute flux level need not match the IRAS 12 micron flux density from the photometry. The 9.7 μ silicate dust feature was found to be in emission. The 8.2, 8.6 and 11.3 μ PAH features also appear to be in emission. The 9.7μ feature is expected to be in emission when the optical depth, τ, of the dust envelope at 9.7μ is less than $\sim$ 4. The peak strength of the feature occurs at $\tau \sim 2$. This feature originates from the circumstellar envelopes of oxygen-rich AGB

stars. Modelling of the circumstellar dust using DUSTY revealed the presence of graphite grains in the warm dust close to the central star and silicate grains in the cold circumstellar dust. The combination of C-rich and O-rich features in the circumstellar environment of the star may suggest a recent change to a C-rich chemistry of the outer envelope.

#IRAS19127+1717(=SS438)

Whitelock & Menzies (1986) discussed the nature of this peculiar object. They found that the object's spectrum has the characteristics of a high-density, moderate excitation PN superimposed on the continuum of a reddened early-type star. From the Hβ, Hγ and Hδ lines, they assigned a spectral classification of B9V to the star. It is not clear whether the nebula is the result of mass-loss of a single star terminating its AGB evolution or a binary system with the outward appearance of a nebula. From the Balmer decrement they obtained E(B−V) = 1.0±0.1. Using our observed (B−V) and the intrinsic (B−V) for a B9V star, we find E(B−V) = 1.14. Using the DUSTY code we obtained a distance of 4.0kpc to the central star of the PN. If on the other hand, the B9V star is the visual binary companion to the hot post-AGB central star of the PN, then using M_v=+0.2 for the B9V star, we obtain a distance of 0.2 kpc to the binary system. Likkel(1989) had detected OH (1667 MHz) emission in this star. CO emission was not detected (Likkel et al., 1991). We detected the presence of a warm dust component at 1300K around the star. The unusually small estimate of the dynamical age from the tip of the AGB may be due to the inability to obtain a good fit to the flux distribution using the DUSTY code and hence the uncertainity in r1.

#IRAS 19157-0247(= LSIV-0229)

This object was classified as a post-AGB star with a spectral type of B1III by Parthasarathy et al.(2000a). From its Hα image, we did not detect nebulosity around the central star. The spectral energy distribution, high galactic latitude and mass-loss rate suggest that it may be a low mass star in the post-AGB phase of evolution.

#IRAS 19200+3457(= StHA161)

It was found to be an H_α emission star (Stephenson, 1986). Preite-Martinez(1988)

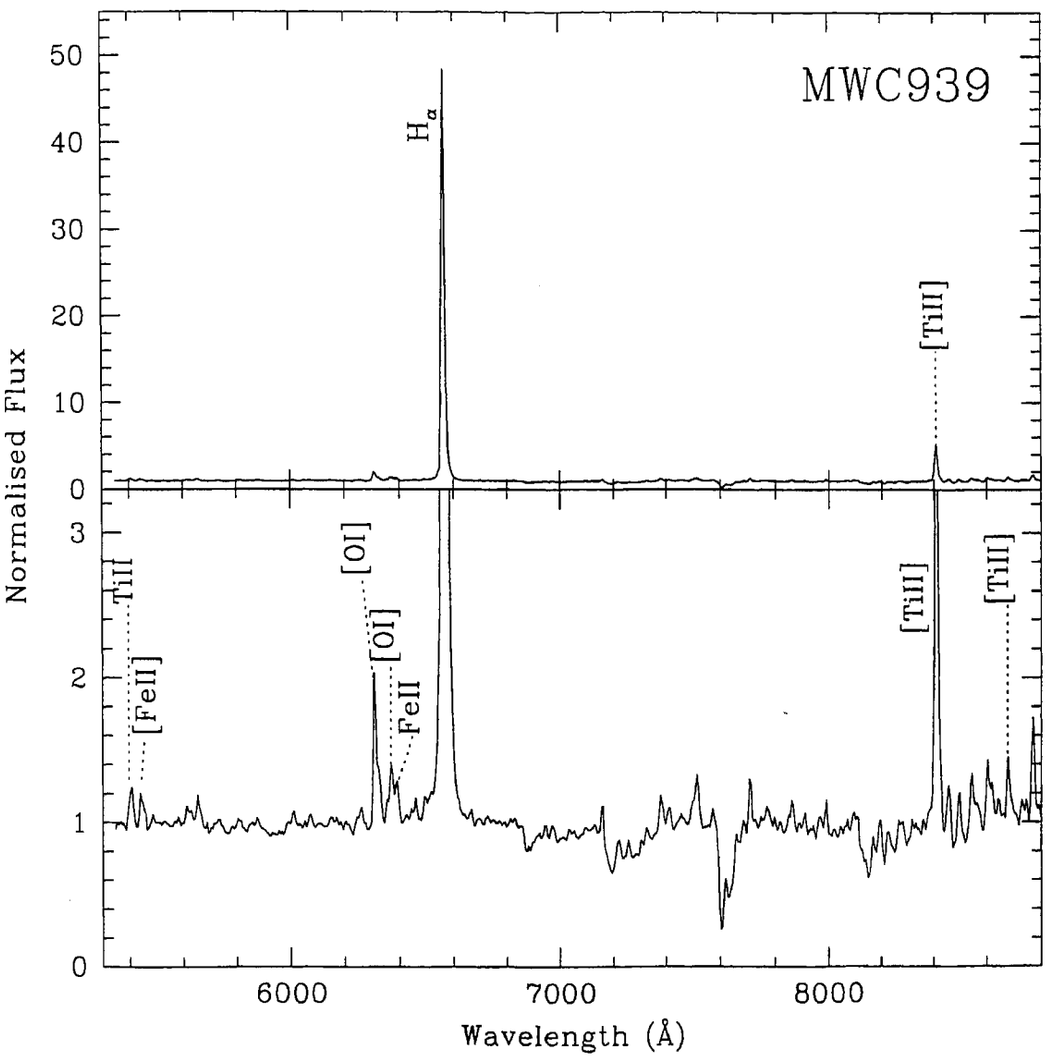

Figure 2.5a: Low resolution spectrum of the hot post-AGB candidate IRAS18313−1738 (=MWC 939)

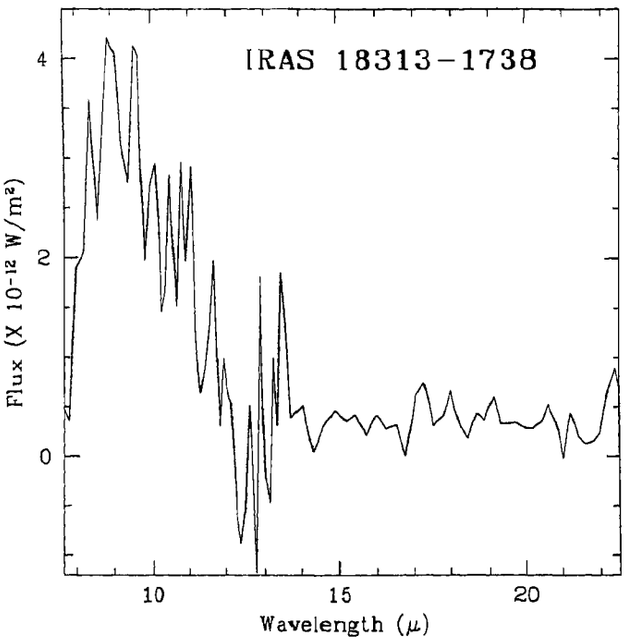

Figure 2.5b: The IRAS LRS spectrum of IRAS 18313-1738 (=MWC 939)

classified it as a possible PN. They estimated the H_β flux to be $4.8X10^{-12}$ erg s^{-1} cm^{-2} for this star. Using the modified Shlowskii method, they estimated a distance of 4.3 kpc to the star. From the dust model for the star, we estimated a distance of 3.8kpc. The angular radius of the envelope inner boundary suggests a low excitation compact nebula (< 1″).

#IRAS 19399+2312(= LSII+2317)

It was classified as B1III by Parthasarathy et al. (2000a). Reed (1998) had obtained the UBV magnitudes of this star (U=11.00, B=11.20, V=10.42). We found them to be in good agreement with our B,V, magnitudes. The spectral energy distribution showing the presence of a cold dust component at 127 K around the hot central star (T_{eff} = 24000 K) and IRAS colors similar to PNe suggest that it may be a post-AGB star. From our short exposure Hα image (120s) we did not detect nebulosity around the central star.

2.6 Discussion and conclusions

We have studied a small sample of hot post-AGB candidates selected on the basis of their IRAS colors. The near and far-infrared flux distributions of the stars were modelled using the DUSTY code. We were able to estimate the inner radii of the circumstellar shells, the distance to the stars, the mass-loss rates and angular extent of the inner boundary of the circumstellar envelopes from the best fit models. We also estimated the dynamical ages from the tip of the AGB to the present stage. However, DUSTY has certain shortcomings. It does not allow simultaneous modelling of warm and cold circumstellar dust shells. The warm and cold dust have to be modelled independent of each other and their simultaneous influence on the evolution of the nebulae cannot be accounted for. IRAS17423-1755, IRAS18313-1738 and IRAS19127+1717 show the presence of both warm and cold dust in their circumstellar environment. The inner shell radii for these three objects were calculated from the model fits to the cold dust shells. Since the influence of ongoing post-AGB mass-loss (warm dust) on the remnant AGB envelope (cold dust) has not been accounted for, the derived r1 values in these cases are uncertain. The uncertainity in r1 translates into an uncertainity in the dynamical ages of the nebulae. Independent modelling of the warm and cold dust shells may also explain the inability to obtain a good fit in the case of IRAS19127+1717. Besides, DUSTY allows only a spherical or slab geometry of the dust density distribution. This again may not be adequate for the hot post-AGB stars rapidly evolving into PNe of varied morphologies. In conclusion, the physical parameters derived from the modelling of the circumstellar envelopes are within the limits of the current model and may not be very precise indicators of the circumstellar envelopes of these stars.

The dust models were generated with different grain types - silicates, graphite and amorphous carbon. From the grain types for the best fit models we can infer the chemical composition of the circumstellar envelopes. IRAS17074-1845 has only silicates in the circumstellar environment while the low excitation PN, IRAS17395-0841 shows a carbon-rich circumstellar envelope. Other stars such as IRAS17423-1755, IRAS18313-1738 and IRAS19127+1717 show a combination of silicates and

carbon in the circumstellar environment. The warm dust in these stars, is composed of amorphous carbon or graphite dust grains. Since the warm dust indicates ongoing post-AGB mass-loss, the envelope chemistry appears to change from oxygen-rich to carbon-rich as the stars evolve towards the PN stage.

The stars in this chapter show Balmer lines in emission. Some also show several permitted and forbidden FeII lines (eg. MWC939) in emission and low excitation forbidden lines of SII and NII (eg. Hen3-1475, Riera et al., 1995). Emission lines have been detected in several other hot post-AGB stars (Parthasarathy et al., 2000b). As the central stars become hotter and evolve towards the PN stage we expect to see these emission lines in their optical spectra. The objects with strong emission lines in our sample are not young stars. These objects are not associated with star forming regions. These are at high galactic latitudes with far-IR colors similar to PNe. These are most likely hot post-AGB stars and as the central stars evolve to higher temperatures they will evolve into PNe.

Chapter 3

UV(IUE) spectra of hot post-AGB candidates

Abstract

Analysis of the low resolution UV(IUE) spectra (1150 to 3200Å) of 15 hot post-AGB candidates is presented. The UV(IUE) spectra of 10 stars suggest partial obscuration of the hot stars due to circumstellar dust. The reddened continua of these 10 stars were used to model and estimate the circumstellar extinction. The circumstellar extinction law was found to be linear in λ^{-1} in the case of IRAS13266-5551 (CPD-55 5588), IRAS14331-6435 (Hen3-1013), IRAS16206-5956 (SAO 243756), IRAS17074-1845 (Hen3-1347), IRAS17311-4924 (Hen3-1428), IRAS18023-3409 (LSS 4634), IRAS18062+2410 (SAO 85766), IRAS18371-3159 (LSE 63), IRAS22023+5249 (LSIII +5224) and IRAS22495+5134 (LSIII +5142). There seems to be no significant circumstellar extinction in the case of IRAS17203-1534, IRAS17460-3114 (SAO 209306) and IRAS18379-1707 (LSS 5112). The UV(IUE) spectrum of IRAS12584-4837 (Hen3-847) shows several emission lines including that of HeII. It may be a massive young OB-supergiant or a low mass star in the post-AGB phase of evolution. IRAS16206-5956 (SAO 243756) and IRAS 18062+2410 (SAO 85766) show variability in the UV which in addition to stellar pulsations may be attributed to a dusty

torus in motion around the hot central stars. The UV spectrum of the bipolar PPN, IRAS17423-1755 (Hen3-1475) indicates that the central B-type star is obscured by a dusty disk. The stars were placed on the log g−log T_{eff} diagram showing the post-AGB evolutionary tracks of Schönberner. Terminal wind velocities of the stars were estimated from the CIV and NV stellar wind features. The presence of stellar wind in some of these stars indicates ongoing post-AGB mass-loss.

3.1 Introduction

Low and intermediate mass stars ($M \simeq 0.8$ - $8\ M_{\odot}$) pass through the post-asymptotic giant branch (post-AGB) phase of evolution on their way to becoming planetary nebulae (PNe). From an analysis of the Infrared Astronomical Satellite Point Source Catalog (IRAS PSC), cooler post-AGB stars having G,F,A supergiant-like character were first identified (Parthasarathy & Pottasch 1986, Lamers et al. 1986, Pottasch & Parthasarathy 1988b, Hrivnak et al. 1989). These stars were found to have circumstellar dust shells with far-IR colors and flux distributions similar to the dust shells of PNe. Later, from an analysis of IRAS data, Parthasarathy & Pottasch (1989) found a few hot (OB spectral types) post-AGB candidates. Their supergiant-like character, the presence of cold detached dust shells, far-IR colors similar to PNe and high galactic latitudes suggested that they may be in a post-AGB phase of evolution. Thus, there seems to be an evolutionary sequence ranging from the cooler G,F,A supergiant-like stars to hotter O-B types, evolving from the tip of the AGB towards young PN stage (Parthasarathy, 1993b).

Pottasch et al. (1988a) and van der Veen & Habing (1988) identified a region of the IRAS color-color diagram ($F(12\mu)/F(25\mu) < 0.35$ and $F(25\mu)/F(60\mu) > 0.3$) which was mainly populated by stars in transition from the AGB to the PN phase. Based on their far-IR colors and low resolution optical spectra, several hot post-AGB candidates were identified (Parthasarathy & Pottasch 1989, Parthasarathy 1993a, 1993b, Parthasarathy et al., 2000a). The optical spectra of these objects show strong Balmer emission lines and in some cases low excitation nebular emission lines such as [NII] and [SII] superposed on the OB stellar continuum. The absence of [OIII]

5007Å line and the presence of low excitation nebular emission lines indicate that photoionisation has just started. It is important to study these stars in the UV to obtain better estimates of their temperatures and to look for signatures of circumstellar reddening, mass-loss and stellar winds. The UV(IUE) spectra of some hot post-AGB stars (eg. Hen3-1357, Parthasarathy et al. 1993c, 1995, Feibelman, 1995) have revealed violet shifted stellar wind P-Cygni profiles of CIV, SiIV and NV, indicating hot and fast stellar wind, post-AGB mass-loss and rapid evolution. In this chapter we have analysed the UV(IUE) spectra of 15 hot post-AGB candidates.

3.2 Target selection and observations

The hot post-AGB candidates in this chapter (Table 3.1) were identified on the basis of their IRAS colors ($F(12\mu)/F(25\mu) < 0.35$ and $F(25\mu)/F(60\mu) > 0.3$), high galactic latitudes and OB-giant or supergiant spectra in the optical (Parthasarathy et al., 2000a) with Balmer lines in emission. Young massive OB supergiants are not expected at high galactic latitudes and also they are not expected to have detached cold circumstellar dust shells. High galactic latitude OB supergiants with detached dust shells and far-IR colors similar to PNe were found to be in the post-AGB phase of evolution (Parthasarathy, 1993b, Parthasarathy et al., 2000a).

Low resolution ($\sim 6 - 7$Å), large aperture, UV(IUE) spectra of the hot post-AGB candidates from 1150Å to 3200Å were extracted from the Multimission Archive at STScI (Table 3.2). The spectra obtained by centering the stars in the 10″X 23″aperture were processed using the IUE NEWSIPS (new spectral image processing system) pipeline which applies the signal weighted extraction technique (SWET) as well as the latest flux calibration and close-out camera sensitivity corrections. An increased signal-to-noise (S/N) ratio of 10% – 50% has been demonstrated for low dispersion IUE spectra reprocessed with the NEWSIPS software (Nichols & Linsky, 1996). Well exposed IUE NEWSIPS spectra have S/N of $\sim$ 50 while weak, high-background, under-exposed spectra have S/N of $\sim$ 20 (Nichols et al., 1994, Nichols & Linsky, 1996). From our sample, IRAS14331-6435 (Hen3-1013), IRAS17074-1845 (Hen3-1347), IRAS17203-1534, IRAS18023-3409 (LSS 4634), IRAS18379-1707 (LSS

Table 3.1: Hot post-AGB candidates

Star No.	IRAS	Name	l	b	IRAS Fluxes (Jy.)			
					12μ	25μ	60μ	100μ
1.	12584-4837	Hen3-847	304.60	+13.95	36.07	48.75	13.04	3.31
2.	13266-5551	CPD-55 5588	308.30	+6.36	0.76	35.90	35.43	11.66
3.	14331-6435	Hen3-1013	313.89	-4.20	4.04	108.70	70.71	20.61
4.	16206-5956	SAO 243756	326.77	-7.49	0.36L	11.04	12.30	4.83
5.	17074-1845	Hen3-1347	4.10	+12.26	0.50	12.20	5.66	3.47:
6.	17203-1534		8.55	+11.49	0.32	10.70	6.88	3.37
7.	17311-4924	Hen3-1428	341.41	-9.04	18.34	150.70	58.74	17.78
8.	17423-1755	Hen3-1475	9.36	+5.78	7.05	28.31	63.68	33.43
9.	17460-3114	SAO 209306	358.42	-1.88	6.26	20.82	12.20	220.40L
10.	18023-3409	LSS 4634	357.61	-6.31	0.26L	2.94	1.82	25.64L
11.	18062+2410	SAO 85766	50.67	+19.79	3.98	19.62	2.90	1.00L
12.	18371-3159	LSE 63	2.92	-11.82	0.25L	6.31	5.16	1.95
13.	18379-1707	LSS 5112	16.50	-5.42	1.67	23.76	7.12	3.66L
14.	22023+5249	LSIII +5224	99.30	-1.96	1.02	24.69	14.52	3.93L
15.	22495+5134	LSIII +5142	104.84	-6.77	0.54	12.37	7.18	3.12

A colon : indicates moderate quality IRAS flux, **L** is for an upper limit

5112) and IRAS22023+5249 (LSIII +5224) have S/N $\sim$ 20. IRAS12584-4837 (Hen3-847), IRAS17460-3114 (SAO 209306) and IRAS18371-3159 (LSE 63) have well exposed spectra with S/N $\sim$ 50. The spectra of the remaining hot post-AGB candidates are of intermediate quality with S/N $\sim$ 30. The LWP spectra 18412 and 27936 of IRAS12584-4837 and IRAS18371-3159 respectively, were saturated and have not been used in the analysis. Line-by-line images were inspected for spurious features.

3.3 Analysis

Tables 3.3, 3.4a and 3.4b list the V magnitudes and B−V values of the 15 hot post-AGB candidates from literature. The optical spectral types are mainly from Parthasarathy et al. (2000a). For the optical spectral types of the stars, the corresponding intrinsic B−V values, $(B-V)_o$, were taken from Schmidt-Kaler (1982). Using the observed and intrinsic B−V values we derived the total (interstellar plus circumstellar) extinction, $E(B-V)_{total}$ $(=(B-V)_{obs} - (B-V)_o)$ towards these stars. These values were compared with interstellar extinction $(E(B-V)_{I.S.})$ at the galactic latitudes and longitudes of these stars, estimated using the Diffuse Infrared Background Experiment (DIRBE)/IRAS dust maps (Schlegel et al., 1998). The DIRBE/IRAS dust maps do not give reliable estimates of the interstellar extinction for $|b| < 5°$. The accuracy of the DIRBE/IRAS extinction estimates are 16%. Comparing $E(B-V)_{total}$ and $E(B-V)_{I.S.}$ we found considerable circumstellar extinction in most cases (Tables 3.4a and b).

The 2200Å feature in the UV gives an estimate of the interstellar extinction. The merged LWP and SWP spectra of the hot post-AGB candidates were dereddened (Tables 3.3, 3.4a and b) using the 2200Å feature in the UV. Using the UNRED routine in the IUE data analysis software package, we adopted the average extinction law by Seaton (1979) and tried different values of E(B−V) till the 2200Å bump in the UV disappeared and smooth continua from 1150Å to 3200Å were obtained for all the stars. In the absence of an LWP spectrum of IRAS17460-3114 (SAO 209306), the SWP spectrum of the star was dereddened using $E(B-V)_{total}$ $((B-V)_{obs}-(B-V)_o)=0.54$. In the rest of this chapter, "dereddened spectra" would always refer to the observed IUE

Table 3.2: Log of observations

IRAS	Camera	Image	Aperture	DateObs	Exposure Time(s)
12584-4837	SWP	39271	LARGE	21 July 1990	2999.781
= Hen3-847	LWP	18412	LARGE	21 July 1990	1799.659
	LWP	19726	LARGE	10 Feb 1991	299.704
13266-5551	SWP	39270	LARGE	20 July 1990	1799.652
= CPD-55 5588	LWP	18411	LARGE	20 July 1990	1199.595
14331-6435	SWP	33601	LARGE	22 May 1988	2399.717
= Hen3-1013	LWP	13295	LARGE	22 May 1988	1199.595
16206-5956	SWP	33953	LARGE	21 July 1988	2399.717
= SAO 243756	SWP	50195	LARGE	12 March 1994	2399.716
	SWP	50640	LARGE	28 April 1994	3599.844
	LWP	13714	LARGE	21 July 1988	1199.595
	LWP	26175	LARGE	19 August 1993	1019.781
	LWP	27667	LARGE	12 March 1994	599.531
17074-1845	SWP	39276	LARGE	21 July 1990	1799.652
= Hen3-1347	LWP	18418	LARGE	21 July 1990	599.531
17203-1534	SWP	50657	LARGE	30 April 1994	2399.716
	LWP	28020	LARGE	30 April 1994	1199.595
17311-4924	SWP	33600	LARGE	21 May 1988	2099.480
= Hen3-1428	SWP	48127	LARGE	17 July 1993	3599.844
	LWP	13294	LARGE	22 May 1988	959.570
	LWP	25934	LARGE	17 July 1993	899.768
17423-1755	SWP	35860	LARGE	26 March 1989	2099.480
= Hen3-1475					
17460-3114	SWP	54660	LARGE	12 May 1995	89.572
= SAO 209306					
18023-3409	SWP	55458	LARGE	9 August 1995	4199.499
= LSS 4634	LWP	31272	LARGE	9 August 1995	1559.634
18062+2410	SWP	44446	LARGE	21 April 1992	1200
= SAO 85766	SWP	55916	LARGE	12 Sept. 1995	1800
	LWP	22865	LARGE	21 April 1992	300
	LWP	31454	LARGE	12 Sept. 1995	600

Table 3.2: contd..

IRAS	Camera	Image	Aperture	DateObs	Exposure Time(s)
18371-3159	SWP	50588	LARGE	19 April 1994	4799.563
= LSE 63	LWP	27936	LARGE	19 April 1994	2399.723
	LWP	27972	LARGE	23 April 1994	899.768
18379-1707	SWP	47531	LARGE	23 April 1993	3899.672
= LSS 5112	LWP	25398	LARGE	23 April 1993	1199.595
22023+5249	SWP	48454	LARGE	24 August 1993	2399.716
= LSIII +5224	SWP	48593	LARGE	9 Sept 1993	4799.563
	SWP	55915	LARGE	12 Sept 1995	7199.819
	LWP	26209	LARGE	24 August 1993	1199.595
	LWP	31453	LARGE	12 Sept 1995	2399.723
22495+5134	SWP	48453	LARGE	24 August 1993	2399.716
= LSIII +5142	LWP	26322	LARGE	9 Sept. 1993	2099.487

spectra corrected for interstellar extinction as determined from the 2200Å feature in the UV.

For stars with multiple LWP and SWP spectra, we overplotted the observed LWP (and SWP) spectra of each star to check for variability. The LWP and SWP spectra of IRAS16206-5956 (SAO 243756) and IRAS18062+2410 (SAO 85766) were found to show variation (Fig. 3.1). Coadded LWP and SWP spectra of IRAS17311-4924 and IRAS22023+5249 were used in the analysis.

The dereddened merged spectra of the hot post-AGB candidates were compared with the dereddened spectra of standard stars from the atlas by Heck et al. (1984) The spectral types of the standard stars chosen for comparison were as close as possible to the optical spectral types of the hot post-AGB candidates. Tables 3.3, 3.4a and 3.4b list the standard stars used for comparison, their spectral types and E(B−V) values. For comparison, the flux of the standard stars were scaled in accordance with the difference between the V magnitudes (after correcting for interstellar exintinction as determined from the 2200Å feature) of the standard star and the corresponding hot post-AGB candidate.

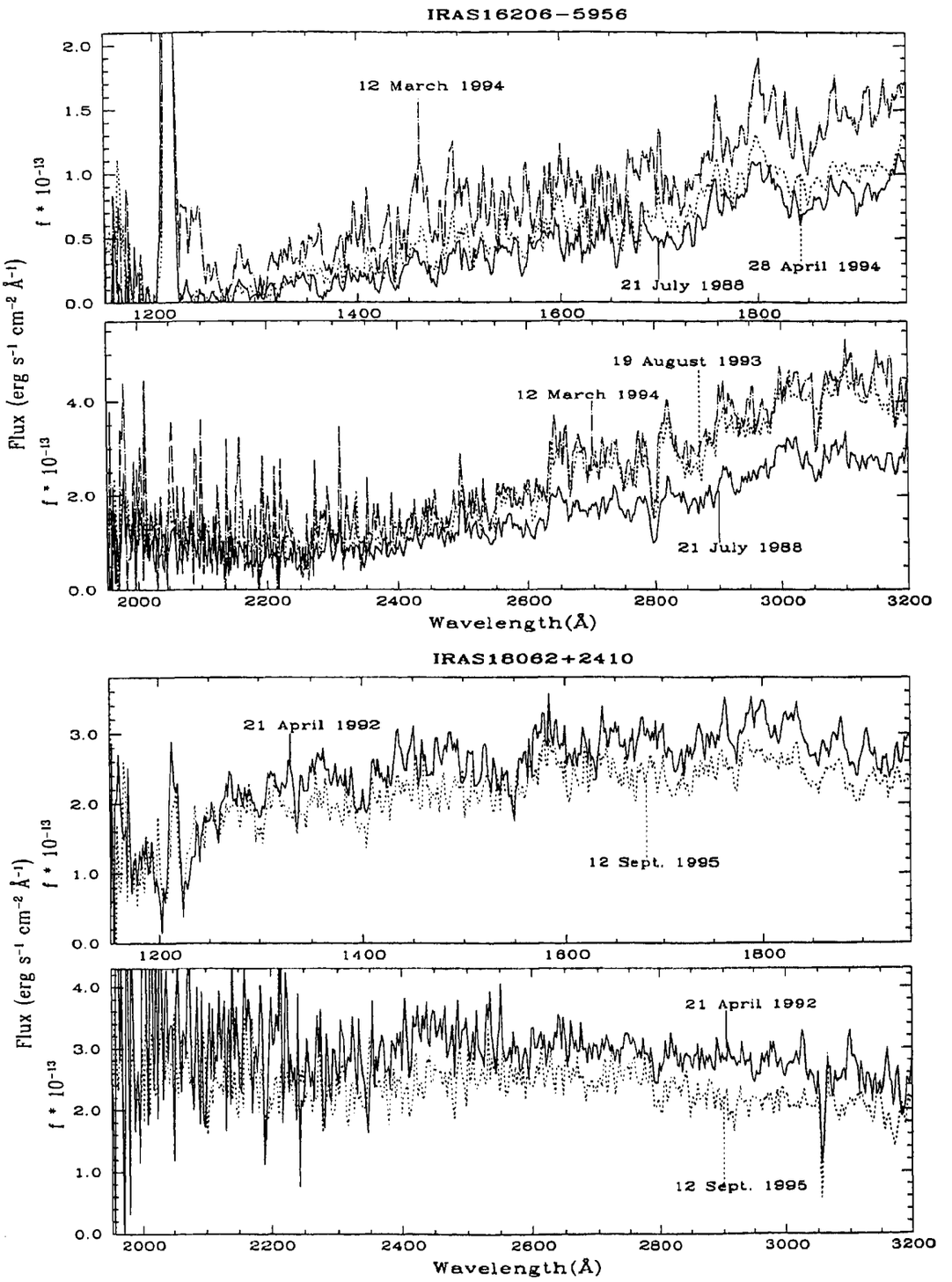

Figure 3.1: The observed LWP and SWP spectra of IRAS16206-5956(SAO 243756) and IRAS18062+2410(SAO 85766) showing the variability.

3.3.1 Spectral features in the UV

The spectra from 1150Å to 3200Å dereddened with E(B−V) determined from the 2200Å feature are shown in Figs. 3.2, 3.3, 3.5a and 3.6a. Lines of NV(1240Å), CII(1335Å), SiIV(1394, 1403Å), CIV(1550Å), NIV(1718Å), FeII(2586-2631Å) and MgII(2800Å) typical of hot stars (Heck et al., 1984) and central stars of PNe were identified in the spectra of these stars. The UV line strengths in the hot post-AGB candidates were compared with the line strengths in the standard stars. The absence of CIV in the B3-supergiant star, IRAS14331-6435 (Hen3-1013) alongwith near normal line strengths of SiIV and NIV suggests the underabundance of carbon in this star. From the SiIV and CIV features it appears that IRAS17074-1845 (Hen3-1347) and IRAS17460-3114 (SAO 209306) may be slightly metal deficient. Based on its optical spectra, IRAS18062+2410 (SAO 85766) was found to be metal poor and underabundant in carbon (Parthasarathy et al. 2000b, Mooney et al., 2002). In the UV also the line strengths appear to be weaker compared to a standard B1-supergiant. Metal deficiency has been observed in some high latitude hot post-AGB stars (see eg. McCausland et al. 1992, Napiwotzki et al. 1994).

3.3.2 Stars with negligible circumstellar extinction

The UV continua and spectral features of IRAS17203-1534, IRAS17460-3114 (SAO 209306) and IRAS18379-1707 (LSS 5112) were in good agreement with the dereddened UV(IUE) spectra of standard stars (Table 3.3) of similar optical spectral types (Fig. 3.2). The E(B−V) values of these stars determined from the 2200Å feature are nearly the same as $E(B-V)_{total}$ (Table 3.3) suggesting negligible extinction of starlight due to circumstellar dust in these three cases. Emission lines of SiII(1533, 1808, 1817Å), HeII(1640Å), NI(1743Å) and FeII(1785, 2746Å) in the spectrum of IRAS12584-4837 (Hen3-847) indicate the presence of hot plasma or a nebula.

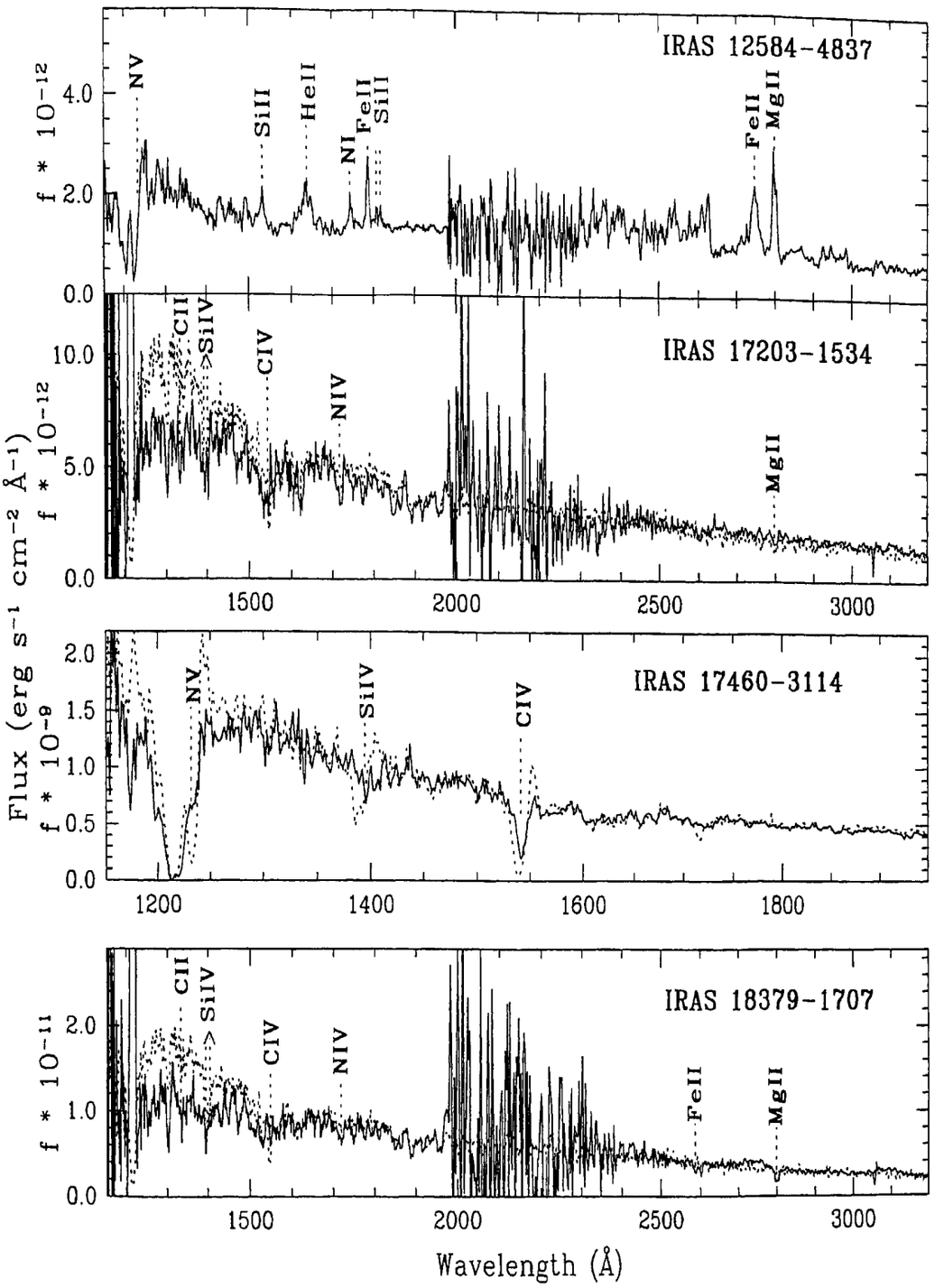

Figure 3.2: The dereddened UV(IUE) spectra of hot post-AGB candidates with negligible circumstellar extinction (solid lines) compared with the dereddened UV(IUE) spectra of standard stars (dotted lines) from the atlas by Heck et al. (1984, Table 3.3). The spectra were dereddened using E(B−V) estimated from the 2200Å feature in the UV. IRAS17460-3114 was dereddened using $E(B-V)_{total}$ for the star. IRAS12584-4837 is a Be star in the optical.

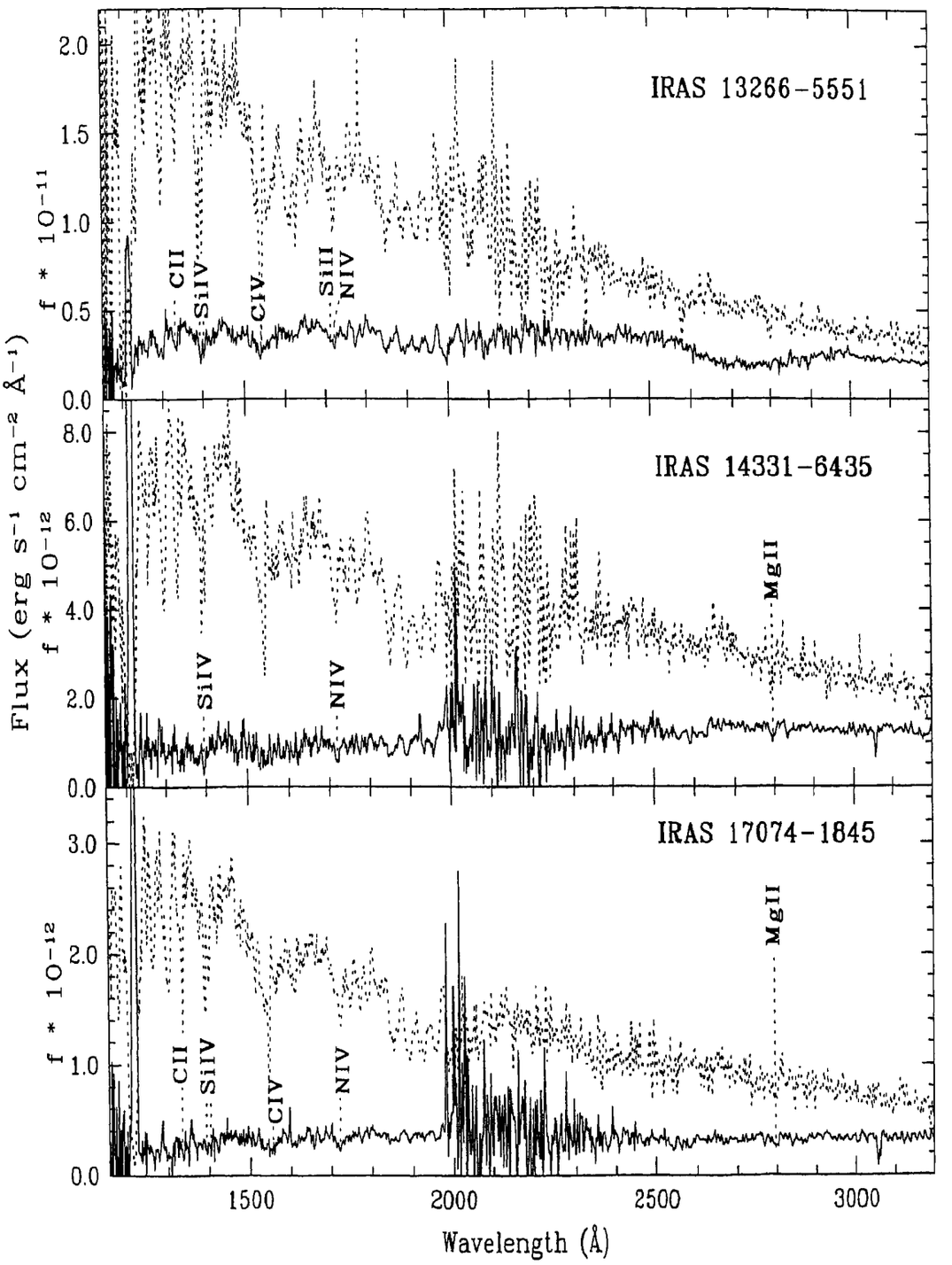

Figure 3.3: The dereddened UV(IUE) spectra of hot post-AGB candidates (solid line) plotted alongwith the dereddened spectra of standard stars (dotted line) of similar optical spectral types from the atlas by Heck et al. (1984, Table 3.4a). The spectra have been dereddened using the 2200Å feature in the UV. Notice the reddened continua of the hot post-AGB candidates in comparison with the standard stars. The hot central star of IRAS17423-1755 is not observed in the UV, possibly due to obscuration of the star by a dusty torus.

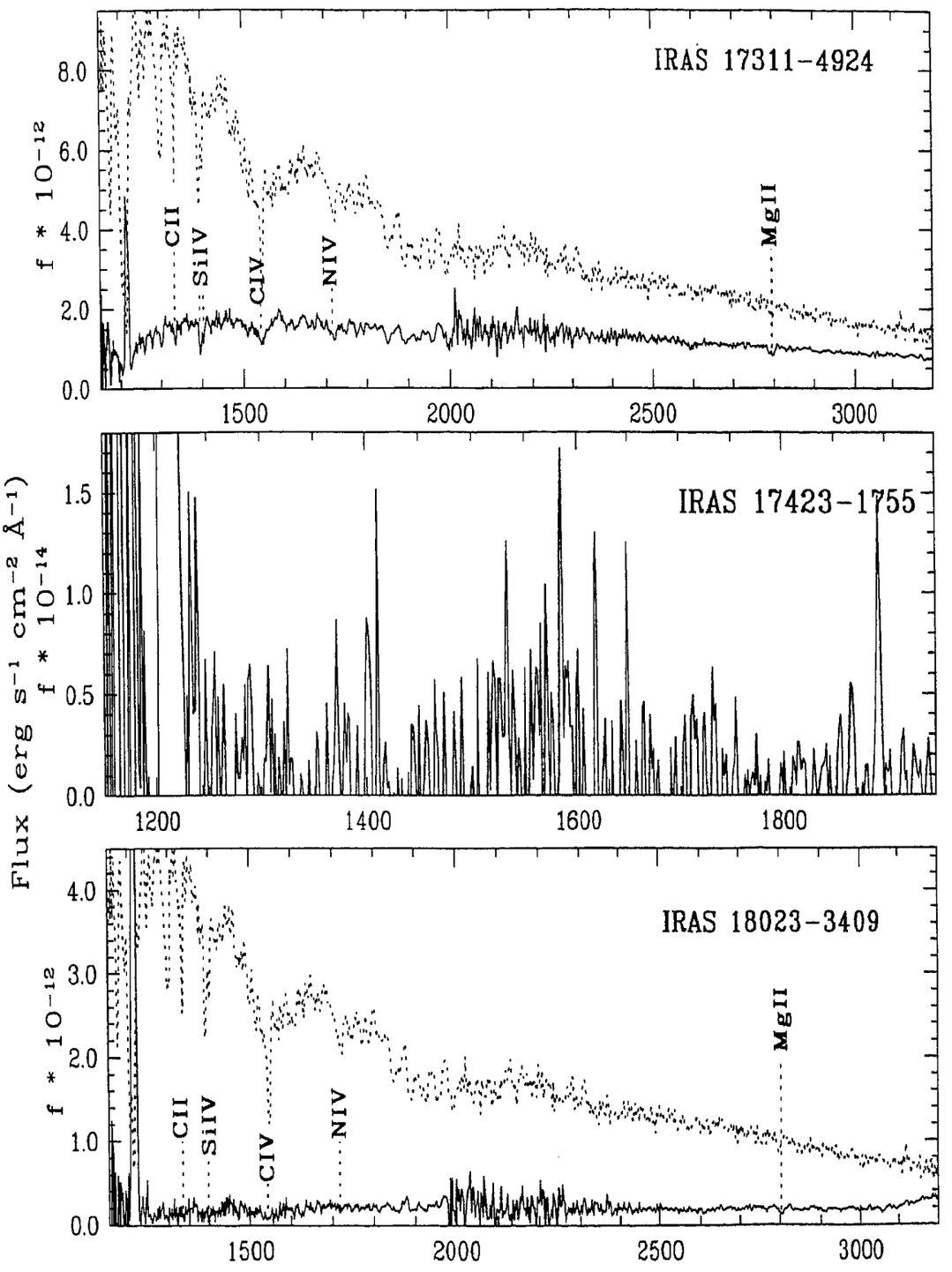

Figure 3.3: contd....

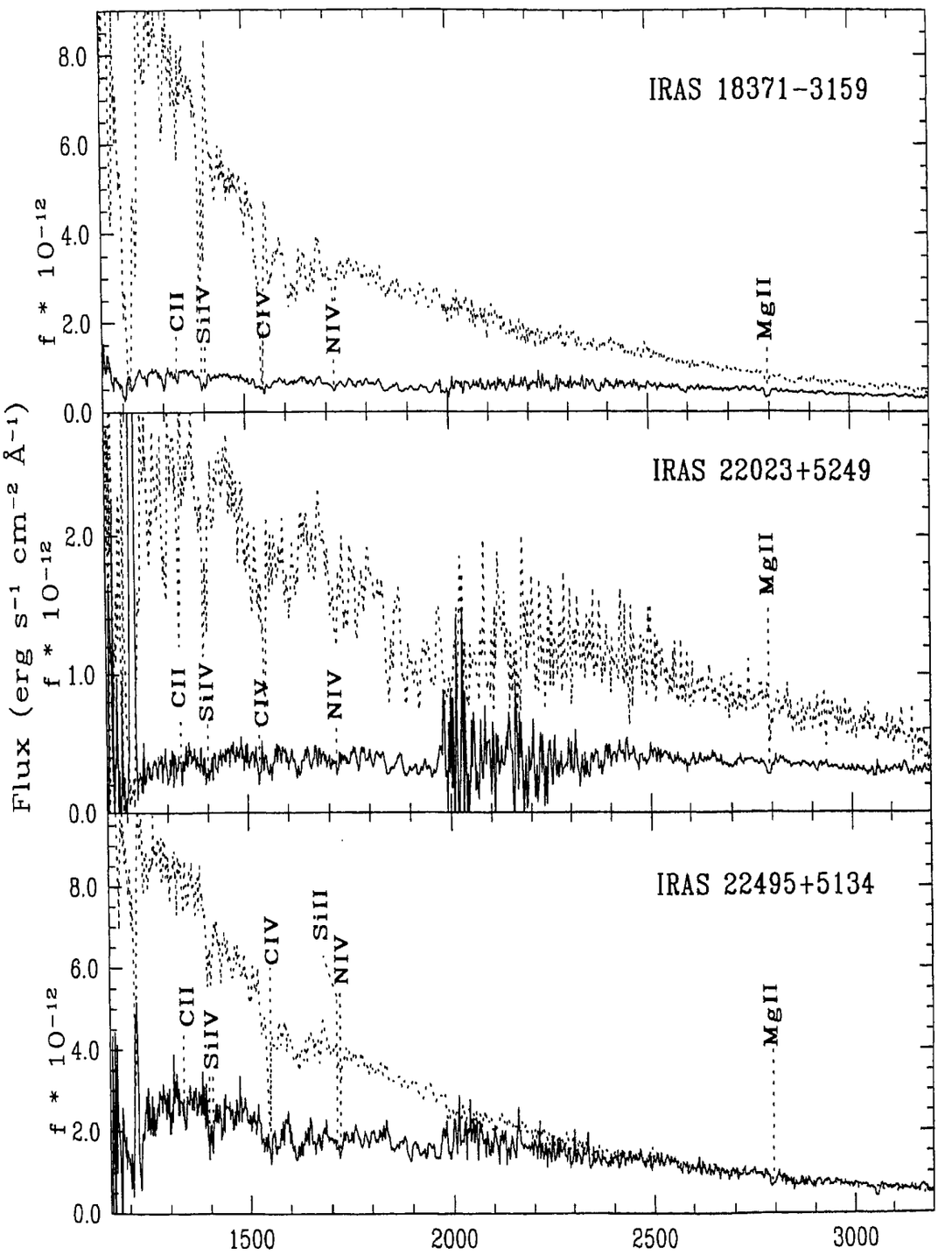

Figure 3.3: contd....

Table 3.3: Hot post-AGB candidates with negligible circumstellar extinction

IRAS	V mag	$(B-V)_{obs}$	E(B−V) I.S.	E(B−V) (2200Å)	Sp. Type Optical	E(B−V) total	Standard star	Sp.Type std. star	E(B−V) std. star
12584-4837	10.58[a]	0.07[a]	0.18	0.25	Be[1]	-	-	-	-
17203-1534	12.02[a]	0.35[a]	0.44	0.56	B1IIIpe	0.61	HD173502	B1II	0.09
17460-3114	7.94[b]	0.23[b]	-	0.54	O8III	0.54	HD162978	O7.5II	0.35
18379-1707	11.93[b]	0.45[b]	-	0.70	B1IIIpe	0.71	HD173502	B1II	0.11

Photometry is from : [a]Hog et al.(2000); [b]Reed(1998). Spectral types of the hot post-AGB candidates are from Parthasarathy et al. (2000a) except [1]Kazarovets et al. (2000).

Table 3.4a: Hot post-AGB candidates with observable circumstellar extinction

IRAS	V mag	$(B-V)_{obs}$	E(B−V) I.S.	E(B−V) (2200Å)	Sp. Type Optical	E(B−V) total	Standard star	Sp.Type std. star	E(B−V) std. star	E(B−V) C.S.
13266-5551	10.68[b]	0.31[b]	0.53	0.38	B1Ibe	0.51	HD77581	B0.5Ia	0.77	0.15
14331-6435	10.90[b]	0.58[b]	-	0.44	B3Ie	0.71	HD198478	B3Ia	0.58	0.26
17074-1845	11.47[a]	0.46[a]	0.28	0.24	B3IIIe	0.66	HD51309	B3II	0.13	0.39
17311-4924	10.68[c]	0.40[c]	0.22	0.28	B1IIe	0.66	HD51283	B2III	0.02	0.39
17423-1755	12.64[d]	0.66[d]	0.67	-	Be	-	-	-	-	-
18023-3409	11.55[b]	0.46[b]	0.44	0.30	B2IIIe	0.70	HD51283	B2III	0.02	0.43
18371-3159	11.98[a]	0.11[a]	0.15	0.13	B1Iabe	0.30	HD122879	B0Ia	0.42	0.11
22023+5249	12.52[a]	0.69[a]	-	0.37	B[1]	-	HD41117	B2Ia	0.52	0.44
22495+5134	11.78[a]	0.22[a]	0.357	0.33	PN[2]	-	HD38666	09V	0.02	0.20

Photometry is from : [a]Hog et al.(2000); [b]Reed(1998); [c]Kozok (1985a); [d] Gauba et al.(2003)

Spectral types of the hot post-AGB candidates are from Parthasarathy et al. (2000a) except

[1]Simbad database; [2]Acker et al.(1992)

Table 3.4b: Hot post-AGB candidates showing variation in the UV

IRAS	V mag	(B−V) obs.	E(B−V) I.S.	E(B−V) (2200Å)	Sp. Type Optical	E(B−V) total	Standard star	Sp.Type std. star	E(B−V) std. star	E(B−V) C.S.
16206-5956	9.76[a]	0.31[a]	0.22	0.13	A0Ia[1]	0.29	HD21389	A0Ia	0.79	0.54 (21/07/88)
										0.24 (12/03/94)
18062+2410	11.54[b]	0.05[b]	0.11	0.08	B1I[2]	0.24	-	-	-	0.03 (21/04/92)
										0.30 (12/09/95)

Photometry is from : [a]Reed(1998); [b]Arkhipova et al.(1999)

Spectral types are from : [1]Schild et al.(1983); [2]Parthasarathy et al. (2000b)

3.3.3 Stars with circumstellar extinction

The UV(IUE) spectra of 10 stars (IRAS13266-5551 (CPD-55 5588), IRAS14331-6435 (Hen3-1013), IRAS16202-5956 (SAO 243756), IRAS17074-1845 (Hen3-1347), IRAS17311-4924 (Hen3-1428), IRAS18023-3409 (LSS 4634), IRAS18062+2410 (SAO 85766), IRAS18371-3159 (LSE 63), IRAS22023+5249 (LSIII +5224), IRAS22495+5134 (LSIII +5142)), dereddened using the 2200Å feature in the UV, showed considerably reddened continua in comparison with the dereddened spectra of standard stars of similar optical spectral types (Figs. 3.3, 3.5 and 3.6). Comparing the interstellar extinction estimates from the 2200Å feature with the total extinction ($E(B-V)_{total}$) towards these stars, we find that these stars have considerable UV deficiency and circumstellar extinction. The hot central star of the bipolar proto-planetary nebula (PPN), IRAS17423-1755 (Hen3-1475) was not detected in a 35 minute exposure with the SWP camera. This may be due to obscuration of the central star by a dusty disk. HST WFPC2 images of the object showed the presence of a dusty torus with a spatial extent of 2″ (Borkowski et al., 1997).

3.3.3.1 Modelling the circumstellar extinction

To account for the observed UV deficiency in the 10 hot post-AGB candidates mentioned in Sec. 3.3.3 and to understand the shape of the UV continuum in these stars, we investigated the circumstellar extinction law in these cases. Waters et al. (1989) modelled the circumstellar extinction in the case of the post-AGB star, HR4049. We followed the same procedure here.

We plotted the logarithmic difference between the dereddened UV flux of a hot post-AGB candidate (normalised to its V-band flux) and the dereddened UV flux of the corresponding standard star (normalised to its V-band flux), i.e.
$\Delta = \log(f_\lambda/f_v)_{star} - \log(f_\lambda/f_v)_{standard}$ Vs. λ^{-1}.
Fig. 3.4 shows the plot of the logarithmic flux deficiency due to circumstellar dust from 3.2 to 8 μ^{-1} for the 10 stars. Best fit lines were obtained by minimising the chi-square error statistic. Eg., in the case of IRAS17311-4924 (Hen3-1428), we obtained, $\Delta = 0.07 - 0.10\lambda^{-1}$. To derive the circumstellar extinction ($E(B-V)_{C.S.}$) in

magnitudes (Tables 3.4a and b) Δ had to be multiplied by -2.5 and $\lambda = 0.44\mu$ was used.

For IRAS22023+5249 (LSIII +5224), only a B spectral type is listed in literature. We compared the spectrum of this star with that of a B2-supergiant standard star. IRAS22495+5134 (LSIII +5142) was detected as a PN with an angular extent of 4″(Acker et al., 1992) Central stars of PNe have temperatures in excess of $\sim$ 30000K corresponding to spectral types of O9 or hotter. We compared the UV(IUE) spectra of this star with a standard O9V star (HD38666).

For each of the 10 hot post-AGB candidates we found that the circumstellar extinction varies as λ^{-1} (Fig. 3.4). The derived $E(B-V)_{C.S.}$ values in Table 3.4a account well for the difference between the total and the interstellar extinction (from the 2200Å feature) values. $E(B-V)_{C.S.}$ values in Table 3.4b are in excess of the difference between $E(B-V)_{total}$ and the interstellar extinction from 2200Å . This may be because of the variable nature of these stars and because the V and (B−V) magnitudes at each epoch of the IUE observations are not known. Mean V and (B−V) magnitudes from literature have been used for each of these two stars (see Sec. 3.3.3.2 below).

3.3.3.2 Variations in the UV(IUE) spectra of IRAS16206-5956 (SAO 243756) and IRAS 18062+2410 (SAO 85766)

IRAS 16206-5956 was found to be variable in the UV (Fig. 3.1). The spectrum of the star has changed from 21 July 1988 to 12 March 1994 and from 12 March 1994 to 28 April 1994 suggesting both long term and short term variability. The maximum flux in the UV was observed on 12 March 1994. Schild et al (1983) found it to be variable in the optical with ΔV=0.13. Since the V magnitudes of the star at the epochs of the UV(IUE) observations are not known, we used a mean V magnitude (=9.76) from the photometric and spectroscopic database for Stephenson-Sanduleak Luminous Stars in the Southern Milky Way (Reed, 1998). Its spectral type in literature is listed as A3Iabe (Humphreys, 1975, Parthasarathy et al., 2000a) and A0Iae (Schild et al. 1983, Garrison et al., 1977). Oudmaijer (1996) listed it as B8Ia, citing the Simbad

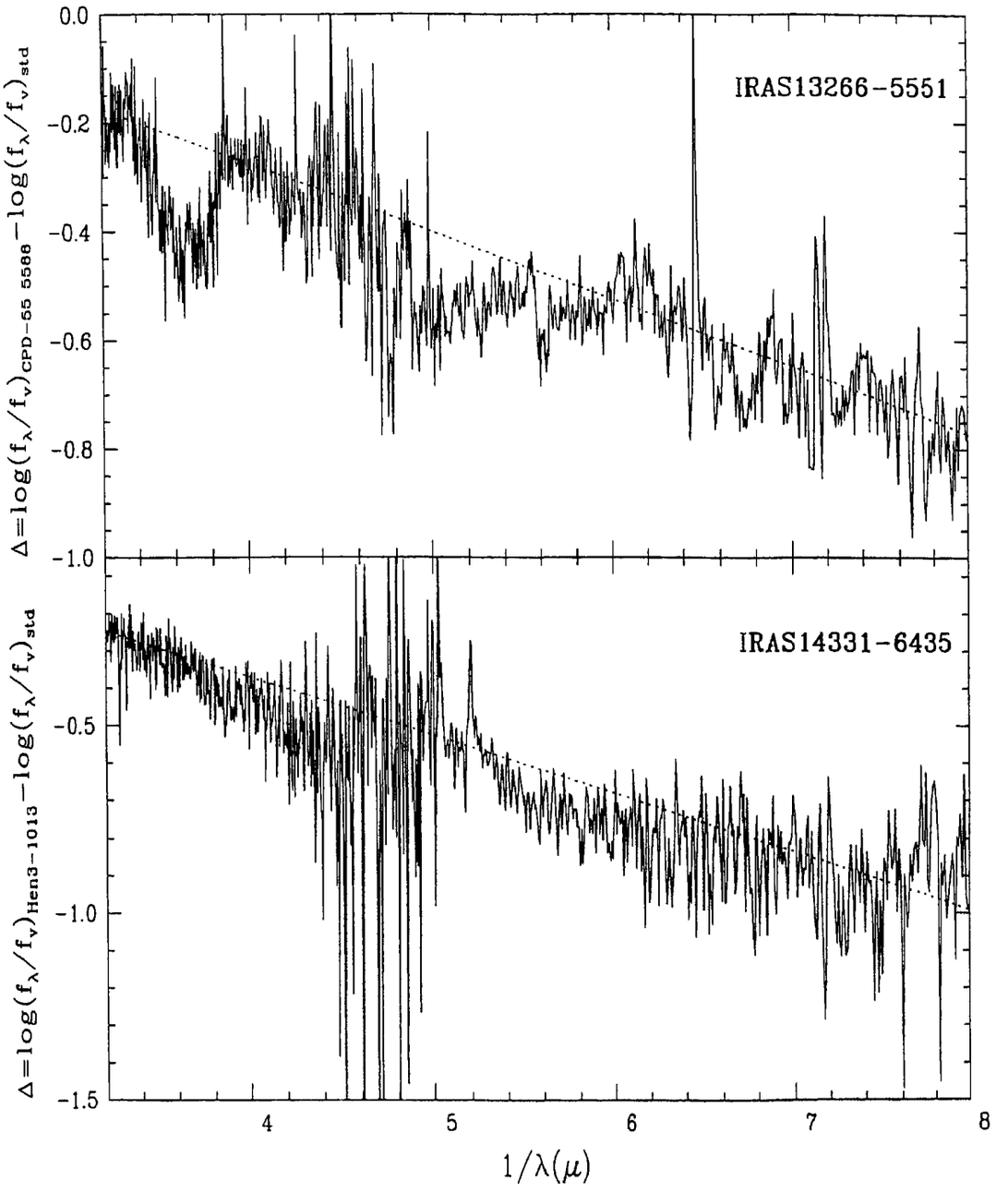

Figure 3.4: 10 hot post-AGB candidates showed a pronounced UV deficiency when compared with standard stars of similar optical spectral types. Here, we have plotted the logarithmic flux deficiency of these stars in the UV from 3.2 to 8 μ^{-1}. The straight line fits are obtained by minimising the chi-square statistic. We find that the flux deficiency in the UV is proportional to λ^{-1}. The bump at $\sim 3.7\mu^{-1}$ in the plot of IRAS13266-5551 is due to the saturated LWP spectrum of the star. This region was not used in obtaining a fit. Similarly, for IRAS18023-3409, the LWP spectrum appears to have saturation effects. For IRAS18371-3159, the bump from ~ 5 to $5.6\mu^{-1}$ is observed because of spurious broad absorption features from 1800Å to 1950Å in the SWP spectrum of the star.

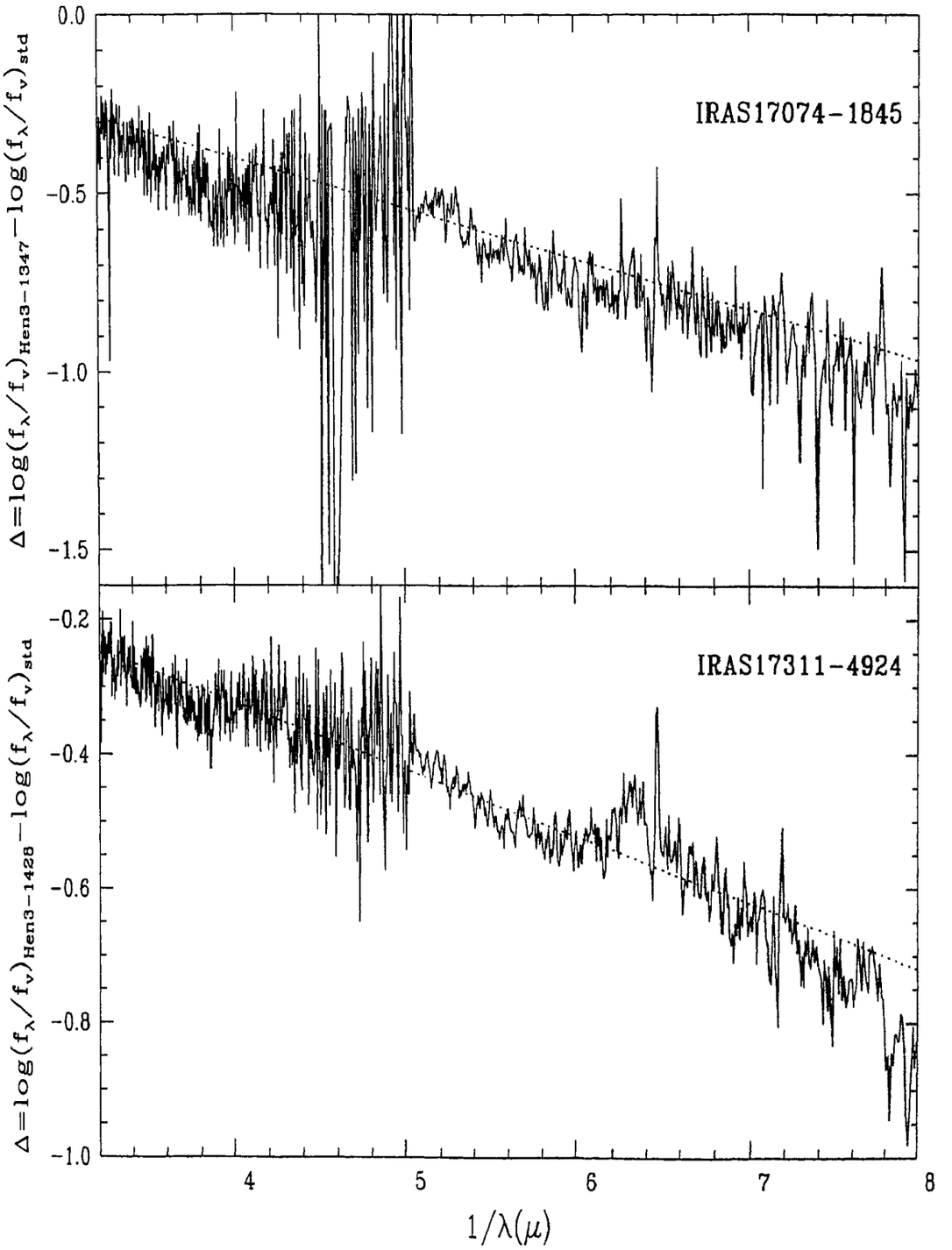

Figure 3.4: contd...

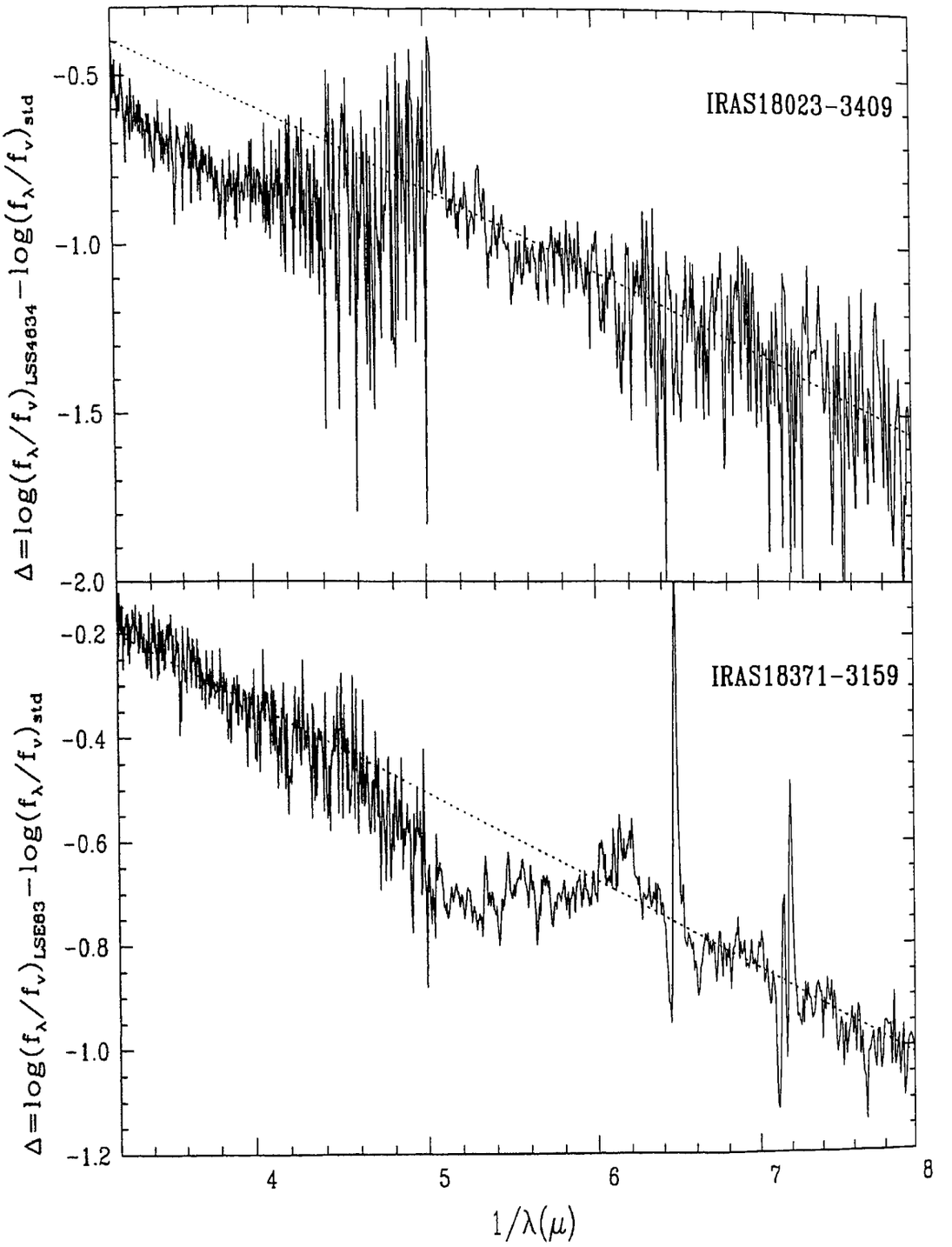

Figure 3.4: contd...

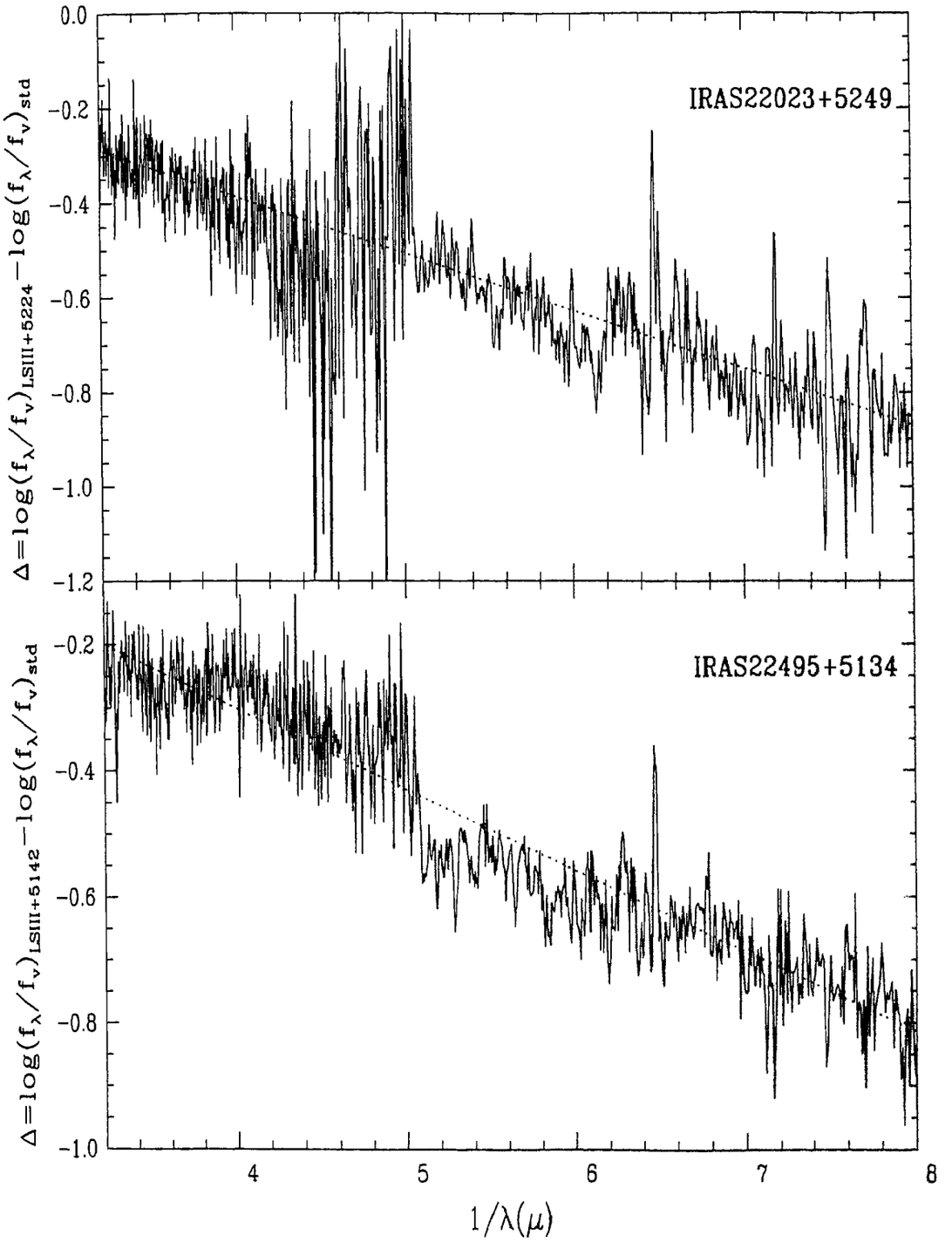

Figure 3.4: contd...

database. However, we could not find a reference for the same. We compared the dereddened IUE spectra of the star at different epochs with the dereddened spectra of A3Ib (HD104035) and A0Ia (HD21389) standard stars (Fig. 3.5a). A match could not be obtained in either case. Finally, we adopted the A0Ia standard star (HD21389) and modelled the circumstellar extinction in the case of SAO 243756 (as outlined in Sec. 3.3.3.1) for the spectra taken on 12 March 1994 (maximum observed IUE flux) and 21 July 1988 (minimum observed IUE flux). The circumstellar extinction was found to be linear in λ^{-1} at both epochs (Fig. 3.5b, Table 3.4b).

The UV flux from IRAS18062+2410 has decreased in Sept. 1995, compared to the flux from the hot central star in April, 1992 (Fig. 3.1). From an analysis of the high resolution optical spectra of the star, Parthasarathy et al. (2000b) and Mooney et al. (2002), found it to be metal-poor ([M/H] ~ -0.6). Since there are no hot (OB-spectral types), metal-poor standard stars in the UV, we compared the UV spectrum of this star with a Kurucz model closest to the effective temperature, gravity and metallicity of the star in the optical (Parthasarathy et al. 2000b, Mooney et al., 2002) We adopted T_{eff}=23000K, log g=3.0 and [M/H]=-0.5 (Fig. 3.6a). Arkhipova et al. (1999, 2000) found that it shows irregular rapid light variations in the optical with an amplitude of upto $0\overset{m}{.}3$. in V. We adopted mean V = $11\overset{m}{.}54$ (Arkhipova et al., 1999). Following the prescription in Sec. 3.3.3.1, we find that the circumstellar extinction varies as λ^{-1} (Fig. 3.6b, Table 3.4b) and has increased in magnitude from 1992 to 1995.

3.3.4 Central star parameters and energy budget

For the 3 hot post-AGB candidates with negligible circumstellar extinction, IRAS17203-1534, IRAS17460-3114 (SAO 209306) and IRAS18379-1707 (LSS 5112), we modelled the spectra using solar metallicity Kurucz (1994) model atmospheres (Fig. 3.7) and derived the effective temperatures and gravities of these stars. The V-band fluxes of the stars were corrected for extinction assuming the normal interstellar extinction law, i.e. $A_v = 3.1 \times E(B-V)_{2200\mathring{A}}$ (see eg. Seaton, 1979). The stellar flux distributions normalised to the corrected V-band flux of each star were compared with

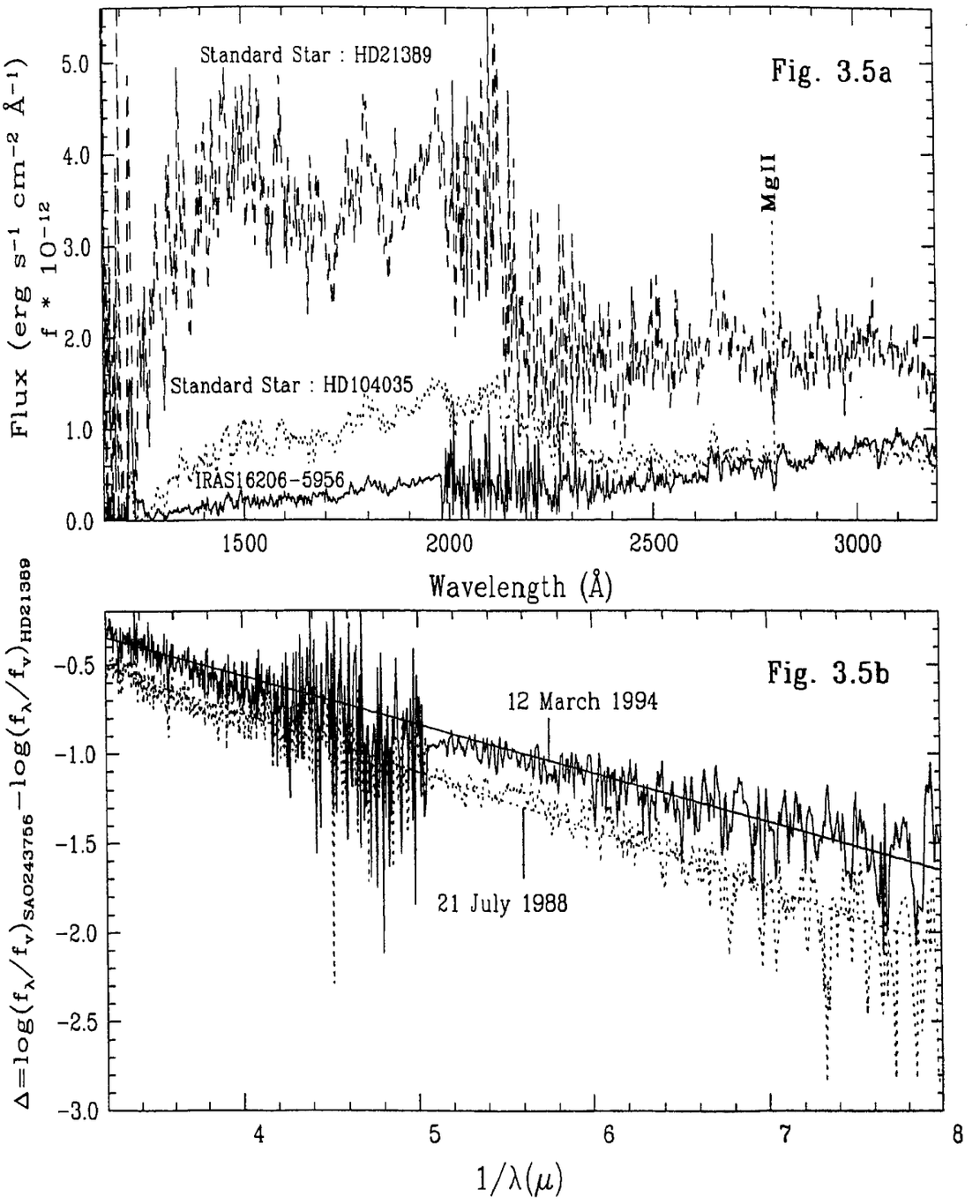

Figure 3.5: IRAS16206-5956 (SAO243756) and the standard A3Ib (HD104035) and A0Ia (HD166937) stars were dereddened using the 2200Å feature in the UV. Fig. 3.5a shows the dereddened 12 March 1994 spectrum of SAO 243756 (solid line) alongwith the dereddened spectra of the standard A0Ia (dash line) and A3Ib stars (dotted line). SAO 243756 is fainter in the spectrum taken on 21 July 1988 (ref. Fig. 3.1). Adopting the A0Ia standard star, Fig. 3.5b shows the modelled circumstellar extinction for the spectrum on 12 March 1994 (solid line) and 21 July 1988 (dotted line) respectively.

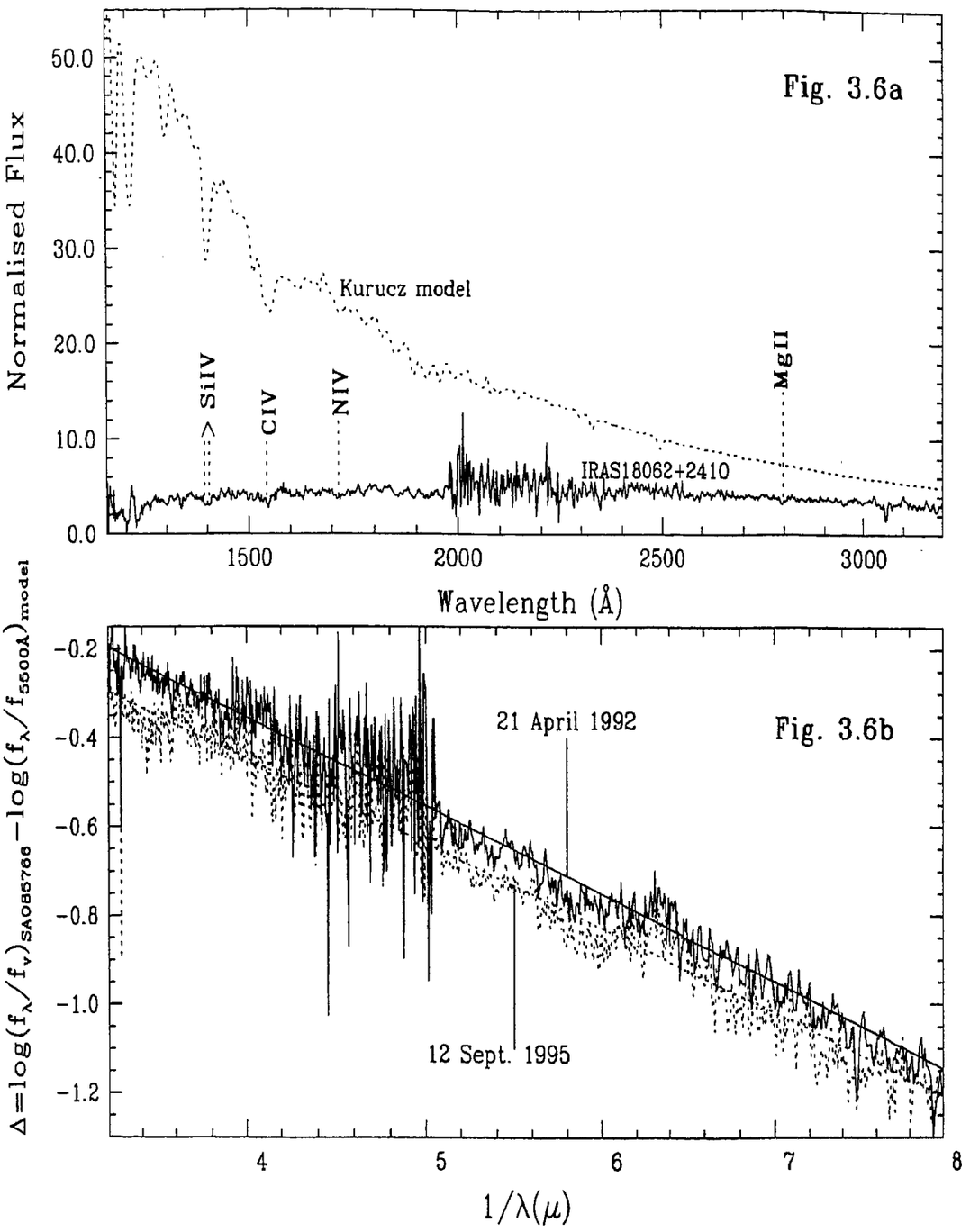

Figure 3.6: IRAS18062+2410 (SAO 85766) was dereddened using the 2200Å feature in the UV. Fig. 3.6a shows the dereddened 1992 spectrum of SAO 85766 normalised to its V-band flux (solid line) alongwith Kurucz model (dotted line) of T_{eff}=23000K, log g=3.0, [M/H]=−0.5 normalised to the flux at 5500Å . SAO 85766 has become fainter in the 1995 spectrum of the star. Fig. 3.6b shows the modelled circumstellar extinction for 1992 (solid line) and 1995 (dotted line).

Kurucz models normalised to the respective model's flux at 5500Å . Log g in the case of the O8III star, IRAS17460-3114 (SAO 209206) was estimated to be 4.0. This value is uncertain due to the non-availability of Kurucz models of lower gravity at the high temperature (T_{eff}=35000K) of the star. The star may also be slightly metal deficient as discussed in Sec. 3.3.1. For the remaining stars, we obtained the effective temperatures and gravities based on their optical spectral types (Lang, 1992). Table 3.5 lists the adopted T_{eff} and log g values. The T_{eff} and log g values estimated from the optical spectral types of the stars may be uncertain by $\sim \pm$ 1000K and $\pm$ 1.0 respectively. High resolution optical spectra of these stars are required for an accurate determination of T_{eff} and log g. The stars were placed on Schönberber's (1983, 1987) post-AGB evolutionary tracks for core masses (M_c) of 0.546, 0.565, 0.598 and 0.644 $M_{\odot}$ (Fig. 3.8).

The far-IR flux distributions of the hot post-AGB candidates must necessarily be due to flux from the hot central stars absorbed and re-radiated by the cold circumstellar dust envelopes which are a remnant of mass-loss on the AGB phase of the star. Hence, the integrated far-IR flux (F_{fir}) must be comparable to or less than the integrated stellar flux (F_{star}). We estimated F_{fir} from the 12μ to 100μ IRAS flux distributions for the stars. The integrated stellar flux (F_{star}) from 1150Å to 5500Å was estimated by combining the IUE spectra with the U,B,V magnitudes of the stars from literature. The IUE spectra and the U,B,V magnitudes were corrected for interstellar extinction derived from the 2200Å feature. IRAS17423-1755 was not detected in the UV. Its U,B,V,R,I magnitudes (Gauba et al., 2003) were corrected for interstellar extinction using the standard extinction law (Rieke & Lebofsky, 1985) and the integrated stellar flux from 3650Å (U-band) to 9000Å (I-band) was estimated. In the three cases with negligible circumstellar extinction (IRAS 17203-1534, IRAS17460-3114 and IRAS18379-1707), F_{fir} was comparable to or significantly less than F_{star}. In contrast stars with circumstellar extinction in the UV, eg. IRAS14331-6435, IRAS17074-1845, IRAS17311-4924, IRAS17423-1755, IRAS18062+2410 and IRAS22023+5249) showed a high ratio of F_{fir}/F_{star} indicating partial obscuration of the central stars. These stars may have dusty circumstellar disks.

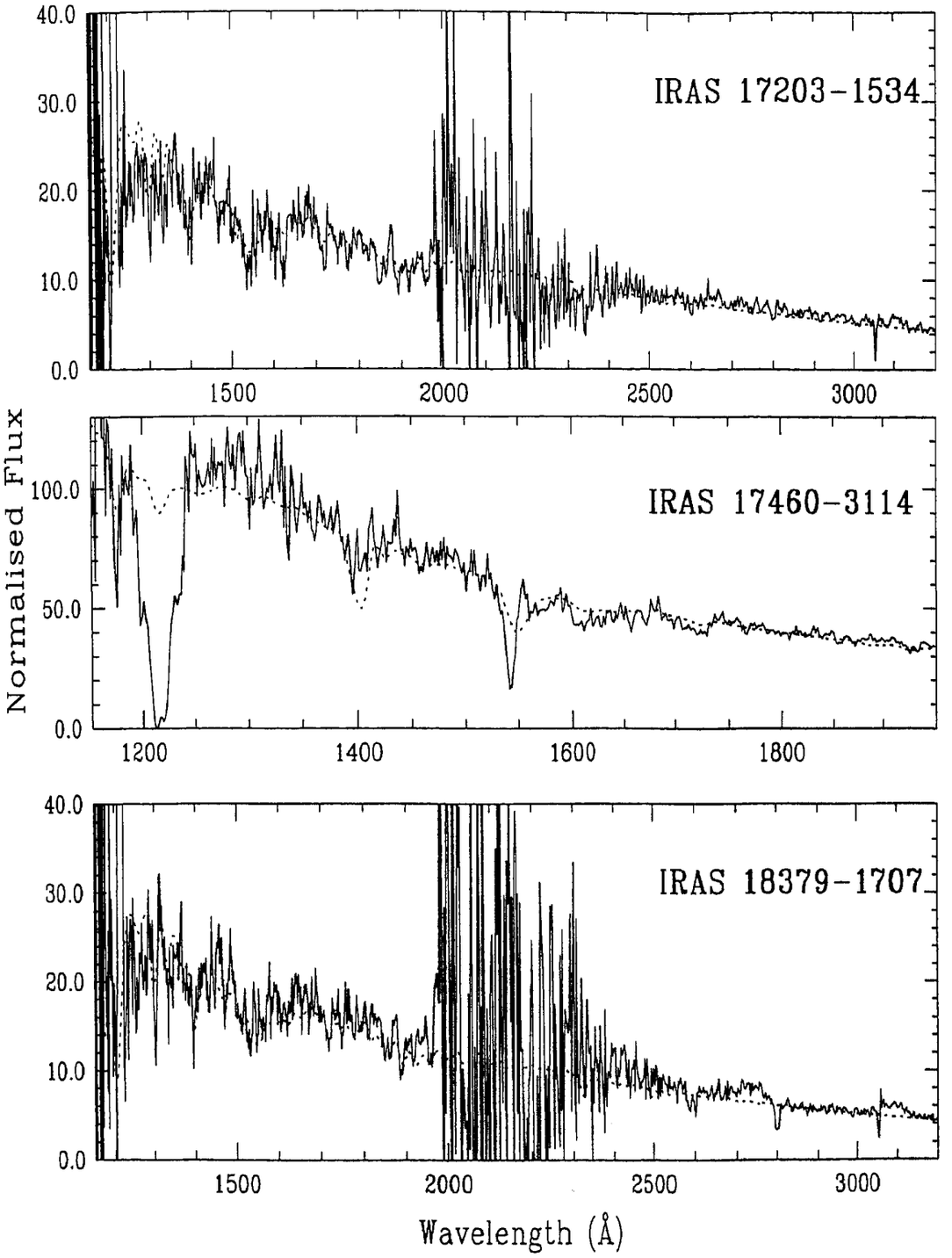

Figure 3.7: The dereddened UV(IUE) spectra of hot post-AGB candidates with negligible circumstellar extinction (solid line), normalised to their V-band fluxes are plotted alongwith solar metallicity Kurucz (1994) model spectra (dotted line), normalised to each model's flux at 5500Å .

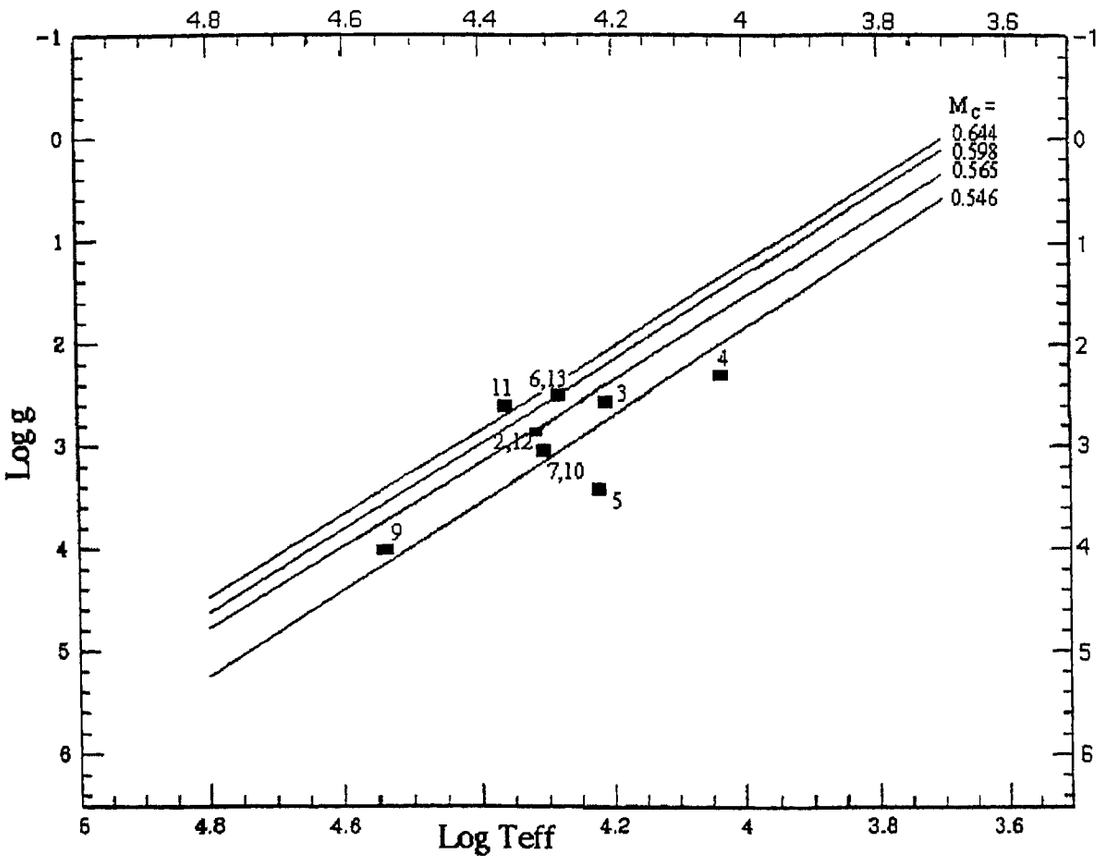

Figure 3.8: Positions of the hot post-AGB candidates on the Log g–Log T_{eff} diagram showing the post-AGB evolutionary tracks of Schönberner (1983, 1987) for core masses of 0.546, 0.565, 0.598 and $0.644 M_{\odot}$

Table 3.5: Central star parameters and Energy budget

Star No.	IRAS	T_{eff}(K)	log g	F_{fir} $X10^{-12}$ Wm^{-2}	F_{star} $X10^{-12}$ Wm^{-2}	F_{fir}/F_{star}	Wind velocity kms^{-1}
1.	12584-4837	-	-	10.90	6.07	1.79	-3769
2.	13266-5551	20800	2.8	5.41	9.29	0.58	-1821
3.	14331-6435	16200	2.6	15.40	4.50	3.42	-
4.	16206-5956	11200	2.3	1.73	2.61 (21/07/88)	0.66	-
					2.97 (12/03/94)	0.58	-
5.	17074-1845	17100	3.4	1.67	1.44	1.16	-
6.	17203-1534[1]	19000±1000	2.5±0.5	1.51	8.86	0.17	-2402
7.	17311-4924	20300	3.0	21.80	4.01	5.44	-1066
8.	17423-1755	-	-	6.41	1.17	5.48	-
9.	17460-3114[1]	35000±2500	4.0±1.0	4.95	876.8	0.006	-1463
10.	18023-3409	20300	3.0	0.58	1.13	0.51	-2048
11.	18062+2410[2]	23000	2.6	2.90	1.64 (21/04/92)	1.77	-
					1.33 (12/09/95)	2.18	-
12.	18371-3159	20800	2.9	0.93	2.17	0.43	-
13.	18379-1707[1]	19000±1000	2.5±0.5	3.20	16.96	0.19	-
14.	22023+5249	-	-	3.45	1.14	3.03	-3978
15.	22495+5134	-	-	1.74	3.72	0.47	-

[1] The effective temperatures and gravities were estimated using solar metallicity Kurucz (1994) models.

[2] Effective temperature and gravity are from Mooney et al. (2002)

3.3.5 Terminal wind velocity

The wavelength at which the shortward edge of the CIV (or NV) absorption profile intersects the stellar continuum is usually used to estimate the terminal wind velocities (v_∞) of hot stars from low resolution IUE spectra. However, this value is usually an upper limit to the true v_∞. Alternatively, the difference between the absorption and emission line centers (Δv) are used to estimate v_∞ from low resolution IUE spectra (Prinja, 1994). But high dispersion studies (see eg. Perinotto et al., 1982) have shown that Δv is less than v_∞.

Considerable circumstellar extinction in 10 of the 15 stars discussed in this chapter, has significantly distorted the continuum flux distributions and line intensities of the CIV profiles. Hence, the point where the blue absorption edge of the CIV profile

intersects the UV continuum is not reliable. These factors also contribute to the fact that the CIV P-Cygni profiles are not clearly observed in the low resolution spectra of these stars. The emission peaks may be too weak or lost in the reddened continuum. Hence it is not possible to estimate v_∞ from the shortward edge of the CIV absorption profile or from the difference between the absorption and emission line centers.

The CIV resonance doublet (1548Å , 1550Å) is not resolved in the IUE low resolution spectra. Stellar wind may be assumed to be absent in a B0V star. We measured the absorption minimum of the CIV feature in the UV(IUE) spectrum of a B0V standard star, HD36512 (1548.4Å) from the atlas by Heck et al. (1984). The difference between this wavelength and the absorption minima of the CIV feature in the IUE spectra of our hot post-AGB candidates was used to estimate the wind velocities in these stars. If instead, we had used the mean laboratory wavelength of the CIV resonance doublet (1549Å), the estimated terminal wind velocites would have been greater by 116kms^{-1}. The NV resonance doublet (1238Å , 1242Å) is also unresolved in low resolution IUE spectra. Moreover, the NV feature is often contaminated by geocoronal Lyman α. From the standard star atlas (Heck et al., 1984) we were unable to find a star in which the NV line is distinguishable from Lyman α and unaffected by stellar wind. Hence, in the case of IRAS12584-4837, we estimated the wind velocity from the difference between the NV absorption minimum and the mean laboratory wavelength of the line (1240Å). The estimated wind velocities are listed in Table 3.5. No shift was observed in the case of IRAS17074-1845, IRAS18062+2410, IRAS18379-1707 and IRAS22495+5134. CIV (or NV) lines were not observed in IRAS14331-6435 and IRAS16206-5958. The SiIV (1394Å) absorption line in IRAS14331-6435 did not show a wavelength shift due to stellar wind. For low resolution IUE spectra, the FWHM of the instrumental width is 5Å (Castella & Barbero, 1983). Assuming a 3Å measurement error in estimating the blue shift of the lines from our low resolution spectra, would correspond to an error of $\sim$ 580 kms^{-1} and 726kms^{-1} in the estimate of wind velocites from CIV and NV respectively. However, our terminal wind velocities exceeded this error estimate. So, we may conclude that although a crude estimate is obtained of the terminal wind velocities, it nevertheless indicates the presence of stellar winds and post-AGB mass-loss in some of these stars.

3.4 Notes on individual objects :

#IRAS 12584-4837 (Hen3-847)

Henize (1976) identified it as an Hα emission line star. Based on its far infrared flux distribution and high galactic latitude (b=+13.95°) Parthasarathy(1993a) classified it as a post-AGB star. It was found to be variable in the optical (Kazarovets et al., 2000, de Winter et al., 2001). The Hipparchos magnitudes at maximum and minimum are $10^{m}.52$ and $10^{m}.70$ respectively. Thé et al. (1994) listed it as a candidate Herbig Ae/Be star. The presence of HeII line (1640Å) indicates a very high temperature. The UV spectrum and the presence of several emission lines (Fig. 3.2) suggest that it may be a massive young star. Another possibility is that it may be a luminous blue variable. Photometric monitoring and high resolution spectroscopy may enable us to further understand the evolutionary stage of this star. From the NV profile we estimated a terminal wind velocity of -3769 kms^{-1}.

#IRAS 13266-5551 (CPD-55 5588)

It was classified as a post-AGB star on the basis of its far infrared flux distribution (Parthasarathy, 1993a). From the optical spectra, Parthasarathy et al. (2000a) classified it as B1Ibe. They found the Balmer lines in emission upto Hδ. The LWP spectrum of the star is saturated from 2600Å to 3000Å . The central star has a terminal wind velocity of -1821 kms^{-1}.

#IRAS 14331-6435 (Hen3-1013)

Henize(1976) identified it as an Hα emission line star. It is listed as a Be star in Wackerling (1970). Based on its far infrared flux distribution it was classified as a post-AGB star (Parthasarathy & Pottasch 1989, Parthasarathy 1993a). Assuming a Be spectral type, Kozok (1985b) derived a distance of 1.9 kpc to the star. Loup et al. (1990) detected CO emission in this object and derived an expansion velocity of 15kms^{-1}. They derived a distance of 1.3kpc using the total IR flux in IRAS bands and assuming a post-AGB luminosity of $10^4 L_{\odot}$. Parthasarathy et al. (2000a) found it to be a B3 supergiant (B3Ie) with Hβ in emission and Hγ filled in. Modelling yielded a circumstellar extinction value of $0^{m}.26$. The F_{fir}/F_{star} (= 3.42) ratio also suggests obscuration of the hot central star.

#IRAS 16206-5956 (SAO 243756)

On the basis of IRAS data, high galactic latitude, and supergiant spectrum, Parthasarathy (1993a) considered it to be a post-AGB star. Hα and Hβ were detected in emission (Oudmaijer 1996, Parthasarathy et al., 2000a). The variation in the UV may be attributed to variable circumstellar extinction.

#IRAS 17074-1845 (= Hen3-1347)

Henize (1976) identified it as an Hα emission line object. It was classified as a hot post-AGB star on the basis of its high galactic latitude, far-IR colors similar to PNe and Be spectral type (Parthasarathy, 1993a). It was classified as a B3IIIe star (Parthasarathy et al., 2000a).

#IRAS 17203-1534

On the basis of its high galactic latitude, early spectral type (B1IIIpe), Balmer line emission (Hβ) and far-IR colors similar to PNe, Parthasarathy et al. (2000a) classified it as a possible post-AGB star. We found that the UV spectrum closely follows that of a standard B1II star (HD173502). Using solar metallicity Kurucz (1994) models we obtained T_{eff} = 19000 $\pm$ 1000K and log g = 2.5 $\pm$0.5.

#IRAS 17311-4924 (Hen3-1428)

It was classified as a post-AGB star on the basis of its IRAS data (Parthasarathy & Pottasch 1989, Parthasarathy 1993a). Loup et al. (1990) detected CO emission in this object typical for circumstellar shells around evolved objects. They derived a distance of 1.1 kpc and an expansion velocity of 11 kms^{-1}. Nyman et al. (1992) found an expansion velocity of 14.1 kms^{-1} from CO observations similar to that found by Loup et al. (1993). Assuming a Be star, Kozok (1985b) derived a photometric distance of 2.6kpc. Parthasarathy et al. (2000a) classified it as B1IIe. We found no apparent change between the UV(IUE) spectra taken in 1988 and 1993.

#IRAS17423-1755 (= Hen3-1475)

It was found to be a B-type emission line star (Henize, 1976). On the basis of IRAS data, Parthasarathy & Pottasch (1989) first classified it as a hot post-AGB star. It is a bipolar PPN (Bobrowsky et al. 1995, Riera et al. 1995, Borkowski et al., 1997) with wind velocities greater than 1000 km s^{-1} (Sánchez Contreras &

Sahai, 2001, Borkowski & Harrington, 2001). Borkowski et al. (1997) concluded that Hen3-1475 is a point symmetric nebula. HST images of the object revealed outflows perpendicular to the dusty torus obscuring the hot central star. From the spectral energy distribution, Gauba et al. (2003) detected a hot dust component ($\sim$ 1000K) indicating cirumstellar dust close to the central star as a result of ongoing post-AGB mass-loss. The non detection of the B-type central star in the SWP spectrum (35 minutes exposure) may be due to obscuration of the star by the dusty torus seen in the HST image. The F_{fir}/F_{star} (= 5.48) ratio also suggests obscuration of the hot central star by the dusty disk.

#IRAS 17460-3114 (SAO 209306)

It shows far-IR colors similar to PNe (Parthasarathy, 1993a). Based on low resolution spectra, it was classified as O8III (Parthasarathy et al., 2000a). In the UV(IUE) spectrum of the star, CIV (1550Å) shows a P Cygni profile with a strong absorption and weak emission component. The NV (1240Å) feature is contaminated by Lyman α.

#IRAS 18023-3409 (LSS 4634)

It is listed in the LSS (Luminous stars in the southern Milky Way) catalogue (Stephenson & Sanduleak, 1971) as an OB+ star. Parthasarathy et al.(2000a) found Hβ in emission and Hγ filled in. They classified it as B2IIIe. The UV(IUE) spectrum of the star shows considerable circumstellar extinction ($E(B-V)_{C.S.}$=0.43).

#IRAS 18062+2410 (SAO 85766)

Stephenson(1986) identified it as an Hα emission line star. The star appears to have rapidly evolved in the last 20-30 years (Arkhipova et al. 1999, Parthasarathy et al. 2000b). It was classified as a high galactic latitude, post-AGB star having far-IR colors similar to PNe (Volk and Kwok, 1989, Parthasarathy, 1993a). According to the HDE Catalog, its spectral type in 1940 was A5. The UV colors of this star listed in the Catalogue of Stellar Ultraviolet Fluxes (Thompson et al., 1978) and based on observations with the Ultraviolet Sky Survey Telescope (S2/68) onboard the ESRO satellite TD-1 indicated that in 1973 its spectral type was still A5I (Parthasarathy et al., 2000b). However, the spectral energy distribution of this star obtained in

1985-87 indicated a Be spectral type. (Downes and Keyes, 1988). An analysis of its high resolution spectra, revealed the underabundance of carbon and metals, high radial velocity and the presence of low excitation nebular emission lines (Arkhipova et al. 1999, Parthasarathy et al., 2000b). On the post-AGB evolutionary tracks of Schönberner (1983, 1987), it appears to be evolving into the PN phase with $M_c \simeq 0.644 M_\odot$. Variable circumstellar extinction, which may be due to a dusty torus in motion around the hot central star may explain the observed variations in the UV.

#IRAS 18371-3159 (LSE 63)

It is listed as OB+ in the extension to the Case-Hamburg OB-star surveys (Drilling & Bergeron 1995). Parthasarathy et al. (2000) classified it as B1Iabe. Preite-Martinez (1988) classified it as a possible new PN and estimated a distance of 2.4 kpc to the star. On the post-AGB evolutionary tracks of Schönberner (Fig. 3.8), it appears to be evolving into the PN stage with $M_c = 0.565 M_\odot$.

#IRAS 18379-1707 (LSS 5112)

Parthasarathy et al. (2000) classified it as B1IIIpe. The photometry of the star is from Reed (1998). IRAS colors similar to PNe, high galactic latitude, early B-type giant spectra in the UV and optical and the presence of CII (1335Å), SiIV (1394,1403Å), CIV(1550Å), NIV (1718Å) and MgII (2800) lines in the IUE spectrum support its classification as a hot post-AGB star. Using solar metallicity Kurucz (1994) models we determined T_{eff}=19000 $\pm$ 1000K and log g = 2.5 $\pm$ 0.5.

#IRAS 22023+5249 (LSIII +5224)

Its IRAS colors were found to be similar to PNe and Parthasarathy et al. (2001b) classified it as a hot post-AGB star. The photometry of the star was obtained from the Tycho-2 Catalogue (Hog et al., 2000). It is listed in Wackerling's (1970) catalog of early-type emission-line stars. The B spectral type of the star was obtained from the Simbad database. We compared the UV spectrum of this star with that of a B2I standard star (HD41117) and found it to be similar. The F_{fir}/F_{star} (=3.03) ratio suggests obscuration of the hot central star and lends support to the modelled circumstellar extinction value of $0^m.44$. There was no difference between the 1993 and 1995 UV(IUE) spectra.

#IRAS 22495+5134 (LSIII +5142)

It is classified as a PN in the Strasbourg-ESO catalogue of Galactic planetary nebulae (Acker et al., 1992). Acker et al. (1992) and Tylenda & Stasińska (1994) reported an angular diameter of 4″, expansion velocity of 10 kms^{-1} and V=12.08. The V magnitude from the Tycho-2 Catalogue (Hog et al., 2000) is $11^m.78$. Handler (1999) found it to be variable with amplitude variations of $0^m.3$ in the Johnson V band. While the long term variations (several days) were non periodic, the short term variations were quasi-periodic with time scales of either 8.9 or 14.3 hours. Variations in the stellar mass-loss coupled with stellar pulsation may explain the observed long and short-term variability. From the Hipparchos catalog, the Hipparchos magnitudes at maximum and minimum are $12^m.11$ and $12^m.47$ respectively. From the logarithmic extinction at Hβ using radio flux at 5Gz (c=0.41), Kaler(1983) obtained E(B-V)=$0^m.28$. Using the Hα to Hβ ratio (c=0.55), Tylenda et al. (1992) obtained E(B-V)=0.37. These values are in good agreement with the interstellar E(B-V)=0.33 derived from the 2200Å feature in the UV.

3.5 Discussion & conclusions

We analysed the UV(IUE) spectra of 15 hot post-AGB candidates. In 11 cases (IRAS13266-5551 (CPD-55 5588), IRAS14331-6435 (Hen3-1013), IRAS16206-5956 (SAO 243756), IRAS17074-1845 (Hen3-1347), IRAS17311-4924 (Hen3-1428), IRAS17423-1755 (Hen3-1475), IRAS18023-3409 (LSS 4634), IRAS18062+2410 (SAO 85766), IRAS18371-3159 (LSE 63), IRAS22023+5249 (LSIII +5224) and IRAS22495+5134 (LSIII +5142)), the UV spectra revealed obscuration of the hot central stars due to circumstellar dust. While IRAS17423-1755 (Hen3-1475) was not detected at all in a 35 minute exposure, the UV continua of the remaining 10 stars were found to be considerably reddened. We found that the circumstellar extinction in these 10 stars varies linearly as λ^{-1}. A λ^{-1} law for the circumstellar extinction was also found in the case of the post-AGB star, HR4049 (Waters et al., 1989, Monier & Parthasarathy, 1999). In the context of Mie scattering (Spitzer, 1978), linear extinction arises from dust grains small compared to the wavelength of light. The shortest

wavelength of light at which the extinction is linear can give an estimate of the size of the smallest grains in the circumstellar environment of these stars ($\lambda = 2\pi a$, where, a is the radius of the dust grain). However our IUE SWP observations are limited to 1150Å ($\lambda^{-1} \approx 8.7\mu^{-1}$). Shortward of 1300Å the spectra are noisy and often contaminated by Lyman α. Taking 1300Å as the shortest observed wavelength at which the extinction is linear in λ^{-1}, we may infer an upper limit of $a \approx 200$Å for the radii of the small grains. Waters et al. (1989) speculate that the destruction of these grains in the vicinity of the hot central stars of PPNe and PNe may give rise to smaller grains and polyaromatic hydrocarbons (PAHs). PAH features at 8.2, 8.6 and 11.3 μ have been detected in the circumstellar environment of several post-AGB stars, PPNe and PNe (see eg. Beintema et al., 1996). It would be interesting to study the infrared spectra of our hot post-AGB candidates to know more about the chemical compositions (carbon-rich or oxygen-rich nature) of the dust grains and the evolution of these grains in the circumstellar environment of these stars. Variation of IRAS16206-5956 (SAO 243756) and IRAS18062+2410 (SAO 85766) in the UV may be due to stellar pulsations and/or due to variable circumstellar extinction similar to that observed in the case of HR4049 (Waters et al., 1989, Monier & Parthasarathy, 1999). Significant circumstellar extinction was not observed in the case of IRAS17203-1534, IRAS17460-3114 (SAO 209306) and IRAS18379-1707 (LSS 5112). The effective temperatures and gravities of these three stars were estimated using Kurucz model atmospheres.

$F_{fir}/F_{star} >> 1.0$ in the case of IRAS14331-6435 (Hen3-1013), IRAS17311-4924 (Hen3-1428), IRAS17423-1755 (Hen3-1475), IRAS18062+2410 (SAO 85766) and IRAS22023+5249 (LSIII +5224) indicates the presence of dusty disks around these stars. From the UV(IUE) spectra we found that 7 (IRAS12584-4837, IRAS13266-5551 (CPD-55 5588), IRAS17203-1534, IRAS17311-4924 (Hen3-1428), IRAS17460-3114 (SAO 209306), IRAS18023-3409 (LSS 4634) and IRAS22023+5249 (LSIII +5224)) of the 15 hot post-AGB candidates have stellar wind velocities in excess of 1000kms^{-1} indicating post-AGB mass-loss.

Acknowledgements : Based on observations obtained with the International Ultraviolet Explorer (IUE), retrieved from the Multimission Archive at STScI

Chapter 4

Circumstellar dust shells of hot post-AGB stars

Abstract

Using a radiative transfer code (DUSTY) parameters of the circumstellar dust shells of 15 hot post-AGB stars have been derived. Combining the optical, near and far-infrared (ISO, IRAS) data of the stars, we have reconstructed their spectral energy distributions (SEDs) and estimated the dust temperatures, mass loss rates, expansion velocites, angular radii of the inner boundary of the dust envelopes, dynamical ages from the tip of the AGB and the distances to these stars. The mass loss rates (10^{-6} – $10^{-5}$$M_{\odot}yr^{-1}$) and expansion velocities (6 – 26 kms^{-1}) are intermediate between stars at the tip of the AGB and the PN phase. The derived dynamical ages ranging from a few hundred to a few thousand years are consistent with the evolutionary models of Schönberner & Blöcker (1993). We have also studied the ISO spectra of 7 of these stars. Amorphous and crystalline silicate features were observed in IRAS14331-6435 (Hen3-1013), IRAS18062+2410 (SAO85766) and IRAS22023+5249 (LSIII +5224) indicating oxygen-rich circumstellar dust shells. The presence of unidentified infrared (UIR) band at 7.7μ, SiC emission at 11.5μ and the "26μ" and "main 30μ" features in the ISO spectrum of IRAS17311-4924 (Hen3-1428)

suggest that the central star may be carbon-rich. The ISO spectrum of IRAS17423-1755 (Hen3-1475) shows a broad absorption feature at 3.1μ due to C_2H_2 and/or HCN which is usually detected in the circumstellar shells of carbon-rich stars.

4.1 Introduction

In the evolution of low and intermediate mass stars (0.8 – 8$M_\odot$), the post-asymptotic giant branch (post-AGB) or protoplanetary nebula (PPN) phase is a transition stage from the tip of the AGB to the planetary nebula (PN) stage (Kwok, 1993). The hot post-AGB stars form an evolutionary link between the cooler G,F,A supergiant post-AGB stars (Parthasarathy & Pottasch, 1986) and the hotter O-B central stars of PNe (Parthasarathy, 1993b).

Analysis of the UV(IUE) spectra of hot post-AGB stars (Gauba & Parthasarathy, 2003b), revealed that in many cases, the hot (OB) central stars of PPNe are partially obscured by circumstellar dust shells. Stars on the AGB and beyond are characterised by severe mass loss (10^{-8} – 10^{-3} $M_\odot$ yr^{-1}) which results in the formation of circumstellar envelopes. The physical mechanisms responsible for the intensive mass loss from AGB stars are not well understood although the most promising mechanism to date involves radiation pressure on the dust grains (Tielens, 1983). While AGB stars appear to have spherically symmetric dust outflows (eg. Habing & Blommaert, 1993), PN tend to have axially symmetric inner regions and spherical outer halos (eg. Schwarz et al., 1992). Inorder to understand the mass loss mechanisms, wind velocities and time scales responsible for the evolution of PNe, we need to study the circumstellar environment of the stage intermediate between the AGB and the PN phase, i.e. the post-AGB/PPN phase. Circumstellar dust shells of some cooler post-AGB stars (eg. Hoogzaad et al., 2002; Hony et al., 2003) and PNe (eg. Siebenmorgen et al., 1994) have been modelled to derive the dust composition, mass loss rates and dynamical ages.

As a consequence of dredge-up of byproducts of helium burning to the surface of stars on the AGB, the oxygen-rich atmospheres of some of these stars may be trans-

formed into carbon-rich atmospheres (see eg. Iben & Renzini, 1983). This change of chemistry would also be reflected in the composition of the dust grains formed in the cirumstellar envelopes of AGB and post-AGB stars. With the resolution and wavelength coverage of the ISO mission (Kessler et al.,1996) the detection of prominent gas and solid state features specific to oxygen-rich and carbon-rich chemistries became possible. Amorphous and crystalline silicate features and crystalline water have been reported in the ISO spectra of some AGB and post-AGB stars and the nebulae surrounding [WC] central stars of PNe (see eg. Waters & Molster, 1999; Hoogzaad et al., 2002). Hrivnak et al. (2000) detected the "21μ" and "30μ" emission features besides the unidentified infrared (UIR) emission bands at 3.3, 6.2, 7.7 and 11.3μ in the ISO spectra of a sample of carbon-rich PPNe.

Bogdanov (2000, 2002) modelled the complete spectral energy distribution (SED) of two hot post-AGB stars, IRAS18062+2410 (SAO85766) and IRAS20462+3416 (LSII+34 26) using radiative transfer codes and derived their mass loss rates, inner radii of the dust envelopes, optical depth of the envelopes and the distances to these stars. We need to study a bigger sample of such stars to understand the evolution of the infrared spectrum as the stars evolve from the cooler post-AGB phase to the hot central stars of PNe. In this chapter, we have used the radiative transfer code, DUSTY (Ivezić et al., 1999) to model the circumstellar dust shells of 15 hot post-AGB stars. Additionally, 7 stars from our list were found to have ISO spectra. We also report the analysis of the ISO spectra of these stars.

4.2 Target Selection

The hot post-AGB stars for this study (Table 4.1) were selected from the papers of Parthasarathy & Pottasch 1989, Parthasarathy, 1993a and Parthasarathy et al., 2000a. High and low resolution optical spectra have confirmed the post-AGB nature of several of these stars, eg. IRAS17119-5926 (Hen3-1357; Parthasarathy et al., 1993c, 1995; Bobrowsky et al., 1998), IRAS18062+2410 (SAO 85766; Parthasarathy et al., 2000b; Mooney et al., 2002; Ryans et al., 2003), IRAS19590-1249 (LSIV-12 111; McCausland et al., 1992; Conlon et al., 1993a, 1993b; Mooney et al., 2002; Ryans et

Table 4.1: Hot post-AGB stars

IRAS	Name	Optical Sp. Type	l	b	IRAS Fluxes (Jy.)			
					12μ	25μ	60μ	100μ
12584-4837	Hen3-847	Be[1]	304.60	+13.95	36.07	48.75	13.04	3.31
13266-5551	-55 5588	B1Ibe	308.30	+6.36	0.76	35.90	35.43	11.66
14331-6435	Hen3-1013	B3Ie	313.89	-4.20	4.04	108.70	70.71	20.61
16206-5956	SAO 243756	A0Ia[2]	326.77	-7.49	0.36L	11.04	12.30	4.83
17203-1534		B1IIIpe	8.55	+11.49	0.32	10.70	6.88	3.37
17311-4924	Hen3-1428	B1IIe	341.41	-9.04	18.34	150.70	58.74	17.78
17423-1755	Hen3-1475	Be	9.36	+5.78	7.05	28.31	63.68	33.43
17460-3114	SAO 209306	O8III	358.42	-1.88	6.26	20.82	12.20	220.40L
18023-3409	LSS 4634	B2IIIe	357.61	-6.31	0.26L	2.94	1.82	25.64L
18062+2410	SAO 85766	B1I[3]	50.67	+19.79	3.98	19.62	2.90	1.00L
18371-3159	LSE 63	B1Iabe	2.92	-11.82	0.25L	6.31	5.16	1.95
18379-1707	LSS 5112	B1IIIpe	16.50	-5.42	1.67	23.76	7.12	3.66L
19590-1249	LSIV-12 111	B1Ibe	29.18	-21.26	0.29:	10.26	6.45	1.77:
22023+5249	LSIII +5224	B[4]	99.30	-1.96	1.02	24.69	14.52	3.93L
22495+5134	LSIII +5142	PN[5]	104.84	-6.77	0.54	12.37	7.18	3.12

A colon : indicates moderate quality IRAS flux, L is for an upper limit.

The spectral types are from Parthasarathy et al. (2000a) except [1]Kazarovets et al. (2000); [2]Schild et al. (1983); [3]Parthasarathy et al. (2000b); [4]Simbad database; [5]Acker et al. (1992)

al., 2003) and IRAS20462+3416 (LSII+34 26; Parthasarathy, 1993b; García-Lario et al., 1997b). The UV(IUE) spectra of some hot post-AGB stars listed in Table 4.1 showed violet shifted P-Cygni profiles of CIV and NV indicating stellar wind and post-AGB mass loss (Gauba & Parthasarathy, 2003b).

4.3 ISO observations

The ISO data archive was searched for spectra of the hot post-AGB stars listed in Table 4.1. Six of the fifteen sources were found to have only SWS (Short Wavelength Spectrometer) spectra while one source, IRAS 17423-1755 (Hen3-1475) had both SWS and LWS (Long Wavelength Spectrometer) spectra. Log of the observations is given

Table 4.2: Log of ISO observations

IRAS	Name	Date of Obs.	Duration of Obs.(s)	TDT[a]	Mode[b]	Speed[c]
14331-6435	Hen3-1013	14 July 1997	3454	60600607	SWS01	3
16206-5956	SAO 243756	6 Sept. 1996	6538	29401311	SWS01	4
17311-4924	Hen3-1428	28 Feb. 1996	1834	10300636	SWS01	2
17423-1755	Hen3-1475	17 March 1997	1140	48700267	SWS01	1
		17 March 1997	800	48700168	LWS01	-
18062+2410	SAO 85766	18 Feb. 1997	1140	46000275	SWS01	1
22023+5249	LSIII +5224	5 Jan. 1997	1140	41600993	SWS01	1
22495+5134	LSIII +5142	5 Jan. 1997	1140	41601295	SWS01	1

[a]TDT number uniquely identifies each ISO observation. [b]SWS observing mode used (see de Graauw et al., 1996). [c]Speed corresponds to the scan speed of observation.

in Table 4.2. ISO SWS spectra have a wavelength coverage from $2.38 - 45.2\mu$. The LWS spectra extend from $43 - 197\mu$.

Our objects were observed in the low resolution (AOT 01) mode of the SWS instrument (de Graauw et al., 1996). A spectrum scanned with SWS contains 12 subspectra, that each consist of two scans, one in the direction of decreasing wavelength ('up' scan) and the other in the direction of increasing wavelength ('down' scan). There are small regions of overlap in the wavelength between the sub-spectra. Each sub-spectrum is recorded by 12 independent detectors.

The LWS observations were carried out in LWS01 mode, covering the full spectral range at a resolution ($\lambda/\Delta\lambda$) of ~ 200. The characteristics of the ISO LWS instrument are described in Clegg et al. (1996) and the calibration of the instrument is described in Swinyard et al. (1996).

4.4 Analysis

In this section we describe the analysis of the ISO spectra and the modelling of the SEDs of the hot post-AGB stars.

4.4.1 ISO Data Analysis

Offline processed ISO SWS01 (OLP version 10.1) and LWS01 (OLP version 10) data were retrieved from the ISO data archive. These were further processed using ISAP (ISO Spectroscopic Analysis Package) version 2.1.

4.4.1.1 SWS

The data analysis using ISAP consisted of extensive bad data removal primarily to minimize the effect of cosmic ray hits. All detectors were compared to identify possible features. For each sub-band, the flux level of the 12 detectors were shifted and brought to a mean value. They were then averaged, using median clipping to discard points that lay more than 2.5σ from the median flux. The spectra were averaged typically to a resolution of of 300, 500, 800 and 1500 for SWS01 data taken with speed 1, 2, 3 and 4 respectively (Table 4.2). Appropriate scaling factors were applied to the averaged spectra of each sub-band to form a continous spectrum from $2.38 - 45.2\mu$. The data of subband 3E ($27.5-29.0\ \mu$) are generally noisy and unreliable (see eg. Hrivnak et al., 2000, Hony et al., 2002). Figs. 4.1a, b, c and 4.2a show the SWS spectra of the hot post-AGB stars. The SWS data of IRAS14331-6435 (Hen3-1013), IRAS18062+2410 (SAO 85766) and IRAS22023+5249 (LSIII +5224) below 7μ and that of IRAS16206-5956 (SAO 243756), IRAS22495+5134 (LSIII +5142) below 12.5μ were noisy and have been excluded. This is also evident from the low IRAS 12μ flux (< 5 Jy) of these stars. Identification of the infrared spectral features is based on Waters & Molster (1999), Cox (1993), Hrivnak et al. (2000), Volk et al. (2002), Cernicharo et al. (1999) and Jørgensen et al. (2000).

4.4.1.2 LWS

Reduction of the LWS observation of IRAS17423-1755 (Hen3-1475) consisted of extensive bad data removal using ISAP rebinning on a fixed resolution grid of $\lambda/\Delta\lambda = 250$. Appropriate scaling factors were applied to the data from different LWS detectors to form a continuous spectrum (Fig. 4.2c). The LWS spectrum of IRAS17423-1755 (Hen3-1475) appears featureless.

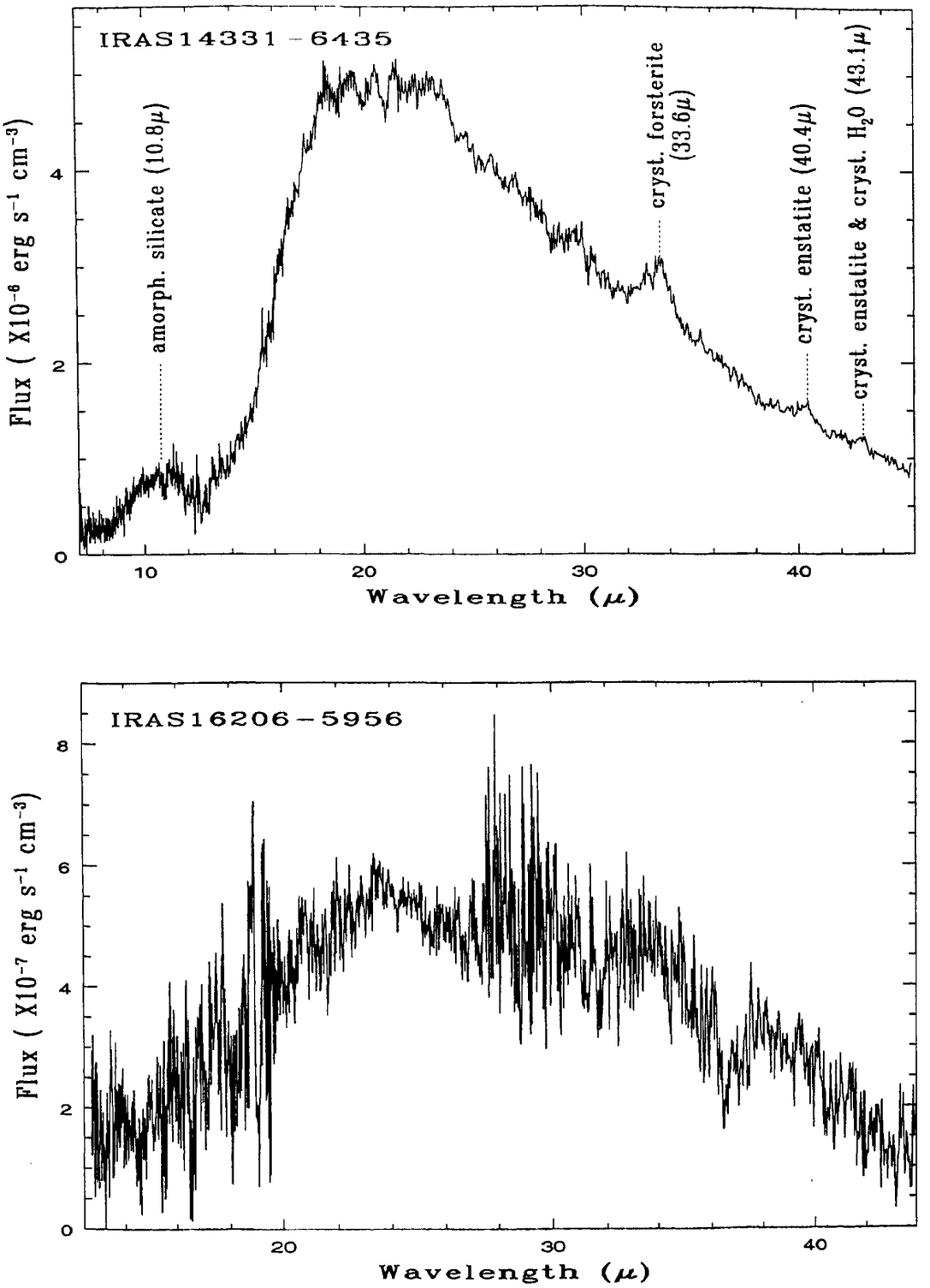

Figure 4.1a: The ISO SWS spectrum of IRAS14331-6435 (Hen3-1013) shows emission due to amorphous (10.8μ) and crystalline silicates and/or H_2O (33.6μ, 40.4μ, 43.1μ) (see eg. Waters & Molster, 1999). ISO spectrum of IRAS16206-5956 (SAO 243756) is noisy and only the continuum is seen here.

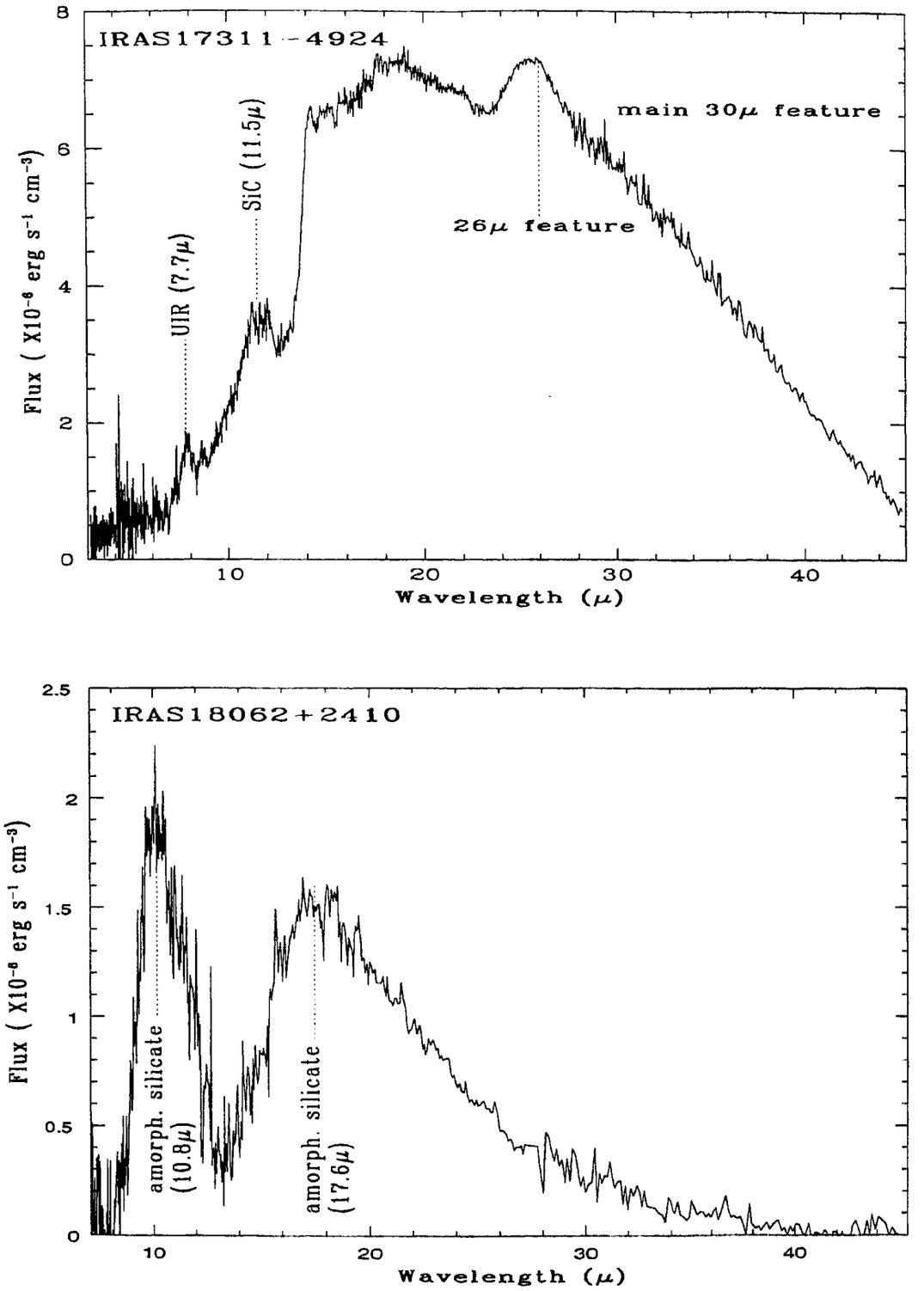

Figure 4.1b: The ISO SWS spectrum of IRAS17311-4924 (Hen3-1428) shows emission due to the UIR band at 7.7μ, SiC (11.5μ) and the "30μ feature" (see eg. Hrivnak et al., 2000; Volk et al., 2002). IRAS18062+2410 (SAO 85766) shows emission due to amorphous silicates at 10.8μ and 17.6μ (see eg. Waters & Molster, 1999).

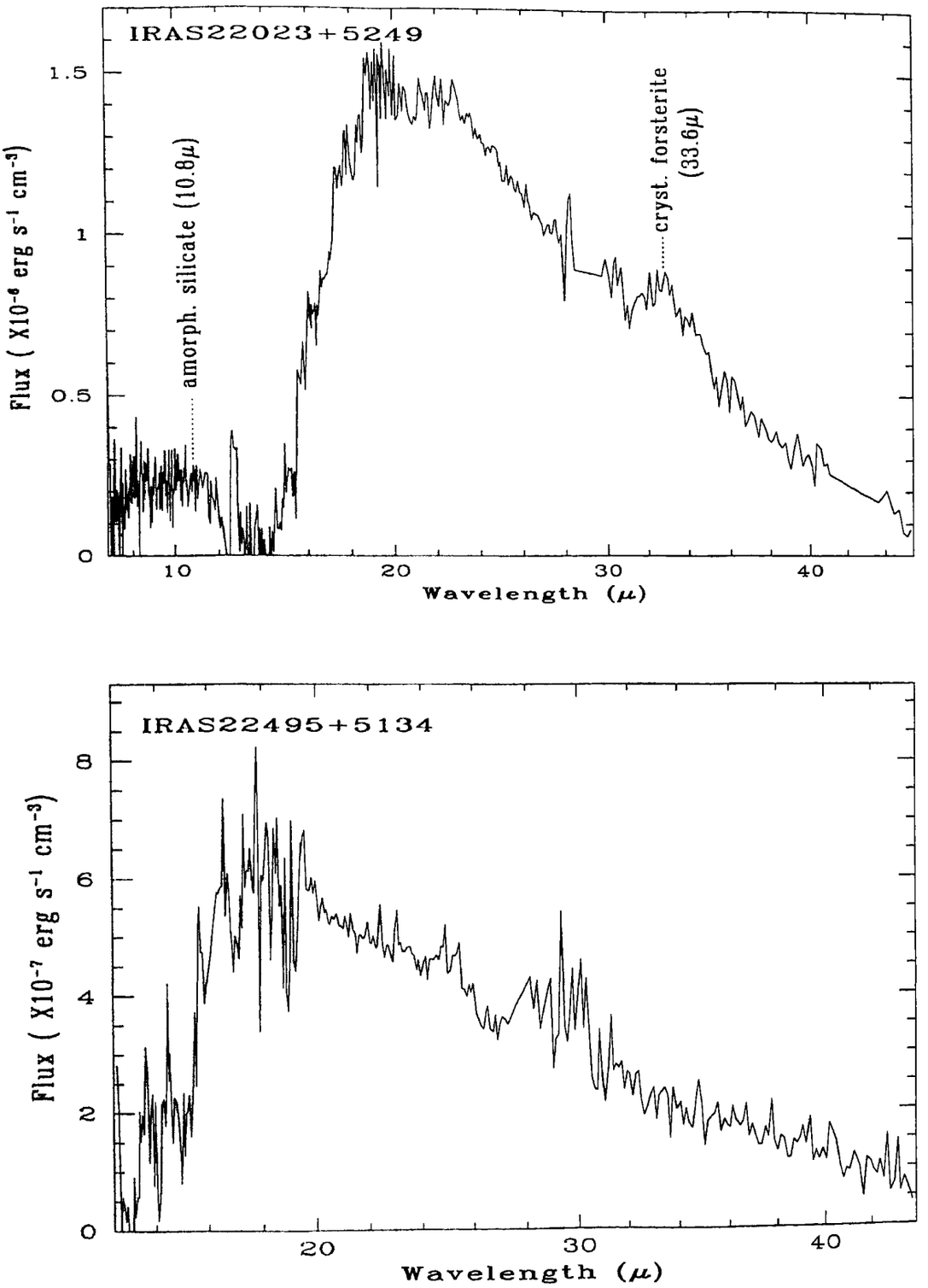

Figure 4.1c: The ISO SWS spectrum of IRAS22023+5249 (LSIII +5224) shows emission due to amorphous (10.8μ) and crystalline (33.6μ) silicates (see eg. Waters & Molster, 1999). ISO SWS spectrum of IRAS22495+5134 (LSIII +5142) is noisy and only the continuum is seen here.

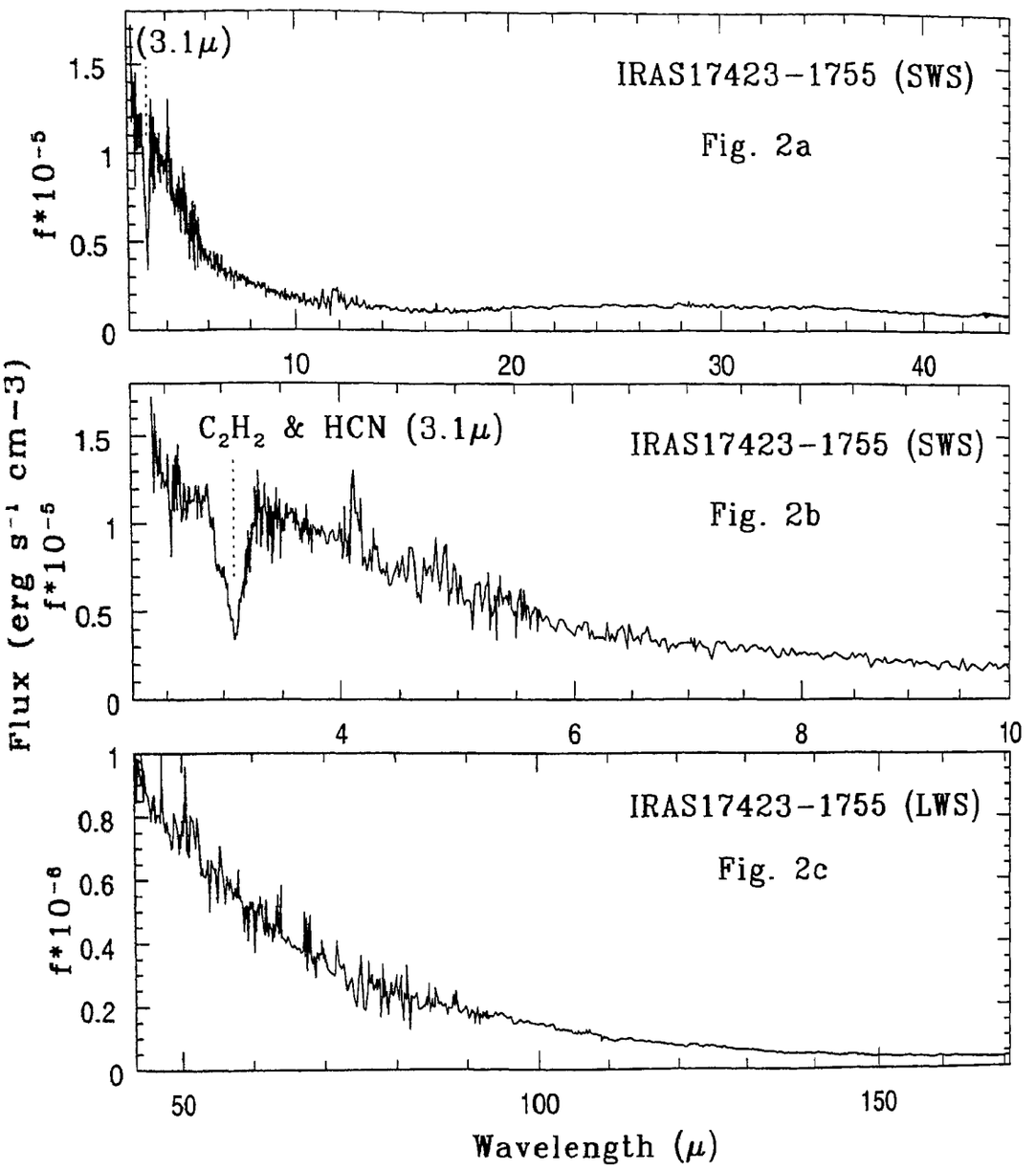

Figure 4.2: ISO SWS (2.4μ – 44.4μ) and LWS (43μ – 171μ) spectra of IRAS17423-1755 (Hen3-1475) are presented in Figs. 4.2a and 4.2c respectively. The SWS spectrum shows a broad absorption feature at 3.1μ due to C_2H_2 and/or HCN (see eg. Cernicharo et al. 1999; Jørgensen et al., 2000). This broad absorption feature is seen clearly in Fig. 4.2b showing the SWS spectrum of the star from 2.4μ – 10μ only. The LWS spectrum of the star (Fig. 4.2c) appears featureless.

4.4.1.3 Joining the SWS and LWS spectra

Although the spectral shape is very reliable, the absolute flux calibration uncertainity is 30% for the SWS at 45μ (Schaeidt et al., 1996) and $10-15\%$ for the LWS at 45μ (Swinyard et al., 1998). The SWS and LWS spectra of IRAS17423-1755 (Hen3-1475) were scaled according to their fluxes in the overlap region. The difference between the flux levels of LWS and SWS in the overlap region was smaller than 30% which is acceptable within the limits of the combined error bars. The combined SWS-LWS spectra of IRAS17423-1755 (Hen3-1475) was used in Fig. 4.3.

4.4.2 Spectral energy distributions (SEDs)

To re-construct the spectral energy distributions (SEDs) of the objects, we combined the ISO data with available U,B,V,R,I,J,H,K,L,L' and M magnitudes of the stars from literature (Table 4.3a). We also searched the 2MASS (2Micron All Sky Survey) Catalog within 15″of each object for their JHK magnitudes, and the Midcourse Space Experiment (MSX) catalog within 3″of each object. MSX fluxes were found only for IRAS17460-3114 (SAO 209306; Table 4.3b). Infrared data (8.7, 10, 11.4, 12.6 and 19.5μ) on IRAS18062+2410 (SAO 85766; Table 4.3c) was obtained from Lawrence et al. (1990).

4.4.2.1 Central star temperatures

The temperatures of the central stars (Table 4.4) are mainly from Gauba & Parthasarathy (2003b). For IRAS12584-4837 (Hen3-847) and IRAS17423-1755 (Hen3-1475), we estimated the central star temperatures based on their spectral types. For the PN, IRAS22495+5134 (LSIII +5142) we used a central star temperature of 35000K (Tylenda & Stasińska, 1994). Gauba & Parthasarathy (2003b) found that the UV(IUE) spectrum of IRAS22023+5249 (LSIII +5224) closely resembles that of a B2-supergiant. Hence we adopted a temperature of 18500K for the star, corresponding to the spectral type B2I. LTE analysis of the high resolution optical spectra of IRAS18062+2410(SAO85766) was carried out by Mooney et al. (2002) and

Table 4.3a: Photometric data on hot post-AGB stars

IRAS	U mag	B mag	V mag	R mag	I mag	J mag	H mag	K mag	L mag	L' mag	M mag
12584-4837		10.65[a]	10.58[a]			9.99[b]	9.14[b]	7.49[b]		4.53[b]	3.59[b]
13266-5551	10.33[c]	10.99[c]	10.68[c]			9.96[d]	9.84[d]	9.70[d]			
14331-6435	11.11[c]	11.48[c]	10.90[c]			9.35[d]	9.03[d]	8.72[d]			
16206-5956	9.87[c]	10.07[c]	9.76[c]								
17203-1534		12.37[a]	12.02[a]			10.95[e]	10.81[e]	10.66[e]			
17311-4924	10.52[f]	11.08[f]	10.68[f]			9.74[d]	9.54[d]	9.19[d]			
17423-1755	13.57[g]	13.3[h]	12.64[g]	11.75[g]	10.91[g]	9.61[d]	8.32[d]	6.80[d]			
17460-3114	7.45[c]	8.17[c]	7.94[c]			7.32[e]	7.31[e]	7.26[e]			
18023-3409	11.70[c]	12.01[c]	11.55[c]								
18062+2410	10.86[i]	11.59[i]	11.54[i]			11.22[d]	10.97[d]	10.84[d]; 10.21[j]	9.61[j]		7.30[j]
18371-3159		12.09[a]	11.98[a]								
18379-1707	11.94[c]	12.38[c]	11.93[c]			10.76[d]	10.55[d]	10.33[d]			
19590-1249	10.75[k]	11.41[k]	11.32[k]			11.08[d]	10.96[d]	10.78[d]		10.34[l]	
22023+5249		13.21[a]	12.52[a]			11.30[d]	11.11[d]	10.83[d]			
22495+5134		12.00[a]	11.78[a]			11.82[e]	11.76[e]	11.57[e]			

Photometry is from : [a]Hog et al.(2000); [b]Fouque et al.(1992); [c]Reed(1998); [d]García-Lario et al.(1997a); [e]2MASS; [f]Kozok (1985a); [g]Gauba et al. (2003a); [h]Monet et al. (1998); [i]Arkhipova et al. (1999); [j]Lawrence et al.(1990); [k]Arkhipova et al. (2002),

[l]Conlon et al. (1993a)

Table 4.3b: MSX data

IRAS	MSX Fluxes (Jansky)			
	Band A 8.28μ	Band C 12.13μ	Band D 14.65μ	Band E 21.34μ
17460-3114	4.0095	5.2726	6.9896	20.730

Table 4.3c: IR data on IRAS18062+2410 (SAO85766)

IRAS	IR data in magnitudes				
	8.7μ	10μ	11.4μ	12.6μ	19.5μ
18062+2410	4.29	2.17	2.22	2.31	−0.25

Parthasarathy et al. (2000b). Recently, using non-LTE analysis, Ryans et al. (2003) reported an effective temperature of 20750K for IRAS18062+2410 (SAO85766) and 20500K for IRAS19590-1249 (LSIV-12 111). In this chapter, we have adopted the temperature estimates by Ryans et al. (2003).

4.4.2.2 Reddening

The interstellar extinction ($E(B-V)_{I.S.}$) in the direction of the stars were estimated using the Diffuse Infrared Background Experiment (DIRBE)/IRAS dust maps (Schlegel et al., 1998; Table 4.4). The optical spectral types of the stars are mainly from Parthasarathy et al. (2000a). The intrinsic B−V values, $(B-V)_o$, for the optical spectral types of the stars, were taken from Schmidt-Kaler (1982). We adopted $(B-V)_o=-0.20$ for IRAS12584-4837 (Hen3-847) and IRAS17423-1755 (Hen3-1475) corresponding to T_{eff}=20000K. For IRAS22023+5249 (LSIII +5224), we used $(B-V)_o=-0.16$ corresponding to B2I spectral type and for the PN, IRAS22495+5134 (LSIII +5142), we adopted $(B-V)_o=-0.30$ correspoding to T_{eff}=35000K. Using the observed and intrinsic B−V values we derived the total (interstellar plus circumstellar) extinction, $E(B-V)_{total}$ $(=(B-V)_{obs} - (B-V)_o)$ towards these stars. Comparing

$E(B-V)_{total}$ and $E(B-V)_{I.S.}$, it is evident that there is considerable circumstellar extinction in most cases. Gauba & Parthasarathy (2003b) found that the circumstellar extinction law in the UV (from $\sim$ 1300Å to 3200Å) varies linearly as λ^{-1} in the case of IRAS13266-5551 (CPD-55 5588), IRAS14331-6435 (Hen3-1013), IRAS16206-5956 (SAO 243756), IRAS17311-4924 (Hen3-1428), IRAS18023-3409 (LSS 4634), IRAS18062+2410 (SAO 85766), IRAS18371-3159 (LSE 63), IRAS22023+5249 (LSIII +5224) and IRAS22495+5134 (LSIII +5142)

Since little is known about circumstellar extinction laws, we corrected the observed optical and near infrared magnitudes of the stars for the total extinction ($E(B-V)_{total}$) using the standard extinction laws by Rieke & Lebofsky (1985). In particular, Rieke & Lebofsky (1985) assume R_v=3.1, where, $R_v=A_v/E(B-V)$. Although this is true for interstellar extinction, it may not be strictly true for circumstellar extinction obeying a λ^{-1} law in the UV. In particular, R_v may be different from 3.1 in the case of circumstellar extinction.

4.4.2.3 Modelling the circumstellar dust shells with DUSTY code

The use of the radiative transfer code, DUSTY (Ivezić et al., 1999) for modelling the circumstellar dust shells of hot post-AGB stars was described in Gauba et al. (2003a). DUSTY uses six different grain types : 'warm' (Sil-Ow) and 'cold' (Sil-Oc) silicates from Ossenkopf et al. (1992), silicates and graphites (Sil-Dl and grf-DL) from Draine and Lee (1984), amorphous carbon (amC-Hn) from Hanner (1988) and SiC (SiC-Pg) from Pégourié (1988). The central stars were assumed to be point sources at the centers of the spherical density distributions. The SEDs of the central stars were assumed to be Planckian. The standard Mathis, Rumpl, Nordsieck (MRN) (Mathis et al., 1977) power-law was used for the grain size (n(a)) distributions, i.e. $n(a) \propto a^{-q}$ for $a_{min} \leq a \leq a_{max}$ with q=3.5, a(min)=0.005μ and a(max)=0.25μ. For each object, the dust temperature (T_d) on the inner shell boundary and the optical depth (τ) at 0.55μ were varied. We assumed an inverse square law (y^{-2}) for the spherical density distribution. The shell was assumed to extend to 1000 times its inner radius. We adopted the fits for which the sum of squares of the deviations between the observed

and modelled fluxes (after scaling) were a minimum. Table 4.4 lists the adopted input parameters. Fig. 4.3 shows the spectral energy distribution of the stars. DUSTY does not allow simultaneous modelling of warm and cold dust shells. Hence, the cold dust in the case of IRAS12584-4837 (Hen3-847) and IRAS17423-1755 (Hen3-1475) had to be modelled and treated independent of the warm dust around these stars.

Having fixed T_d and τ, we then used the gas-dynamical mode of the DUSTY code to derive the inner radii, r1(cm) where the dust temperatures (T_d) are specified and the mass-loss rates ($\dot{M}$). The radius scales in proportion to $L^{1/2}$ where L is the luminosity and the code output value corresponds to $L=10^4 L_\odot$. The mass-loss rate scales in proportion to $L^{3/4}(r_{gd}\rho_s)^{1/2}$ where, the gas-to-dust mass ratio, r_{gd}=200 and the dust grain density, ρ_s=3 g cm^{-3}. The hot post-AGB stars discussed in this chapter have a range of core-masses (Gauba & Parthasarathy, 2003b). Pottasch (1992) pointed out that the white dwarf distribution is sharply peaked with a mean mass between 0.56 and 0.58 $M_\odot$ and central stars of PNe have core-masses which show a peak at approximately $0.6M_\odot$. We carried out calculations for our hot post-AGB stars with core masses of $0.565M_\odot$ and $0.605M_\odot$ corresponding to luminosities of $4500L_\odot$ (Schönberner, 1983) and $6300L_\odot$ (Blöcker, 1995) respectively. Distances (d) to the stars were derived using r1 and the ratio of the observed and modelled fluxes at 0.55μ. θ (=r1/d) is the angular radii of the inner boundary of the cold circumstellar dust envelopes.

For post-AGB stars with core masses of 0.565 $M_\odot$ and 0.605 $M_\odot$ the effective temperatures at the tip of the AGB are 5000K (Schönberner, 1983) and 6000K (Blöcker, 1995) respectively. The dust condensation temperature is taken to be 1200K (Whittet, 2003). Using the gas-dynamical mode of the DUSTY code, we then obtained the terminal outflow velocities (V_e) and the distances (r0) at which the dust grains reached the condensation temperature. Ve scales in proportion to $L^{1/4}(r_{gd}\rho_s)^{-1/2}$. The present inner boundary of the dust envelopes is at r1. Thus, the dynamical age from the tip of the AGB is given by $(r1-r0)/V_e$.

Tables 4.5a and b list the respective values for T_d, r1, r0, d, θ, $\dot{M}$, V_e and Δt. All calculations were carried out using the best fit parameters for the cold circumstellar

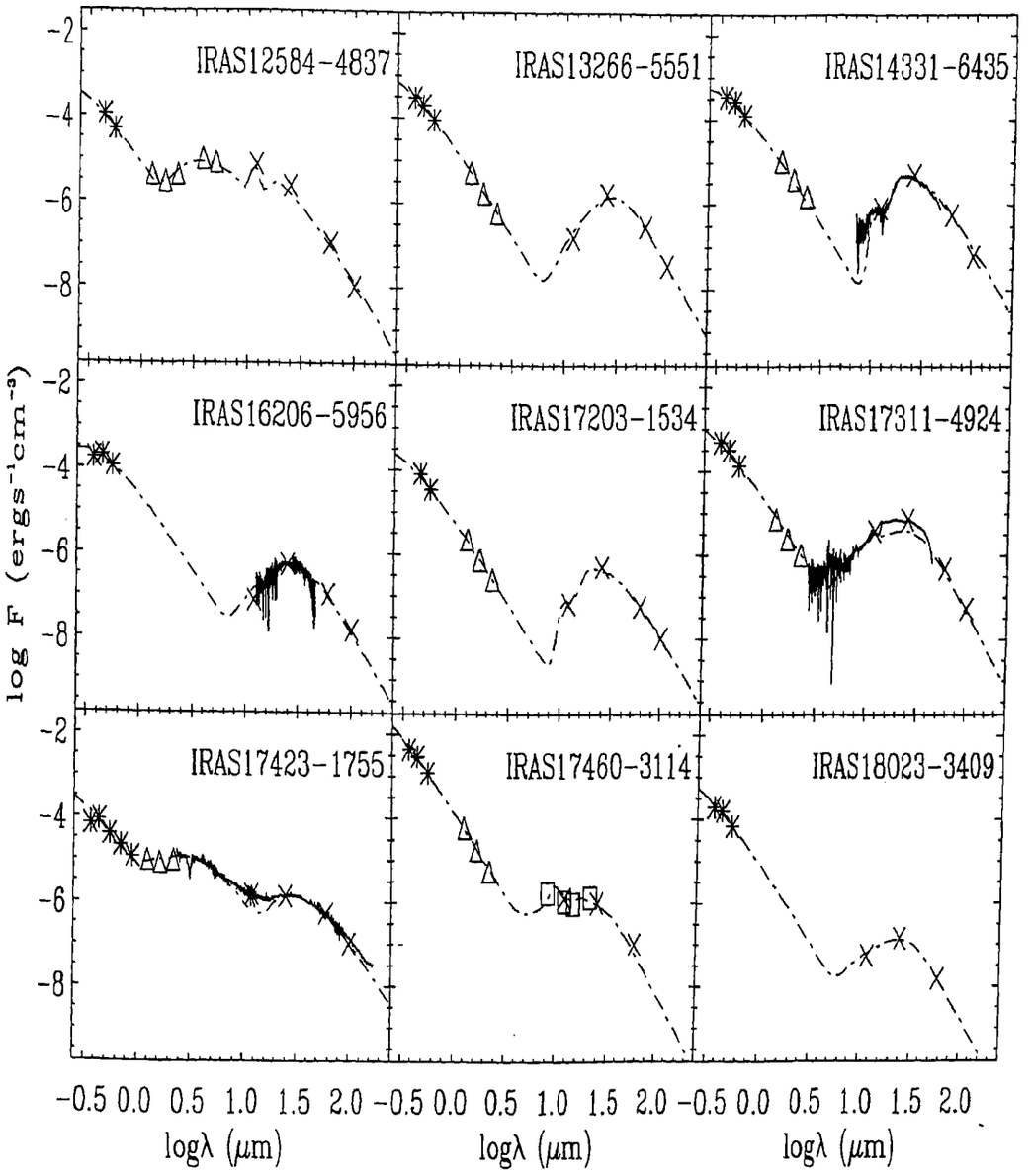

Figure 4.3: Spectral energy distributions (SEDs) of the hot post-AGB stars. UBVRI data (asterisk) are plotted alongwith JHK (triangle), MSX (square) and IRAS data (cross). ISO spectra of the hot post-AGB stars are plotted as solid lines. Dusty model fits are shown by dashed-dotted lines. We could not obtain a fit to the "30μ emission feature" in IRAS17311-4924 (Hen3-1428). The near-IR and K,L,M data of IRAS18062+2410 (SAO85766) by Lawrence et al. (1990) is indicated by diamonds. Notice the mismatch between the K-band flux of Lawrence et al. (1990; diamond) and García-Lario et al. (1997a; triangle) for the star. The L and M-band fluxes also do not lie on the modelled SED of the star (see Sec. 4.4.3).

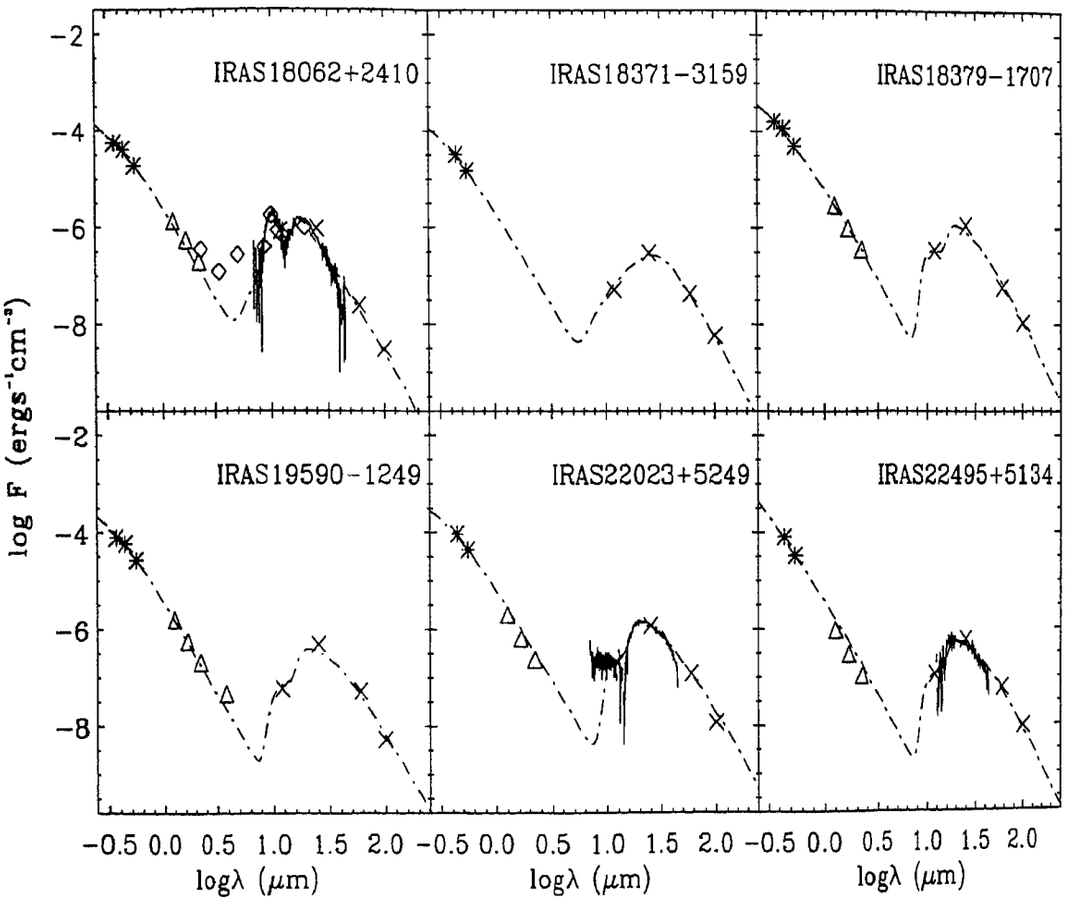

Figure 4.3: contd....

Table 4.4: Input physical parameters for DUSTY and the adopted reddening values

IRAS	dust type	E(B−V) total	E(B−V) I.S.	T_{eff} (K)	grain type	optical depth (τ)	T_d (K)
12584-4837	warm	0.27	0.18	20000	amC-Hn	0.26	775
	cold	0.27	0.18	20000	Sil-DL	0.29	200
13266-5551	cold	0.51	0.53	20800	grf-DL	0.12	160
14331-6435	cold	0.71	-	16200	Sil-Ow	0.50	130
16206-5956	cold	0.29	0.22	11200	grf-DL & amC-Hn	0.16	170
17203-1534	cold	0.61	0.44	19000	Sil-Ow	0.15	117
17311-4924	cold	0.66	0.22	20300	grf-DL & SiC-Pg	0.22	250
17423-1755	warm	0.86	0.67	20000	amC-Hn	0.16	1500
	warm	0.86	0.67	20000	amC-Hn	0.32	1000
	cold	0.86	0.67	20000	SiC-Pg	0.35	100
17460-3114	cold	0.54	-	35000	Sil-DL & grf-DL	0.0015	315
18023-3409	cold	0.70	0.44	20300	grf-DL	0.015	220
18062+2410	cold	0.24	0.11	20750	Sil-Oc & Sil-DL	0.32	230
18371-3159	cold	0.30	0.15	20800	grf-DL	0.13	180
18379-1707	cold	0.71	-	19000	Sil-DL	0.13	140
19590-1249	cold	0.29	0.20	20500	Sil-Ow & Sil-DL	0.08	120
22023+5249	cold	0.85	-	18500	Sil-Oc & Sil-DL	0.29	120
22495+5134	cold	0.52	0.36	35000	Sil-DL	0.011	125

dust shells.

4.4.3 Notes on individual objects

The hot post-AGB stars in this chapter, except IRAS19590-1249 (LSIV-12 111), have been described in Gauba et al. (2003a; Chapter 2) and Gauba & Parthasarathy (2003b; Chapter 3). Here, we describe, the ISO spectra and dust shell characteristics of some of these objects.

#IRAS 12584-4837 (Hen3-847)

The SED of this star showed the presence of both warm (775K) and cold (200K) circumstellar dust. The presence of warm circumstellar dust may indicate ongoing

Table 4.5a: Derived stellar and dust envelope parameters for M_c=0.565$M_\odot$

IRAS	r1 (cm)	r0 (cm)	d (kpc)	θ ($''$)	$\dot{M}$ $M_\odot yr^{-1}$	V_e kms^{-1}	Δt yr.
12584-4837	$2.03X10^{16}$	$1.43X10^{14}$	2.85	0.47	$1.34X10^{-5}$	21.64	311
13266-5551	$3.92X10^{16}$	$1.78X10^{14}$	2.05	1.28	$8.08X10^{-6}$	17.54	741
14331-6435	$5.10X10^{16}$	$1.59X10^{14}$	2.10	1.62	$3.27X10^{-5}$	20.16	840
16206-5956	$2.91X10^{16}$	$1.68X10^{14}$	3.24	0.60	$7.14X10^{-6}$	19.26	500
17203-1534	$5.25X10^{16}$	$1.50X10^{14}$	3.70	0.95	$1.35X10^{-5}$	16.88	1033
17311-4924	$1.72X10^{16}$	$1.79X10^{14}$	1.66	0.70	$8.24X10^{-6}$	19.67	288
17423-1755	$2.98X10^{17}$	$1.52X10^{14}$	3.15	6.39	$5.30X10^{-5}$	23.28	4154
17460-3114	$9.93X10^{15}$	$1.72X10^{14}$	0.30	2.19	$1.86X10^{-7}$	6.20	525
18023-3409	$3.12X10^{16}$	$1.75X10^{14}$	2.46	0.58	$1.25X10^{-6}$	11.06	624
18062+2410	$9.13X10^{15}$	$1.25X10^{14}$	4.48	0.14	$1.03X10^{-5}$	20.90	144
18371-3159	$3.14X10^{16}$	$1.78X10^{14}$	5.04	0.41	$7.69X10^{-6}$	17.87	582
18379-1707	$3.00X10^{16}$	$1.07X10^{14}$	3.10	0.64	$1.12X10^{-5}$	18.20	548
19590-1249	$4.80X10^{16}$	$1.17X10^{14}$	3.93	0.82	$9.89X10^{-6}$	15.90	1004
22023+5249	$4.62X10^{16}$	$1.24X10^{14}$	3.33	0.93	$2.09X10^{-5}$	20.57	747
22495+5134	$5.59X10^{16}$	$1.05X10^{14}$	1.83	2.04	$3.05X10^{-6}$	10.49	1773

Table 4.5b: Derived stellar and dust envelope parameters for M_c=0.605$M_\odot$

IRAS	r1 (cm)	r0 (cm)	d (kpc)	θ ($''$)	$\dot{M}$ $M_\odot yr^{-1}$	V_e kms^{-1}	Δt yr.
12584-4837	$2.40X10^{16}$	$1.94X10^{14}$	3.37	0.47	$1.73X10^{-5}$	24.55	323
13266-5551	$4.63X10^{16}$	$2.40X10^{14}$	2.42	1.28	$1.04X10^{-5}$	19.82	775
14331-6435	$6.03X10^{16}$	$2.20X10^{14}$	2.49	1.62	$4.22X10^{-5}$	22.78	879
16206-5956	$3.44X10^{16}$	$2.25X10^{14}$	3.83	0.60	$9.22X10^{-6}$	21.70	525
17203-1534	$6.21X10^{16}$	$2.05X10^{14}$	4.38	0.95	$1.74X10^{-5}$	19.38	1065
17311-4924	$2.03X10^{16}$	$2.41X10^{14}$	1.96	0.70	$1.06X10^{-5}$	22.14	303
17423-1755	$3.52X10^{17}$	$2.06X10^{14}$	3.72	6.39	$6.84X10^{-5}$	26.07	4481
17460-3114	$1.17X10^{16}$	$2.31X10^{14}$	0.36	2.19	$2.40X10^{-7}$	7.08	541
18023-3409	$2.48X10^{16}$	$2.36X10^{14}$	2.92	0.58	$1.62X10^{-6}$	12.59	651
18062+2410	$1.08X10^{16}$	$1.71X10^{14}$	5.29	0.14	$1.33X10^{-5}$	23.93	148
18371-3159	$3.71X10^{16}$	$2.40X10^{14}$	5.95	0.41	$9.93X10^{-6}$	20.18	609
18379-1707	$3.55X10^{16}$	$1.46X10^{14}$	3.67	0.64	$1.45X10^{-5}$	21.52	548
19590-1249	$5.67X10^{16}$	$1.59X10^{14}$	4.64	0.82	$1.28X10^{-5}$	18.66	1009
22023+5249	$5.46X10^{16}$	$1.71X10^{14}$	3.94	0.93	$2.70X10^{-5}$	23.66	766
22495+5134	$6.61X10^{16}$	$1.40X10^{14}$	2.17	2.04	$3.94X10^{-6}$	12.41	1773

post-AGB mass loss. The use of amorphous carbon grains to model the warm dust and silicate grains for the cold dust, indicates that during its evolution along the AGB, the central star may have evolved from an oxygen-rich to a carbon-rich star.

#IRAS 14331-6435 (Hen3-1013)

The ISO SWS spectrum reveals the presence of amorphous (10.8μ) and crystalline silicates and/or water (33.6μ, 40.4μ, 43.1μ) in the circumstellar environment of this star. Crystalline silicates have been detected in the dust shells around evolved oxygen-rich stars (see eg. Waters et al.,1996, Waters & Molster, 1999). Waters et al. (1996) found that these emission features are more prominent for objects with cooler dust shells ($T < 300K$). Emission from crystalline water has been reported in the $40-70\mu$ spectrum of the Frosty Leo nebula and other cool oxygen-rich envelopes (Omont et al., 1990).

#IRAS 16206-5956 (SAO 243756)

The ISO spectrum of this star is noisy and no features could be identified. The continuum from 12.5μ to 45.2μ was used in addition to the IRAS fluxes to better contrain the model fit to the SED.

#IRAS 17311-4924 (Hen3-1428)

The broad "30 μ emission feature" was detected in several AGB stars and PN sources (Forrest et al., 1981; Cox, 1993). More recently it was also detected in carbon-rich PPNs possessing the 21μ emission feature (Omont et al., 1995). Hony et al. (2002) detected this feature in the ISO SWS spectrum of IRAS 17311-4924 (Hen3-1428) and a large sample of carbon-rich AGB stars (C-stars), post-AGB stars and PNe. Substructure in the 30μ feature was recognised by Szczerba et al. (1999). In the spectra of several PPNs and carbon stars, it was resolved into two components (Hrivnak et al., 2000; Volk et al., 2000, 2002), the "26 μ" and "main 30 μ" feature (Fig. 4.1b). Goebel & Moseley (1985) first suggested that the feature is due to magnesium sulfide (MgS). Hony et al. (2002) too identified MgS as the carrier of the "26 μ" and "main 30 μ" emission features. However, the 30μ band is never seen in oxygen-rich sources (Forrest et al., 1979). Since the feature is seen only in carbon-rich objects, the suggestion that its carrier is a carbonaceous material continues to be

appealing (Volk et al., 2002). We modelled the SED of IRAS 17311-4924 (Hen3-1428) using graphite and silicon carbide (SiC). However, we could not obtain a fit in the 30μ emission region (from $\sim 20 - 30\ \mu$).

The 11.5μ band (Fig. 4.1b) is attributed to SiC (Treffers & Cohen, 1984) and has been detected in carbon-rich evolved objects (see eg., Cernicharo et al., 1989). Cox(1993) pointed out that all AGB stars where a 30μ emission band is present show the 11.5μ band in emission with the notable exception of GL 3068 where it is seen in absorption. However, the reverse is not true and some caron-rich sources with a a prominent 11.5μ emission band do not show the 30μ band (V Cyg, S Cep and Y CVn). Using the DUSTY model, we obtained a good fit to the SiC emission.

We also detected the 7.7 μ UIR feature in the ISO spectrum of this object. UIR features are commonly attributed to polyaromatic hydrocarbons (PAHs) and have been detected in other carbon-rich protoplanetary nebulae (see eg. Beintema et al., 1996; Hrivnak et al., 2000).

#IRAS 17423-1755 (Hen3-1475)

Gauba et al. (2003a) modelled the SED of this star using DUSTY. They found a warm dust component at 1500K in addition to the cold-dust at 100K indicating ongoing post-AGB mass-loss. Plotting the ISO spectrum of the star ($2.38\mu - 171\ \mu$) alongwith the photometric data from Gauba et al (2003a), near-IR data from García-Lario et al. (1997a) and IRAS fluxes and using the DUSTY code, we detected a second warm dust component at 1000K.

The broad absorption feature at 3.1μ seen in the ISO spectrum is due to C_2H_2 and/or HCN (Ridgway et al., 1978; Cernicharo et al., 1999; Jørgensen et al., 2000). This feature is observed in carbon stars (Merrill & Stein, 1976; Noguchi et al., 1977; Groenewegen et al., 1994). The far-IR flux distribution of the star was modelled with amorphous carbon and silicon carbide confirming the carbon rich nature of the circumstellar dust shell. The LWS spectrum appears featureless.

#IRAS 18062+2410 (SAO 85766)

High resolution optical spectra (Parthasarathy et al., 2000b; Mooney et al., 2002; Ryans et al., 2003) indicated the underabundance of carbon in this star. The ISO

spectrum shows strong emission due to amorphous silicates at 10.8μ and 17.6μ in conformity with an oxygen-rich chemistry (i.e. C/O < 1) for the central star.

The K,L,M fluxes by Lawrence et al. (1990) lie above the modelled SED (Fig. 4.3). In particular the K-band flux of Lawrence et al. (1990) lies above the K-band flux estimated by García-Lario et al. (1997a). If the K,L,M fluxes of the star by Lawrence et al. (1990) were not overestimated, the observed mismatch may be due to the variable nature of this object. Optical variations of the star were detected by Arkhipova et al. (1999). Gauba & Parthasarathy (2003b) reported variable circumstellar extinction which in addition to stellar pulsations may be due to a dusty torus in motion around the hot central star.

Bogdanov (2000) modelled the SED of this star using a different radiative transfer code. They derived T_d=410K. This value is much higher than the dust temperature (T_d=230K) derived by us from the model fit. Bogdanov (2000) had used the K,L,M fluxes by Lawrence et al. (1990) only. Besides they did not use the ISO spectrum of the star to constrain the SED. We believe that we have a better estimate of the physical parameters of the star especially since our model gives a very good fit to the IRAS fluxes and ISO spectrum of the star.

#IRAS 19590-1249 (LSIV-12 111)

It was classified from low dispersion spectroscopy by Kilkenny & Pauls (1990) as having a spectral type around B0. Based on an analysis of its high resolution optical spectra, McCausland et al. (1992) and Conlon et al. (1993a, 1993b) concluded that its chemical composition and atmospheric parameters are consistent with a post-AGB evolutionary state. The presence of nebular emission lines of [NII], [OII] and [SII] in its optical spectrum suggest that it may be in the early stages of PN formation. Study of the atmospheric parameters and abundance analysis of the star have also been carried out by Mooney et al (2002) and more recently a non-LTE analysis by Ryans et al. (2003). Based on these studies it has been confirmed that the central star of LSIV-12 111 shows severe carbon deficiency. Using silicate grain composition for the dust envelope, we obtained a good fit to the SED (Fig. 4.3). We estimated a dust temperature of 120K which is in good agreement with the estimate of Conlon

et al. (1993b) based on the 100μ IRAS flux and the color-color diagram of Jourdain de Muizon et al. (1990).

#IRAS 22023+5249 (LSIII +5224)

Amorphous (10.8μ) and crystalline (33.6μ) silicate features were detected in the ISO spectrum of the dust shell surrounding this star indicating the oxygen-rich nature of the central star.

#IRAS 22495+5134 (LSIII +5142)

The ISO spectrum of this PN is noisy and spectral features could not be identified. The expansion velocities (V_e) and angular radius (θ) derived using the DUSTY code (Tables 4.5a and b) are in good agreement with the expansion velocity of 10 kms^{-1} and angular diameter of 4″ reported by Tylenda & Stasińska (1994) and Acker et al. (1992) respectively.

4.5 Discussion and conclusions

We have modelled the circumstellar dust shells of 15 hot post-AGB stars using the radiative transfer code, DUSTY and derived their dust temperatures, distances to the stars, mass loss rates, expansion velocities, angular radii of the inner boundary of the dust envelopes and dynamical ages from the tip of the AGB (Tables 4.5a and b). These stars have detached dust shells (as is evident from the SEDs, Fig. 4.3), OB-giant or supergiant spectra and cold dust between 100−315K, satisfying the observational properties of PPNe as defined by Kwok (1993, 2001). In addition to the cold dust, warm dust was detected in the case of IRAS12584-4837 (Hen3-847) and IRAS17423-1755 (Hen3-1475) indicating ongoing mass loss. From the grain types used for the model fits, we may infer the chemical composition of the circumstellar dust shells. The use of both silicate and amorphous carbon grains to model the SEDs of IRAS12584-4837 (Hen3-847) and IRAS17460-3114 (SAO 209306) suggests that the central stars in these two cases may have undergone a recent change from an oxygen-rich to a carbon-rich chemistry. Such hot post-AGB stars may evolve into the [WC] central stars of PNe. Recently, Waters et al. (1998) detected carbon-rich PAH

features in the near-infrared and crystalline silicates in the far-infrared ISO spectra of two PNe with [WC] central stars, BD+30 3639 and He2-113.

Observational evidence (eg. Chu et al., 1991) suggests that three winds are involved in stripping the outer envelope of the AGB star on its way to becoming a PN (Marten et al., 1993; Frank, 1994) : the spherically symmetric AGB wind (eg. Habing & Blommaert, 1993) when the star loses mass at rates of $10^{-7} - 10^{-6} M_{\odot} yr^{-1}$ with a wind velocity of $\sim$ 10 kms^{-1}; the superwind phase when the mass loss is thought to increase dramatically at the end of the AGB, upto $10^{-5} - 10^{-3} M_{\odot} yr^{-1}$, still with a wind velocity of $\sim$ 10 kms^{-1}; once the superwind exhausts most of the AGB star's envelope, a fast wind with mass loss rate of $10^{-8} M_{\odot} yr^{-1}$ and velocity of $\sim$ 1000 kms^{-1} develops at some point during the PPN phase. Velocities of 1000 kms^{-1} and mass loss rates of $\sim 10^{-8} M_{\odot} yr^{-1}$ have been observed in the central stars of PNe (eg. Gauba et al., 2001). For our hot post-AGB stars, we derived mass loss rates of $10^{-5} - 10^{-6} M_{\odot} yr^{-1}$. Our expansion velocities (6 – 26 kms^{-1}) appear to be in good agreement with the envelope expansion velocities of post-AGB stars from CO measurements (see eg. Likkel et al., 1991) and those of PNe (see eg. Acker et al., 1992). The mass loss rates ($\dot{M}$) and expansion velocities (V_e) scale with the gas-to-dust mass ratio (r_{gd}). We have adopted $r_{gd} = 200$. For carbon-rich AGB and post-AGB stars values between 200 and 250 are often used (eg. Jura, 1986; Meixner et al., 1997). For the cool (F3Ib) post-AGB star, HD161796 with an oxygen-rich circumstellar environment, Hoogzaad et al. (2002) estimated $r_{gd} = 270$. Our derived dynamical ages from the tip of the AGB range from a few hundred to a few thousand years and are in agreement with the ages expected from evolutionary models (Schönberner & Blöcker, 1993). Similar dynamical ages have been also been estimated from hydrodynamical models for the circumstellar dust shells of post-AGB stars like HD56126 (Hony et al., 2003) and HD161796 (Hoogzaad et al., 2002). Furthermore, our models assume that the dust density distribution falls off as y^{-2} in the entire circumstellar dust shell. Such an assumption would break down in the case of episodic mass loss (Olofsson et al., 1990). Eg. episodic mass loss may have been responsible for the rapid evolution (30 – 40 years) of IRAS17119-5926 (Hen3-1357) and IRAS18062+2410 (SAO85766) from B-type post-AGB supergiants to young PNe (Parthasarathy et al., 1993c, 1995;

Bobrowsky et al., 1998, Parthasarathy et al., 2000b).

We also studied the ISO spectra of 7 hot post-AGB stars, IRAS14331-6435 (Hen3-1013), IRAS16206-5956 (SAO243756), IRAS17311-4924 (Hen3-1428), IRAS17423-1755 (Hen3-1475), IRAS18062+2410 (SAO85766), IRAS22023+5249 (LSIII +5224) and IRAS22495+5134 (LSIII +5142). A weak amorphous silicate feature (10.8μ) alongwith crystalline silicate features was found in the dust shells of IRAS14331-6435 (Hen3-1013) and IRAS22023+5249 (LSIII +5224). The 17.6μ amorphous silicate feature was missing in these two stars. The post-AGB star IRAS18062+2410 (SAO85766) did not show evidence for the presence of crystalline silicates but strong amorphous silicate features at 10.8μ and 17.6μ were detected. Volk & Kwok (1989) predict that at dust temperatures of typically a few 100K for post-AGB stars, the spectrum should increase from 8 to 23μ and the 10.8μ and 17.6 μ silicate features should cease to be observable. This appears to be consistent with the observed spectral features and the dust temperatures of 230K, 130K and 120K for IRAS18062+2410 (SAO85766), IRAS14331-6435 (Hen3-1013) and IRAS22023+5249 (LSIII +5224) respectively from our model fits. The presence of silicate features in these stars indicates the O-rich nature of the central stars. The formation of crystalline silicates in the circumstellar shells of post-AGB stars is still not well understood (see eg., Waters et al., 1996). In contrast, PAH emission at 7.7μ, the "26μ" and "main 30μ" features and 11.5μ SiC emission in IRAS17311-4924 (Hen3-1428), are typical of circumstellar dust shells around carbon-rich post-AGB stars. However, the 21μ emission feature detected in several carbon-rich PPNe (Hrivnak et al., 2000) was notably absent in the ISO spectrum of IRAS17311-4924 (Hen3-1428). Volk et al. (2002) pointed out that although all sources with the 21μ emission feature also display the "26μ" and "main 30μ" features, the converse is not true. The hot post-AGB star, IRAS01005+7910 (Klochkova et al., 2002) which showed the "26" and "main 30μ" emission also did not show the 21μ emission feature (Hrivnak et al., 2000). It may be that the dust grains responsible for the 21μ emission are destroyed as the central star evolves towards hotter temperatures. The broad absorption feature at 3.1μ in IRAS17423-1755 (Hen3-1475) attributed to C_2H_2 and/or HCN indicates that the central star may be carbon-rich.

Acknowledgements : Based on observations with ISO, an ESA project with instruments funded by ESA Member States (especially the PI countries: France, Germany, the Netherlands and the United Kingdom) and with the participation of ISAS and NASA. The ISO Spectral Analysis Package (ISAP) is a joint development by the LWS and SWS Instrument Teams and Data Centers. Contributing institutes are CESR, IAS, IPAC, MPE, RAL and SRON.

Chapter 5

High resolution spectroscopy of the hot post-AGB stars: IRAS13266-5551 (CPD-55 5588) and IRAS17311-4924 (Hen3-1428)

Abstract

The high resolution spectra covering the wavelength range 4900Å to 8250Å of the hot post-AGB stars IRAS13266-5551 (CPD-55 5588) and IRAS17311-4924 (Hen3-1428) reveal absorption lines of C II, N II, O II, Al III, Si III and Fe III and a rich emission line spectrum consisting of H I, He I, C II, N I, O I, Mg II, Al II, Si II, V I, Mn II, Fe II, Fe III, [Fe II] and [Cr II]. The presence of [N II] and [O I] lines and absence of [O III] indicates low excitation nebulae around these stars. The detection of Na I absorption lines indicates the presence of neutral circumstellar envelopes in addition to the low excitation nebulae. The H_α lines show P-Cygni profiles indicating ongoing post-AGB mass loss. We derived heliocentric radial velocities to be 67.55 $\pm$ 1.26 kms^{-1} and 26.09 $\pm$ 1.88 kms^{-1} for IRAS13266-5551 (CPD-55 5588) and IRAS17311-4924 (Hen3-1428) respectively. High galactic latitude and large radial velocity of IRAS13266-

5551 (CPD-55 5588) indicate that it is a high velocity star belonging to the old disk population. Preliminary estimates for the CNO abundances in IRAS13266-5551 (CPD-55 5588) are obtained.

5.1 Introduction

IRAS13266-5551 (CPD-55 5588) and IRAS17311-4924 (Hen3-1428) were identified as hot post-AGB stars (Table 5.1) based on their far-IR flux distribution, high galactic latitudes and B-supergiant spectra in the optical (Parthasarathy & Pottasch, 1989; Parthasarathy, 1993a; Parthasarathy et al., 2000a). The UV (IUE) spectra of these stars show C II (1335Å), Si IV (1394Å , 1403Å), C IV (1550Å) and N IV (1718Å) lines typical of the central stars of planetary nebulae (PNe). The C IV (1550Å) resonance lines were blue shifted indicating stellar wind velocities of -1821 kms^{-1} (CPD-55 5588) and -1066 kms^{-1} (Hen3-1428) respectively (Gauba and Parthasarathy, 2003b). The "30μ feature", SiC emission at 11.5μ, and UIR band at 7.7μ were detected in the ISO spectrum of IRAS17311-4924 (Hen3-1428, Gauba and Parthasarathy, 2003c). These features have been detected in the circumstellar dust shells of carbon rich AGB stars (C-stars), post-AGB stars, proto-planetary nebulae (PPNe) and planetary nebulae (PNe) (see eg. Hony et al., 2002; Hrivnak et al., 2000, Volk et al., 2000, 2002). Loup et al. (1990) detected CO emission in IRAS17311-4924 (Hen3-1428) typical for circumstellar shells around evolved objects. They estimated an expansion velocity of 11 kms^{-1}. Based on CO observations, Nyman et al. (1992) estimated an expansion velocity of 14.1 kms^{-1}.

High resolution optical spectra of only a few hot post-AGB stars have been analysed. These include IRAS01005+7910 (Klochkova et al., 2002), IRAS18062+2410 (SAO85766, Parthasarathy et al., 2000b; Arkhipova et al., 2001a; Mooney et al., 2002, Ryans et al., 2003), IRAS19590-1249 (LSIV$-12°111$, McCausland et al., 1992; Conlon et al., 1993b; Ryans et al., 2003) and IRAS20462+3416 (LSII+34°26, Parthasarathy, 1993b; García-Lario et al., 1997b; Arkhipova et al., 2001b). The optical spectra of these stars showed absorption lines due to C II, N II, O II, Si II, Si III, Fe III etc. Emission lines of He I, Fe I, II and III, N I, Ni I, O I have also been detected.

Table 5.1: Details of the stars

IRAS	Name	RA (2000)	DEC (2000)	l	b	Sp. Type Optical	IRAS Fluxes (Jy.) 12μ	25μ	60μ	100μ
13266-5551	CPD-55 5588	13:29:50.8	−56:06:53	308.30	+6.36	B1Ibe	0.76	35.90	35.43	11.66
17311-4924	Hen3-1428	17:35:02.49	−49:26:26.4	341.41	−9.04	B1IIe	18.34	150.70	58.74	17.78

Nebular emission lines of [O II], [N II], [S II] etc., detached cold circumstellar dust shells, OB-supergiant spectral types, high galactic latitudes and chemical composition indicate that these are post-AGB stars rapidly evolving into early stages of PNe (Parthasarathy et al., 1993c, 1995 and 2000b). IRAS13266-5551 (CPD-55 5588) and IRAS17311-4924 (Hen3-1428) are found to be similar to the objects mentioned above. In this chapter we report an analysis of their high resolution spectra.

5.2 Observations

High resolution (R $\sim$ 30,000) spectra of IRAS13266-5551 (CPD-55 5588) and IRAS17311-4924 (Hen3-1428) from 4900Å to 8250Å were obtained on 22nd June, 2002. Each object was observed twice during the night. The echelle spectrograph at the f/7.8 Ritchey-Chretien focus of the Victor M. Blanco 4m. telescope of the Cerro Tololo Inter-American Observatory (CTIO) was used for the purpose. The spectra were recorded using a Tektronix 2048X2048 CCD. Appropriate number of bias frames and flat fields were observed. A Th-Ar comparison lamp was used for wavelength calibration.

5.3 Analysis

The spectra were processed using standard IRAF routines. The spectra were corrected using data in the overscan region of the CCD chip. The other reduction steps included trimming, bias subtraction, flat field correction, correction for scattered light and wavelength calibration. The two sets of reduced spectra for each object were then combined to increase the signal-to-noise (S/N) ratio. The final S/N ratios for

IRAS13266-5551 (CPD-55 5588) and IRAS17311-4924 (Hen3-1428) were estimated to be ~ 120. The reduced spectra were continuum normalised and the equivalent widths (W_λ) of the absorption and emission lines were measured. Whenever required, deblending was done to obtain gaussian fits to the blended line profiles. The continuum normalised spectra are presented in Appendices A and B (Figs. A and B). Regions of the spectra with no observable spectral features have been omitted in these figures. The line identifications (Tables 5.2a, b, c, d and 5. 3a, b, c, d) are based on the Moore multiplet table (1945) and the linelists of Sivarani et al. (1999); Parthasarathy et al. (2000b) and Klochkova et al. (2002). Unidentified lines are denoted by "UN". The log (gf) values and excitation potentials (χ) are from the linelist compiled by Ivan Hubeny and retrieved from the directory /pub/hubeny/synplot by anonymous ftp from tlusty.gsfc.nasa.gov.

5.3.1 Description of the spectra

The high resolution optical spectra of IRAS13266-5551 (CPD-55 5588) and IRAS17311-4924 (Hen3-1428) show absorption lines due to C II, N II, O II, Ne I, Al III and Si III. The O I triplet at $\sim$ 7773Å was detected in both stars. Both stars show a rich emission line spectrum with lines of C II, O I, Mg II, Al II, Si II, Mn II, Fe II and Fe III in emission. Emission lines of N I, [O I], V I, [Fe II] and [Cr II] in IRAS17311-4924 (Hen3-1428) were also detected. The presence of low excitation nebular lines of [N II] in the spectra of both stars and the absence of [O III] 5007Å indicates that photoionisation has just started.

The He I lines in the two stars show a variety of profiles. They appear in absorption, in emission and also show P-Cygni profiles indicating post-AGB mass-loss. The He I(4) 5015.675Å and He I(45) 7281.349Å emission lines in IRAS13266-5551 (CPD-55 5588) are superposed on the corresponding absorption components. The asymmetric nature of these emission lines suggests that they may have P-Cygni profiles. The presence of high excitation lines of He I on the one hand and low excitation emission lines of Na I (see Sec. 5.3.4) and V I on the other hand indicates a range of temperatures for the circumstellar material around these stars. The circumstellar en-

velope around these stars may be extended and the outermost regions may be cooler. The H_α lines in both stars show P-Cygni profiles. The emission peak of the line in IRAS17311-4924 (Hen3-1428) is asymmetric.

5.3.2 Radial velocities

Heliocentric radial velocities (V_r) for the well defined absorption and emission lines are presented in Tables 5.2a, 5.2b, 5.2d, 5.3a, 5.3b and 5.3d. For each species found in absorption in IRAS13266-5551 (CPD-55 5588) and IRAS17311-4924 (Hen3-1428), the average radial velocity along with the probable error and the mean lower excitation potential ($\overline{\text{LEP}}$) of the species is given in Table 5.4. For IRAS13266-5551 (CPD-55 5588), it appears that the lines with smaller ($\overline{\text{LEP}}$) i.e. the Ne I, Al III and Fe III lines have larger radial velocities. The O II, Ne I, Al III and Si III lines in IRAS17311-4924 (Hen3-1428) have a distinct velocity when compared with the C II and N II lines in this star. These lines may be formed in different regions in the atmospheres of these stars. We adopt the mean radial velocity from the C II, N II and O II lines ($+67.55 \pm 1.26$ kms^{-1}) for IRAS13266-5551 (CPD-55 5588) and the mean radial velocity from the C II and N II lines ($+26.09 \pm 1.88$ kms^{-1}) for IRAS17311-4924 (Hen3-1428).

The emission lines do not appear to show any obvious trend with lower excitation potential. The average heliocentric radial velocity of the emission lines is $+58.56 \pm 0.87$ kms^{-1} and $+33.50 \pm 0.81$ kms^{-1} in IRAS13266-5551 (CPD-55 5588) and IRAS17311-4924 (Hen3-1428) respectively.

5.3.3 Diffuse interstellar bands (DIBs)

DIBs are absorption features in the spectra of reddened stars and have their origin in the interstellar and circumstellar medium. They are typically broader than expected from the Doppler broadening of turbulent gas motions in the interstellar and circumstellar medium. DIBs at $\lambda\lambda$ 5780.410Å and 5797.030Å were identified in the spectra of IRAS13266-5551 (CPD-55 5588) and IRAS17311-4924 (Hen3-1428). IRAS13266-5551 (CPD-55 5588) also exhibited DIBs at $\lambda\lambda$ 6195.990Å ,

Table 5.2a: Absorption lines in IRAS13266-5551 (CPD-55 5588)

$\lambda_{obs.}$ (Å)	$\lambda_{lab.}$ (Å)	Ident.	W_λ (Å)	log (gf)	χ (eV)	$\Delta\lambda$ (Å)	V_r kms^{-1}
4942.503	4941.12	O II (33)	0.047	0.080	26.55–29.06	1.38	+68.55
4944.434	4943.06	O II (33)	0.087	0.370	26.56–29.07	1.37	+67.91
4956.941	4955.78	O II (33)	0.040	−0.420	26.56–29.06	1.16	+54.98
4995.447	4994.360	N II (24, 64)	0.028	−0.080	20.94–23.42	1.09	
5002.737	5001.469	N II (19)	0.200	0.450	20.65–23.13	1.27	+60.94
5003.909	5002.692	N II (4)	0.084	−1.020	18.46–20.94		
5006.149	5005.150	N II (19, 6)	0.111	0.610	20.66–23.14	1.00	
5008.762	5007.316	N II (24)	0.051	0.160	20.94–23.41		
5012.132	5010.620	N II (4)	0.156	−0.520	18.46–20.94	1.51	+75.16
5046.551	5045.098	N II (4)	0.170	−0.330	18.48–20.94	1.45	+70.98
5049.261	5047.736	He I (47)	0.146	−1.600	21.22–23.67	1.52	+75.10
5075.435	5073.60	N II (10)	0.042	−1.280	18.49–20.94		
	+ 5073.903	Fe III (5)		−2.557	8.65–11.09		
5088.301	5086.701	Fe III (5)	0.029	−2.590	8.65–11.09	1.60	+79.12
5129.38	5127.463	Fe III (5)	0.029	−2.218	8.65–11.07	1.92	+97.10
5134.133	5132.96	C II (16)	0.102	−0.240	20.70–23.12		
	+ 5133.29	C II (16)		−0.200	20.70–23.12		
5144.575	5143.49	C II (16)	0.045	−0.240	20.70–23.11		
5146.636	5145.16	C II (16)	0.091	0.160	20.71–23.12	1.48	+71.05
5152.531	5151.08	C II (16)	0.067	−0.200	20.71–23.12	1.45	+69.21
5157.668	5156.111	Fe III (5)	0.040	−2.018	8.64–11.04		
5161.381	5160.02	O II (32)	0.145	−0.660	26.56–28.96	1.36	+63.83
5208.261	5206.73	O II (32)	0.086	−0.860	26.56–28.94	1.53	+72.92
5220.938		UN	0.133				
5455.44	5454.26	N II (29)	0.080	−0.740	21.15–23.43	1.18	+49.66
5497.188	5495.70	N II (29)	0.076	−0.170	21.16–23.42		
5641.814	5640.50	C II (15)	0.061	−0.750	20.70–22.90		
5668.177	5666.64	N II (3)	0.287	0.010	18.47–20.65	1.54	+66.29
5677.687	5676.03	N II (3)	0.249	−0.340	18.46–20.65	1.66	+72.50
5681.185	5679.56	N II (3)	0.410	0.280	18.48–20.67	1.62	+70.33
5687.802	5686.21	N II (3)	0.158	−0.470	18.47–20.65	1.59	+68.65
5698.282	5696.47	Al III (2)	0.356	0.230	15.64–17.82	1.81	+80.08

Table 5.2a: contd...

$\lambda_{obs.}$ (Å)	$\lambda_{lab.}$ (Å)	Ident.	W_λ (Å)	log (gf)	χ (eV)	$\Delta\lambda$ (Å)	V_r kms^{-1}
5712.48	5710.76	N II (3)	0.185	−0.470	18.48−20.65	1.72	+75.12
5724.433	5722.65	Al III (2)	0.222	−0.070	15.64−17.81	1.78	+78.07
5741.366	5739.734	Si III (4)	0.400	−0.160	19.72−21.88	1.63	69.95
5780.525	5780.410	DIB	0.156			0.12	−9.01
5797.2	5797.030	DIB	0.095			0.17	−6.44
5835.656	5833.938	Fe III (114)	0.114	0.616	18.51−20.63	1.72	+73.21
5933.567	5931.79	N II (28)	0.042	0.050	21.15−23.24		
5943.397	5941.67	N II (28)	0.062	0.320	21.16−23.25		
6144.813	6143.063	Ne I (1)	0.046	−0.350	16.62−18.64	1.75	+70.22
6196.012	6195.990	DIB	0.020			0.02	−14.27
6203.309	6203.060	DIB	0.030			0.25	−3.15
6381.503	6379.63	N II (2)	0.058	−0.920	18.47−20.41	1.87	+72.70
6404.133	6402.246	Ne I (1)	0.123	0.360	16.62−18.55	1.89	+73.32
6483.965	6482.07	N II (8)	0.218	−0.160	18.50−20.41	1.89	+72.23
6508.396	6506.528	Ne I (3)	0.027	0.030	16.67−18.58	1.87	+70.98
6579.254	6578.03	C II (2)	0.084	0.120	14.45−16.33	1.22	+40.40
6613.854	6613.630	DIB	0.104			0.22	−5.26
6642.834	6640.90	O II (4)	0.081	−0.890	23.42−25.29	1.93	+71.95
6723.375	6721.35	O II (4)	0.165	−0.590	23.44−25.29	2.02	+74.92
6782.063	6780.27	C II (14)	0.034	0.040	20.70−22.53	1.79	+63.96
6785.888	6783.75	C II (14)	0.047	0.320	20.71−22.54	2.14	+79.40
7034.571	7032.413	Ne I (1)	0.033	−0.250	16.62−18.38	2.16	+76.90
7773.521	7771.96	O I (1)	0.273	0.320	9.14−10.74	1.56	+44.98
7776.411	7774.18	O I (1)	0.396	0.170	9.14−10.74	2.23	+70.81
7777.68	7775.40	O I (1)	0.072	−0.050	9.14−10.74	2.28	+72.73

Table 5.2b: Emission lines in IRAS13266-5551 (CPD-55 5588)

$\lambda_{obs.}$ (Å)	$\lambda_{lab.}$ (Å)	Ident.	W_λ (Å)	log (gf)	χ (eV)	$\Delta\lambda$ (Å)	V_r kms^{-1}
5015.675†		He I (4)		−0.820	20.62−23.09		
5042.201	5041.063	Si II (5)	0.070	0.290	10.07−12.52	1.14	+52.60
5057.23	5056.020	Si II (5)	0.143	0.590	10.07−12.52	1.21	+56.56
5199.115	5197.569	Fe II (49)	0.030	−2.116	12.78−10.40		
5201.464	5199.5	N II (66)	0.025	−1.370	27.75−30.13		
5955.094	5953.65	Fe III (115)	0.047	0.186	18.79−20.87	1.44	+57.32
5959.04	5957.612	Si II (4)	0.104	−0.300	10.07−12.15	1.43	+56.77
5980.395	5978.90	Fe III (117)	0.268	−1.792	22.62−24.69		
	+5978.970	Si II (4)		0.000	10.07−12.15		
6000.873	5999.30	Fe III (117)	0.038			1.57	+63.27
6034.08	6032.30	Fe III (117)	0.065	0.497	18.82−20.87	1.78	+73.28
6096.798	6095.37	C II (24)	0.029				
6099.948	6098.62	C II (24)	0.030				
6233.296	6231.78	Al II (10)	0.043	−0.080	13.07−15.06	1.52	+57.93
6241.092	6239.36	Fe II (34)	0.043	−4.538	2.80−4.79	1.73	+67.94
6244.937	6243.36	Al II (10)	0.032	0.670	13.08−15.06	1.58	+60.68
6348.619	6347.091	Si II (2)	0.242	0.300	8.12−10.07	1.53	+57.08
6372.931	6371.359	Si II (2)	0.128	0.000	8.12−10.07	1.57	+57.68
6463.234	6462.210	Mn II (20)	0.018	−0.292	14.13−12.21		
6463.668	6462.454	Mn II (20)	0.021	−0.149	14.13−12.21		
6547.508	6545.8	Mg II (23)	0.032			1.71	+63.13
6549.545	6548.1	[N II] (1F)	0.024			1.44	+50.73
6584.932	6583.6	[N II] (1F)					
7003.696	7001.93	O I (21)	0.031	−1.050	10.99−12.76		
	+7002.22	O I (21)		−1.530	10.99−12.76		
7043.716	7042.06	Al II (3)	0.080	0.350	11.32−13.08	1.66	+55.48
7058.3	7056.60	Al II (3)	0.069	0.130	11.32−13.07	1.70	+57.03
7065.315	7063.64	Al II (3)	0.040	−0.350	11.32−13.07	1.67	+55.69
7067.218	7065.188	He I (10)	0.524	−0.460	20.96−22.72		
	+7065.719	He I (10)		−1.160	20.96−22.72		
7233.257	7231.12	C II (3)	0.316	0.070	16.33−18.05		
7238.254	7236.19	C II (3)	0.488	0.330	16.33−18.05		
7281.349†		He I (45)		−0.840	21.22−22.92		
7794.193		UN					
7878.956	7877.13	Mg II (8)	0.215	0.390	9.99−11.57	1.83	+54.46
7898.231	7896.37	Mg II (8)	0.382	0.650	10.00−11.57	1.86	+55.42
8236.681		UN	0.198				

† : the He I(4) 5015.675Å and He I(45) 7281.349 Å emission lines are superposed on the corresponding absorption profiles of these lines. The asymmetric nature of these emission lines suggests that they may have P-Cygni profiles.

Table 5.2c: Lines with P-Cygni profiles in IRAS13266-5551 (CPD-55 5588). Equivalent widths of the absorption and emission components of the P-Cygni profiles are given.

λ_{lab} (Å)	Ident.	W_λ (absorption) (Å)	W_λ (emission) (Å)	log (gf)	χ (eV)
5875.618	He I (11)	0.079	0.484	0.410	20.97–23.08
+ 5875.650	He I (11)			−0.140	20.97–23.08
+ 5875.989	He I (11)			−0.210	20.97–23.08
6562.817	H_α		6.902	0.710	10.15–12.04
6678.149	He I (46)	0.212	0.076	0.330	21.22–23.08

Owing to the broad wings of the H_α emission component, the absorption component of the P-Cygni profile lies above the normalised continuum (see Fig. 5.2).

Table 5.2d: Absorption (a) and emission (e) components of Na I D_2 (5889.953Å) and Na I D_1 (5895.923Å) lines in the spectrum of IRAS13266-5551 (CPD-55 5588). W_λ are the equivalent widths of the components and V_r are the respective heliocentric radial velocities.

Component		IRAS13266-5551					
		Na I D_2			Na I D_1		
		$\lambda_{obs.}$ (Å)	W_λ (Å)	V_r (kms^{-1})	λ_{lab} (Å)	W_λ (Å)	V_r (kms^{-1})
1.	a	5889.54	0.168	−36.28	5895.432	0.062	−40.22
2.	a	5890.003	0.551	−12.69	5896.002	0.415	−11.22
3.	a	5890.366	0.292	+5.80	5896.38	0.203	+8.01
4.	a	5890.938	0.021	+34.92	5896.913	0.029	+35.13
5.	e	5891.324	1.371	+54.59	5897.373	0.007	+58.54

Table 5.3a: Absorption lines in IRAS17311-4924 (Hen3-1428)

$\lambda_{obs.}$ (Å)	$\lambda_{lab.}$ (Å)	Ident.	W_λ (Å)	log (gf)	χ (eV)	$\Delta\lambda$ (Å)	V_r kms^{-1}
5045.694	5045.098	N II (4)	0.096	−0.330	18.48−20.94	0.60	+33.22
5047.79	5047.2†	C II (35)	0.074	−1.00	24.27−26.71	0.59	+32.61
5133.382	5132.96	C II (16)	0.063	−0.240	20.70−23.12		
	+ 5133.29	C II (16)		−0.200	20.70−23.12		
5143.951	5143.49	C II (16)	0.043	−0.240	20.70−23.12	0.46	+24.37
5145.512	5145.16	C II (16)	0.102	0.160	20.71−23.12	0.35	+17.95
5640.069		UN	0.037				
5667.269	5666.64	N II (3)	0.142	0.010	18.46−20.65	0.63	+30.89
5676.672	5676.02	N II (3)	0.135	−0.340	18.46−20.65	0.65	+31.90
5679.909	5679.56	N II (3)	0.246	0.280	18.48−20.67	0.35	+16.03
5686.549	5686.21	N II (3)	0.093	−0.470	18.47−20.65	0.34	+15.48
5697.325	5696.47	Al III (2)	0.183	0.230	15.64−17.82	0.86	+42.83
5711.253	5710.76	N II (3)	0.084	−0.470	18.48−20.65	0.49	+23.28
5723.467	5722.65	Al III (2)	0.111	−0.070	15.64−17.81	0.82	+40.53
5740.521	5739.734	Si III (4)	0.189	−0.160	19.72−21.88	0.79	+38.83
5780.325	5780.410	DIB	0.126			−0.08	−6.61
5797.062	5797.030	DIB	0.020			0.03	−0.91
6143.324	6143.062	Ne I (1)	0.134	−0.350	16.62−18.64	0.26	+10.24
6163.961	6163.594	Ne I (5)	0.045	−0.590	16.72−18.73	0.37	+15.55
6266.775	6266.495	Ne I (5)	0.045	−0.530	16.72−18.69	0.28	+10.94
6334.777	6334.428	Ne I (1)	0.078	−0.310	16.62−18.58	0.35	+14.12
6380.234	6379.63	N II (2)	0.023	−0.920	18.47−20.41	0.60	+25.75
6383.216	6382.991	Ne I (3)	0.059	−0.260	16.67−18.61	0.22	+7.88
6402.583	6402.246	Ne I (1)	0.230	0.360	16.62−18.56	0.34	+13.47
6482.968	6482.07	N II (8)	0.125	−0.160	18.50−20.41	0.90	+39.19
6506.724	6506.528	Ne I (3)	0.084	0.030	16.67−18.58	0.20	+6.76
6641.881	6640.90	O II (4)	0.069	−0.890	23.42−25.29	0.98	+41.81
6722.322	6721.35	O II (4)	0.105	−0.590	23.44−25.29	0.97	+40.83
7032.739	7032.413	Ne I (1)	0.107	−0.250	16.62−18.38	0.33	+11.62
7772.134	7771.96	O I (1)	0.743	0.320	9.14−10.74	0.17	+4.10
7774.474	7774.18	O I (1)	0.530	0.170	9.14−10.74	0.29	+8.73
7775.758	7775.40	O I (1)	0.206	−0.050	9.14−10.74	0.36	+11.43

† : The identification of this carbon line is uncertain and needs to be confirmed.

Table 5.3b: Emission lines in IRAS17311-4924 (Hen3-1428)

$\lambda_{obs.}$ (Å)	$\lambda_{lab.}$ (Å)	Ident.	W_λ (Å)	log (gf)	χ (eV)	$\Delta\lambda$ (Å)	V_r kms^{-1}
5041.587	5041.063	Si II (5)	0.090	0.290	10.07–12.53	0.52	+28.48
5056.567	5056.020	Si II (5)	0.159	0.590	10.07–12.53		
	+ 5056.353	Si II (5)					
5122.337	5121.69	C II (12)	0.078			0.65	+35.61
5159.448	5158.81	[Fe II] (19F)	0.049			0.64	+34.76
5194.499	5193.89	Fe III (5)	0.018	−2.852	8.66–11.04	0.61	+32.77
5198.536	5197.569	Fe II (49)	0.058	−2.116	12.78–10.40	0.97	+53.53
5200.833		UN	0.021				
5243.995	5243.30	Fe III (113)	0.052	0.405	18.27–20.64	0.69	+37.02
5262.232	5261.61	[Fe II] (19F)	0.039			0.62	+32.89
5273.963	5273.38	[Fe II] (18F)	0.025			0.58	+30.53
5282.827	5282.10	Fe III (113)	0.024	0.108	18.27–20.61	0.73	+39.00
5299.617	5299.00	O I (26)	0.043	−2.140	10.99–13.33	0.62	+32.64
5516.036	5515.083	V I (2)	0.091	−3.570	0.07–2.31		
	± 5515.371	V I (1)					
5535.918	5535.382	V I (1)	0.035	−4.043	0.02–2.25	0.54	+26.81
5538.288	5537.756	Mn I (4)	0.037	−2.017	2.19–4.42		
5555.591	5554.94	O I (24)	0.034	−2.110	10.99–13.22	0.65	+32.64
5577.334	5576.61	Si II (9)	0.033			0.72	+36.27
5577.822	5577.35	[O I] (3F)	0.052			0.47	+22.82
5805.573	5804.91	Fe II (165)	0.093	−3.726	5.57–7.71		
5920.884	5920.00	Fe III (115)	0.064	0.349	22.55–24.64		
5954.28	5953.65	Fe III (115)	0.040	0.186	18.79–20.87		
5958.19	5957.612	Si II (4)	0.160	−0.300	10.07–12.15	0.58	+26.75
5959.218	5958.46	O I (23)	0.042				
	+ 5958.63	O I (23)					
5979.628	5978.970	Si II (4)	0.371	0.000	10.08–12.15	0.66	+30.66
6000.275	5999.30	Fe III (117)	0.058	0.355	18.82–20.88	0.97	+46.04
6033.299	6032.30	Fe III (117)	0.072	0.497	18.82–20.87	1.00	+47.27
6047.116	6046.46	O I (22)	0.059	−1.670	10.99–13.04	0.66	+30.29
6095.937	6095.37	C II (24)	0.032			0.57	+25.59
6099.241	6098.62	C II (24)	0.077			0.62	+28.04
6152.143	6150.90	N II (36)	0.109	−0.930	23.13–25.14	1.24	+58.02
6244.098	6243.11	V I (19)	0.044	−0.878	0.30–2.28		
6257.705	6256.906	V I (19)	0.017	−2.192	0.27–2.25		
6260.245	6258.595	V I (19)	0.027	−1.842	0.26–2.24		
6300.892	6300.23	[O I] (1F)	0.714	−9.820		0.66	+28.97
6347.775	6347.091	Si II (2)	0.330	0.300	8.12–10.07	0.68	+29.68
6364.336	6363.88	[O I] (1F)	0.202	−10.300		0.46	+19.22
6372.12	6371.359	Si II (2)	0.150	0.000	8.12–10.07	0.76	+33.32
6462.481	6462.210	Mn II (20)					
	+ 6462.454	Mn II (20)					

Table 5.3b: contd...

$\lambda_{obs.}$ (Å)	$\lambda_{lab.}$ (Å)	Ident.	W_λ (Å)	log (gf)	χ (eV)	$\Delta\lambda$ (Å)	V_r kms^{-1}
6546.685	6545.80	Mg II (23)	0.029				
6548.828	6548.1	[N II] (1F)	0.151			0.73	+30.98
6611.319	6610.58	N II (31)	0.044	0.430	21.60–23.48		
6731.646	6730.79	C II (21)	0.046				
6751.503	6750.22	C II (21)	0.032				
7002.958	7001.93	O I (21)	0.099	−1.050	10.99–12.76		
	+ 7002.22	O I (21)		−0.780	10.99–12.76		
7042.795	7042.06	Al II (3)	0.070	0.350	11.32–13.08	0.73	+28.64
7053.928	7052.9	C II (26)	0.037			1.03	+41.35
7057.484	7056.60	Al II (3)	0.046	0.130	11.32–13.07	0.88	+34.95
7113.732	7112.36	C II (20)	0.031				
7116.453	7115.13	C II (20)	0.022				
7156.018	7155.14	[Fe II] (14F)	0.033				
7232.061	7231.12	C II (3)	0.850			0.94	+36.54
7237.242	7236.19	C II (3)	1.168			1.05	+41.07
7255.18	7254.19	O I (20)	0.121	−1.320	10.99–12.70		
	+ 7254.47	O I (20)		−1.100	10.99–12.70		
7443.13	7442.28	N I (3)	0.035	−0.450	10.33–11.99	0.85	+31.80
7469.175	7468.29	N I (3)	0.052	−0.270	10.33–11.99	0.88	+32.89
7877.873	7877.13	Mg II (8)	0.184	0.390	10.00–11.57	0.74	+25.72
7897.135	7896.37	Mg II (8)	0.359	0.650	10.00–11.57	0.76	+26.41
8000.937	8000.12	[Cr II] (1F)	0.079			0.82	+28.29
8126.345	8125.50	[Cr II] (1F)	0.045			0.84	+28.55
8188.889	8187.95	N I (2)	0.047			0.94	+31.98
8217.317	8216.28	N I (2)	0.067			1.04	+35.51
8224.207	8223.07	N I (2)	0.094			1.14	+39.13

Table 5.3c: Lines with P-Cygni profiles in IRAS17311-4924 (Hen3-1428). Equivalent widths of the absorption and emission components of the P-Cygni profiles are given.

λ_{lab} (Å)	Ident.	W_λ (absorption) (Å)	W_λ (emission) (Å)	log (gf)	χ (eV)
5015.675	He I (4)	0.183	0.319	−0.820	20.62−23.09
5127.463	Fe III (5)	0.070	0.025	−2.218	8.65−11.07
5156.00	Fe III (5)	0.037	0.035	−2.018	8.64−11.04
5875.618	He I (11)		0.992	0.410	20.97−23.08
+ 5875.650	He I (11)			−0.140	20.97−23.08
+ 5875.989	He I (11)			−0.210	20.97−23.08
6562.817	H_α		9.872	0.710	10.15−12.04
6578.03	C II (2)	0.327	0.082	0.120	14.45−16.33
6582.85†	C II (2)	0.269		−0.180	14.45−16.33
6678.149	He I (46)	0.417	0.412	0.330	21.22−23.08
7065.188	He I (10)	0.137	1.062	−0.460	20.96−22.72
+ 7065.719	He I (10)			−1.160	20.96−22.72
7281.349	He I (45)	0.151	0.229	−0.840	21.22−22.92

Two blended absorption components are visible in the P-Cygni profile of He I(11). The emission peak of the H_α P-Cygni profile is asymmetric indicating two emission components blended together. Owing to the broad wings of the emission component in H_α, the absorption component of the P-Cygni profile lies above the normalised continuum (see Fig. 5.2). †: the emission component of C II(2) 6582.85Å P-Cygni profile is blended with [N II](1F) 6583.6Å

Table 5.3d: Absorption (a) and emission (e) components of Na I D_2 (5889.953Å) and Na I D_1 (5895.923Å) lines in the spectrum of IRAS17311-4924 (Hen3-1428). W_λ are the equivalent widths of the components and V_r are the respecitve heliocentric radial velocities.

Component		IRAS17311-4924					
		Na I D_2			Na I D_1		
		$\lambda_{obs.}$ (Å)	W_λ (Å)	V_r (kms^{-1})	λ_{lab} (Å)	W_λ (Å)	V_r (kms^{-1})
1.	a	5889.886	0.552	−5.87	5895.875	0.479	−4.90
2.	a	5890.334	0.121	+16.94	5896.331	0.121	+18.30
3.	e	5890.677	0.096	+34.41	5896.695	0.020	+36.82

Table 5.4: Average radial velocities measured for individual species along with the probable error. n refers to the number of lines used.

Species	IRAS13266-5551			IRAS17311-4924		
	n	$\overline{LEP}$ (eV)	V_r (kms^{-1})	n	$\overline{LEP}$ (eV)	V_r (kms^{-1})
He I	1	21.22	+75.10			
C II	5	19.46	+64.80 ± 4.44	2	20.70	+21.16 ± 2.16
N II	10	18.96	+68.42 ± 1.68	7	18.47	+27.49 ± 2.28
O II	7	25.66	+67.86 ± 1.72	2	23.43	+41.32† ± 0.33
Ne I	4	16.63	+72.85 ± 1.01	8	16.66	+11.32 ± 0.72
Al III	2	15.64	+79.07 ± 0.68	1	15.64	+40.53
Si III	1	19.72	+69.95	1	19.72	+38.83
Fe III	3	11.94	+83.14 ± 4.84			

Average radial velocity of the O II lines in IRAS17311-4924 (Hen3-1428) indicates that they may originate in a different atmospheric region of the star (see Sec. 5.3.6.3).

6203.060Å and 6613.630Å . Their heliocentric radial velocities (V_r, Tables 5.2a and 5.3a) agree with their interstellar origin. From the strength of the band at 5780.410Å (W_λ = 156mÅ and 126mÅ for IRAS 13266-5551 and IRAS17311-4924 respectively), we estimate interstellar E(B−V) $\simeq$ 0.33 and 0.26 respectively for IRAS13266-5551 (CPD-55 5588) and IRAS17311-4924 (Hen3-1428) (Herbig, 1993). At the galactic latitude and longitude of these stars, using the Diffuse Infrared Background Experiment (DIRBE)/IRAS dust maps (Schlegel et al., 1998), we estimated interstellar extinction values of 0.53 and 0.22 respectively. Herbig (1993) admits that although the DIB strengths increase linearly with E(B−V), there is a real dispersion about the mean relationship. Eg. from their data, HD144470 and HD37061 both have about the same DIB strengths despite large differences in their values of E(B−V), 0.22 and 0.56 respectively.

5.3.4 Na I D_2 and Na I D_1 lines

The Na I D_2 and Na I D_1 lines in the spectra of IRAS13266-5551 (CPD-55 5588) and IRAS17311-4924 (Hen3-1428) show both absorption and emission components (Fig. 5.1, Tables 5.2d and 5.3d). Comparing the radial velocities of these components with the average radial velocities for each star (Sec. 5.3.2), it is evident that the absorption components 1,2 and 3 in IRAS13266-5551 (CPD-55 5588) and component 1 in IRAS17311-4924 (Hen3-1428) are of interstellar origin. Components 4 and 2 in IRAS13266-5551 (CPD-55 5588) and IRAS17311-4924 (Hen3-1428) may be of circumstellar origin indicating the presence of neutral circumstellar envelopes in addition to the cold detached dust shells and low excitation nebulae. Radial velocities of the emission components of the NaI lines are very close to the mean radial velocity of emission lines in IRAS13266-5551 (= +58.56 kms^{-1}) and IRAS17311-4924 (= +33.50 kms^{-1}) respectively indicating that the emission components belong to the circumstellar matter.

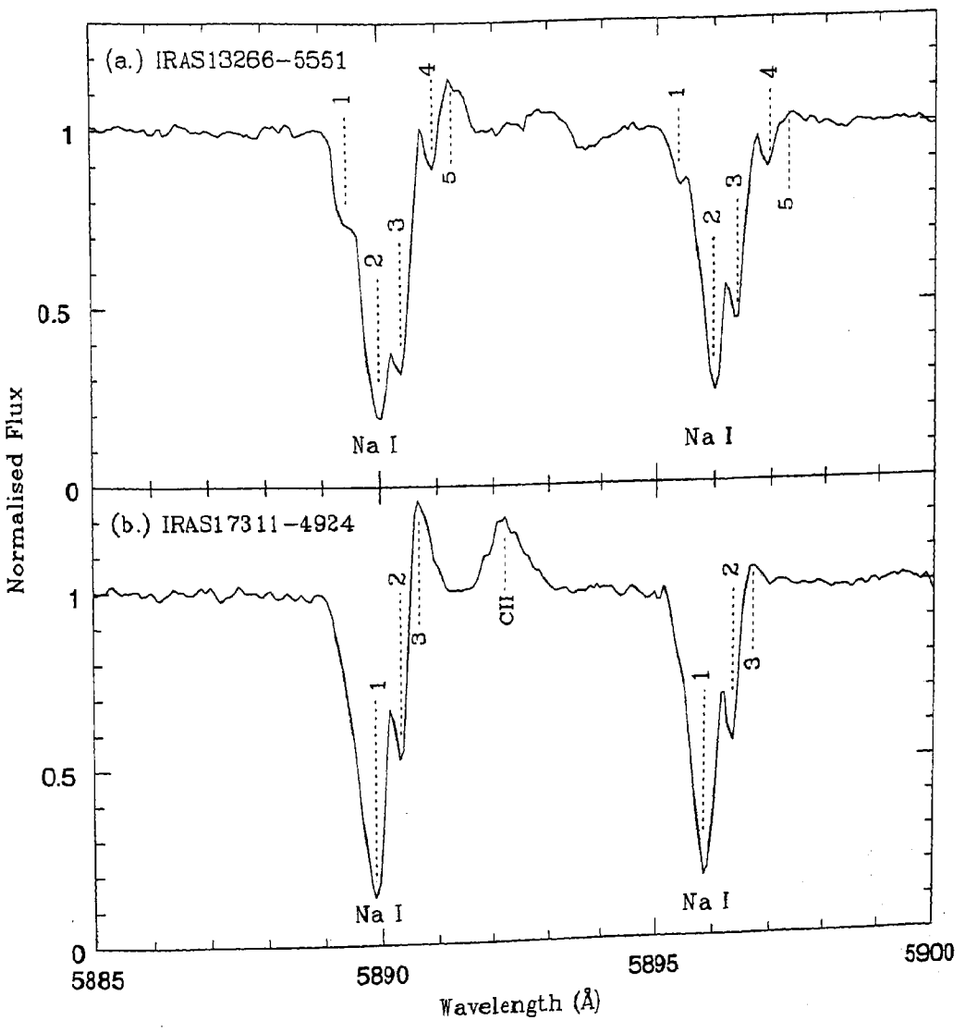

Figure 5.1: Na I D_2 and Na I D_1 lines in the spectra of (a.) IRAS13266-5551 (CPD-55 5588) and (b.) IRAS17311-4924 (Hen3-1428). The various absorption and emission components of the lines have been labelled.

5.3.5 H_α profile and mass loss rate

H_α profiles of the two stars are shown in Fig. 5.2. The wavelengths were converted to velocity units relative to the laboratory wavelength of the H_α line, 6562.817Å The zero point was then adjusted for the heliocentric radial velocity of each star. The wings of H_α can be seen upto about 220 and 180 kms^{-1} in IRAS13266-5551 (CPD-55 5588) and IRAS17311-4924 (Hen3-1428) respectively.

The P-Cygni profile of H_α indicates ongoing mass-loss. Model calculations by Klein and Castor (1978) predicted a tight relationship between the H_α luminosity of the stellar wind and mass loss rate. The H_α luminosity is related to the equivalent width of the H_α emission line (see eg. Conti and Frost, 1977; Ebbets, 1982). The equivalent widths of the H_α emission components are 6.902Å and 9.872Å in IRAS13266-5551 (CPD-55 5588) and IRAS17311-4924 (Hen3-1428) respectively (Tables 5.2c and 5.3c). Modelling the H_α profiles to derive the mass loss rates of post-AGB stars would be the subject of a future paper. Here, we may compare our H_α profiles with the B1.5Ia star, BD-14° 5037. The observed equivalent width of the H_α emission component in this star is 7.4Å . From the H_α profile, Leitherer (1988) derived a mass loss rate of $1.58X10^{-6}$ $M_\odot$ yr^{-1}.

5.3.6 Atmospheric parameters and abundances

The presence of He I lines and the absence of He II lines in IRAS13266-5551 (CPD-55 5588) and IRAS17311-4924 (Hen3-1428) indicates 18000K $\leq T_{eff} \leq$ 25000K (Miroshnichenko et al., 1998). We used Kurucz's WIDTH9 program and the spectrum synthesis code, SYNSPEC (Hubeny et al., 1985) along with solar metallicity Kurucz (1994) model atmospheres to derive the atmospheric parameters and elemental abundances under the LTE approximation.

The usual criterion for determining the effective temperature (T_{eff}), gravity (log g) and microturbulent velocity (ξ_t) of a star, is to obtain a zero slope respectively in plots of (i) log abundances for a particular species Vs. lower excitation potentials of that species (ii) log abundances for two species of a particular element (eg. Fe II

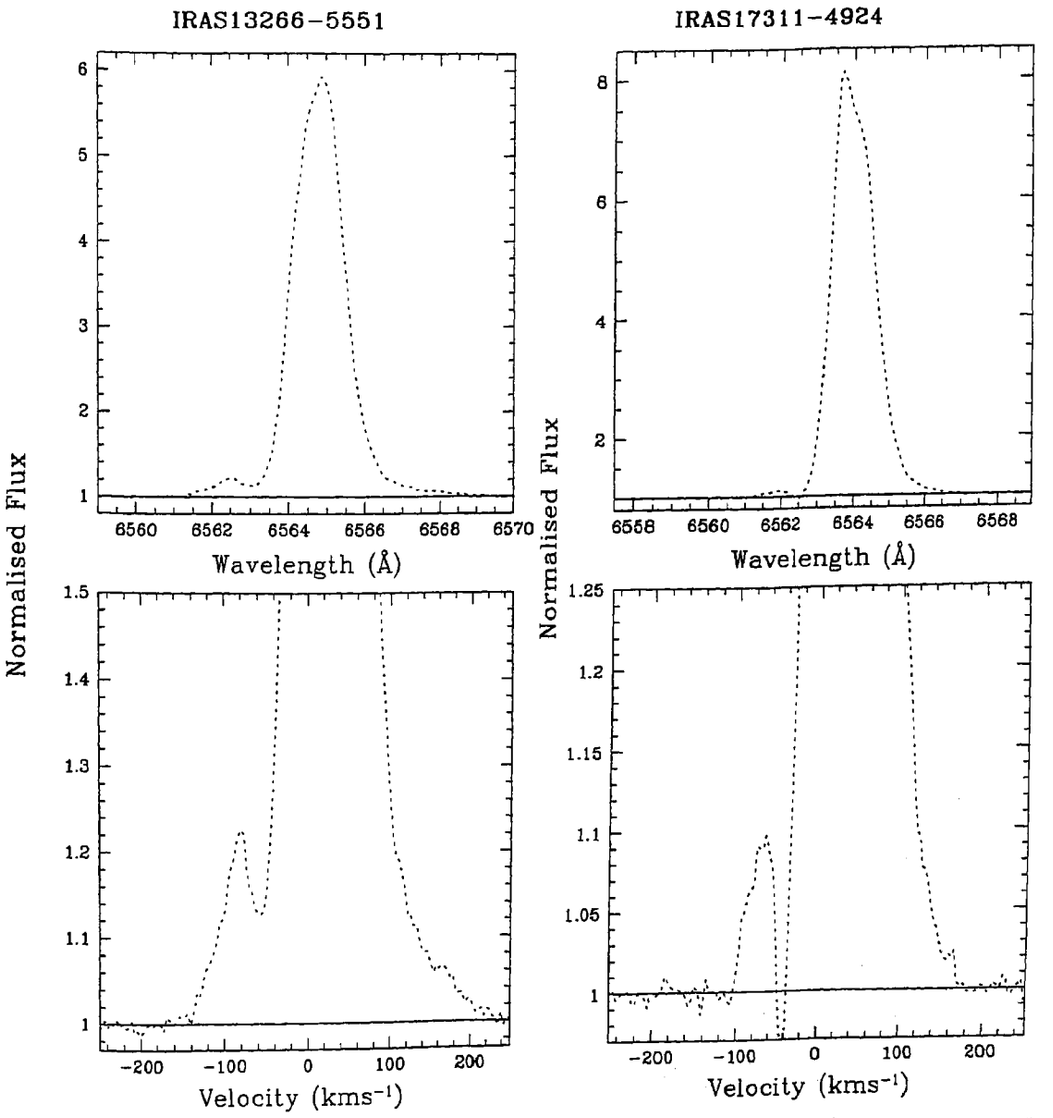

Figure 5.2: The normalised H_α profiles (dotted lines) of IRAS13266-5551 (CPD-55 5588) and IRAS17311-4924 (Hen3-1428)

and Fe III) Vs. lower excitation potentials and (iii) log abundances for a particular species Vs. equivalent widths.

The maximum number of absorption lines in the spectrum of IRAS13266-5551 (CPD-55 5588) are those of N II. The majority of the N II lines are strong with $W_\lambda \geq 100$ mÅ . Besides, the observed N II lines fall in a narrow range of lower excitation potentials (Tables 5.2a and 5.3a). This coupled with the lack of two ionisation species of any element does not allow us to employ the usual criterion for determining T_{eff}, log g and ξ_t. Hence, for IRAS13266-5551 (CPD-55 5588) we obtained abundances of N II, O II, and Fe III with the WIDTH9 program for various combinations of T_{eff}, log g and ξ_t. We covered 18000K $\leq T_{eff} \leq$ 24000K and 5 kms^{-1} $\leq \xi_t \leq$ 45 kms^{-1}. From the Kurucz (1994) model atmospheres, the log g value was limited to a minimum of 3.0. For each combination of these parameters, we then synthesised the spectrum using SYNSPEC. The best fit to the observed spectrum was obtained for T_{eff} = 23000K, log g = 3.0, ξ_t = 10 kms^{-1} (Fig. 5.3).

IRAS17311-4924 (Hen3-1428) has fewer absorption lines. The maximum number (8) of absorption lines that we find in our spectrum are those of N II and Ne I. While the N II lines are strong with $W_\lambda \geq 100$ mA, the Ne I lines are very sensitive to NLTE effects (see Sec. 5.3.6.4 below). Due to the small number of C II, N II and O II lines and the lack of iron lines, we were unable to estimate the atmospheric parameters and metallicity of this star using the WIDTH9 program and the SYNSPEC code. The star suffers significant circumstellar extinction, $E(B-V)_{c.s.}$ = 0.39 (Gauba and Parthasarathy, 2003b) and the circumstellar extinction law in the UV was found to be linear in λ^{-1}. Hence, the (B−V) color of the star cannot be used for temperature estimation. An estimate of the temperature and gravity may be made from the spectral type of the star. Parthasarathy et al. (2000b) classified it as B1IIe which corresponds to T_{eff} = 20300K and log g = 3.0 (Lang, 1992).

5.3.6.1 C II lines

We observed 8 C II lines in IRAS13266-5551 (CPD-55 5588) and 5 C II lines in IRAS17311-4924 (Hen3-1428). Some of these lines are noisy and some of them are

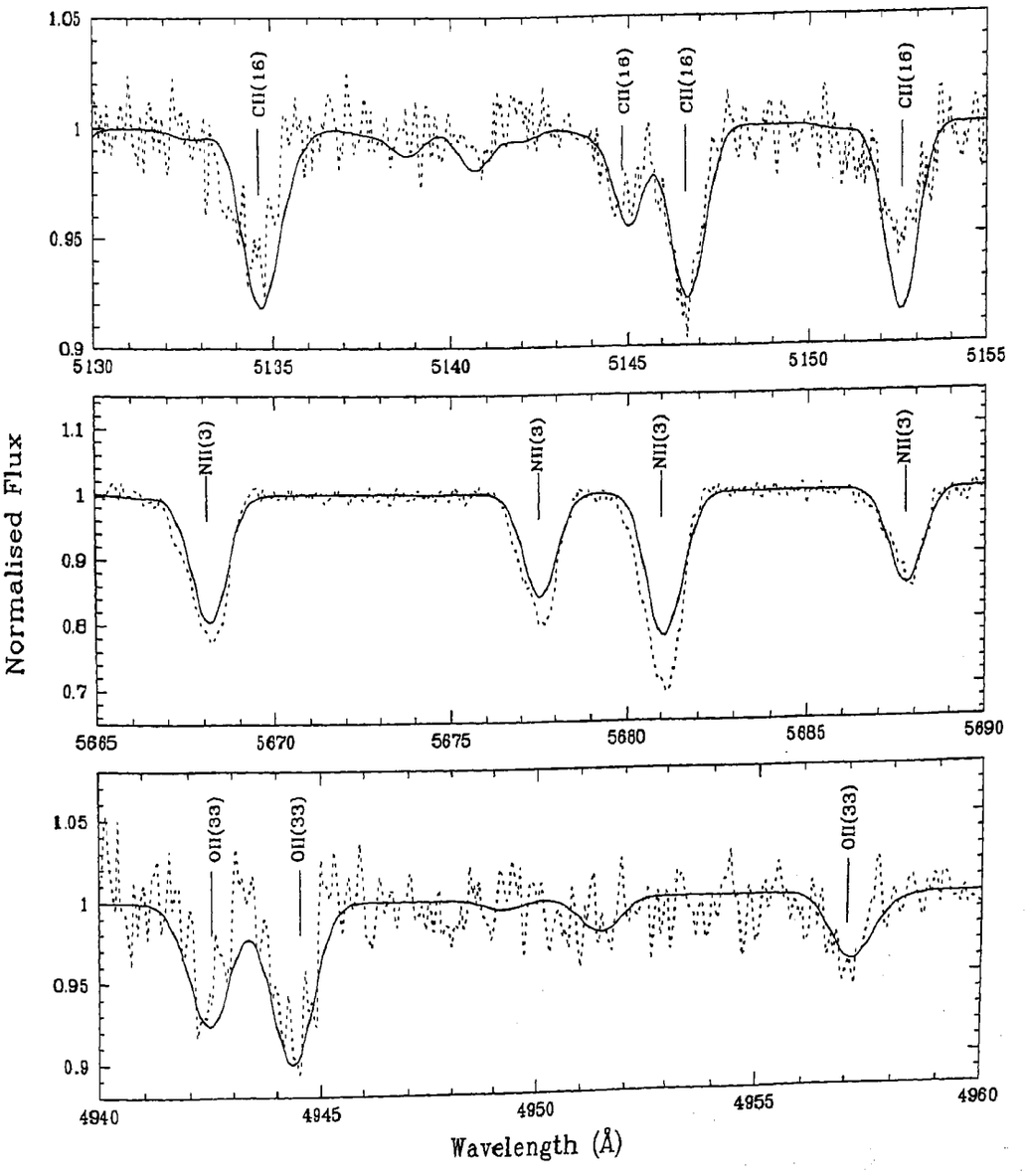

Figure 5.3: Regions showing the C II, N II and O II absorption lines in the observed spectrum (dotted line) of IRAS13266-5551 (CPD-55 5588) plotted along with the synthetic spectrum (solid line) for the derived atmospheric parameters (T_{eff} = 23000K, log g = 3.0, ξ_t = 10 kms^{-1}) and elemental abundances (Table 5.5) of the star.

Table 5.5: Derived chemical composition of IRAS13266-55551 (CPD-55 5588). The abundances are for log ϵ(H) = 12.0. Solar abundances log $\epsilon(X)_\odot$ are from Anders & Grevesse (1989). n refers to the number of lines of each species used for the abundance determination. For comparison we have listed the average abundances of main sequence B-stars from the Ori OB1 association (Kilian, 1992)

	IRAS13266-5551 (CPD-55 5588) (23000, 3.0, 10)					Main sequence B-stars, Ori OB1
X	n	log $\epsilon(X)$	[X/H]	[X/Fe]	log $\epsilon(X)_\odot$	log ϵ(X)
He I	1	11.26†	+0.27		10.99	
C II	5	8.69†	+0.17	+0.55	8.52	8.23
N II	10	8.87±0.27	+0.86	+1.24	8.01	7.72
O II	5	8.97±0.52	+0.08	+0.46	8.89	8.60
Ne I	4	9.05±0.27*	+1.00		8.05	
Fe III	4	7.25±0.32	−0.38		7.63	

The abundances were derived using Kurucz's WIDTH9 program (modified for Unix machines by John Lester at the University of Tornonto, Canada). † : these values were derived from spectrum synthesis analysis using the SYNSPEC code. *: Ne abundances derived using Kurucz's WIDTH9 program appear to be in error. For the atmospheric parameters of the star, the observed Ne I lines are much stronger than the corresponding lines synthesised with the SYNSPEC code. NLTE effects may be significant for these lines (see Sec. 5.3.6.4)

blended with other C II lines. Hence, the carbon abundance in IRAS13266-5551 (CPD-55 5588) was estimated only from spectrum synthesis using SYNSPEC. The ISO spectrum of IRAS17311-4924 (Hen3-1428) (Gauba and Parthasarathy, 2003c) indicated carbon-rich circumstellar dust. The presence of carbon lines and their strengths compared to that of standard stars in the UV (Gauba and Parthasarathy, 2003b) and optical spectra of this star indicate normal or slight overabundance of carbon.

5.3.6.2 N II lines

Maximum number of absorption lines in both the stars are due to N II. The majority of these lines are strong with $W_\lambda \geq 100$ mÅ . Since such strong lines are usually effected by microturbulence, the use of these lines in determining the atmospheric parameters of the star may contribute to systematic errors. The very strong lines eg. N II(3) 5679.56Å ($W_\lambda = 410$ mÅ) and N II(3) 5666.64Å ($W_\lambda = 287$ mÅ) in IRAS13266-5551 (CPD-55 5588) have been excluded from the abundance analysis.

5.3.6.3 O I triplet and O II lines

The intensity of the O I triplet increases with luminosity (Faraggiana et al., 1988). The equivalent widths of the O I triplet in the spectra of the hot post-AGB stars, LSII+34°26 (B1.5 Ia, García-Lario et al., 1997b; Arkhipova et al., 2001b) and IRAS01005+7910 (Klochkova et al., 2002) are 0.95Å and 0.75Å respectively. The (total) equivalent widths of the O I triplet in IRAS13266-5551 (CPD-55 5588) and IRAS17311-4924 are 0.74Å and 1.48Å respectively (Tables 5.2a and 5.3a). NLTE effects and circumstellar shells can enhance the strength of the O I triplet lines in the spectra of these stars. It may not be proper to use the width of these lines to estimate the luminosities of these stars (Parthasarathy, 1994).

The O I triplet at λ7773Å is known to be sensitive to NLTE effects. For the atmospheric parameters of IRAS13266-5551 (CPD-55 5588), using LTE analysis, we attempted to synthesise the O I triplet with the SYNSPEC code. This required oxygen abundances (log ϵ(O)) in excess of 10.5. In contrast, the derived oxygen

abundance using LTE analysis for the O II lines in IRAS13266-5551 (CPD-55 5588) is 8.97 (Table 5.5). Such large discrepancies between the oxygen abundances derived from the O I triplet and the O II lines has also been observed in the hot post-AGB star IRAS01005+7910 (Klochkova et al., 2002).

The O II lines at 5160.02Å (W_λ = 145 mÅ) and 6721.35Å (W_λ = 165 mÅ) in IRAS13266-5551 (CPD-55 5588) may also have significant NLTE effects. We could not obtain a good fit to these lines and they were excluded from the abundance analysis. In IRAS17311-4924 (Hen3-1428) absorption lines at 6641.881Å and 6722.322Å were detected. From the Moore multiplet table (1945), the best identification for these lines corresponded to O II(4) lines at $\lambda\lambda$ 6640.90Å and 6721.35Å respectively. These O II(4) lines have also been detected in the hot post-AGB star, IRAS20462+3416 (LSII+34°26; García-Lario et al., 1997b; Arkhipova et al., 2001b). However, this implied heliocentric radial velocities of +41.81 kms^{-1} and +40.83 kms^{-1} respectively for these two lines. These values are significantly different from the average radial velocities of the C II and N II lines in this star (Table 5.4). This suggests that these lines may originate in a different atmospheric region. No other O II lines were detected in IRAS17311-4924 (Hen3-1428).

5.3.6.4 Ne I lines

The derived neon abundance for IRAS13266-5551 (CPD-55 5588) is unusually high (Table 5.5). However, we could still not obtain a good fit to the majority of Ne I lines in the spectrum of this star. Auer and Mihalas (1973) showed that for stars in the range B2 to B5 the neon abundance deduced from LTE analyses is systematically in error by about a factor of five. They computed equivalent widths of Ne I lines ($\lambda\lambda$ 5852.5Å to 6598.9Å) for 15000K $\leq T_{eff} \leq$ 22500K, log g = 3.0 and 4.0 and solar neon abundance. For T_{eff} = 22500K, log g = 3.0, they found that the LTE equivalent widths were almost a factor of three smaller than the NLTE equivalent widths of these lines.

5.3.6.5 Al III and Si III lines

Only two lines of Al III and one of Si III were identified in each of the two stars. These lines are very strong (ref. Tables 5.2a and 5.3a) in both the stars. Eg. in IRAS13266-5551, Si III, 5739.734Å has $W_\lambda = 400$ mÅ . Using WIDTH9 and spectrum synthesis we derived $\log \epsilon$ (Al) $= 7.96 \pm 0.36$ and $\log \epsilon$ (Si) $= 9.23$ for IRAS13266-5551 (CPD-55 5588). However, these abundances may be an overestimate.

5.3.6.6 Iron lines

From the Fe III absorption lines, we estimated [Fe/H] $= -0.38$ in the case of IRAS13266-5551 (CPD-55 5588). The iron lines in IRAS17311-4924 only appear in emission or as P-Cygni profiles.

5.4 Discussion and conclusions

From LTE analysis of the high resolution optical spectrum of IRAS13266-5551 (CPD-55 5588) we find the atmospheric parameters to be $T_{\rm eff} = 23000$K $\pm$ 1000K, log g =3.0 $\pm$ 0.5 and $\xi_t = 10$ kms^{-1} $\pm$ 5 kms^{-1}. The lines of Ne I, a few O II lines and the O I triplet indicate that NLTE effects may be significant in these stars. Hence, we would like to emphasise that LTE is only a first approximation. Also, being hot stars it is important to obtain observations shortward of 4930Å . The absorption lines in the blue may significantly improve our estimates of the stellar parameters and elemental abundances. Eg. Mooney et al. (2002), Klochkova et al. (2002) and Ryans et al. (2003) have obtained observations from $\sim$ 3700Å onwards. Recently, from NLTE analysis of the absorption lines in the blue region, Ryans et al. (2003) estimated the atmospheric parameters of two hot post-AGB stars, IRAS18062+2410 (SAO85766) and IRAS19590-1249 (LSIV-12°111). A similar analysis is required for IRAS13266-5551 (CPD-55 5588) and IRAS17311-4924 (Hen3-1428). The major shortcoming in our data is that the absorption lines of a particular species are few and most of the lines of a species belong to the same multiplet thus making it difficult to obtain accurate estimates of the chemical abundances.

The F-type supergiant post-AGB star, IRAS11385-5517 (HD101584), also shows several permitted and forbidden emission lines and strong H_α P-Cygni profile (Sivarani et al., 1999). CO millimeter observations (Trams et al., 1990) and OH 1667 MHz maser emission (Te Lintel Hekkert et al., 1992) revealed the presence of bipolar outflows in this star. Te Lintel Hekkert et al. (1992) suggest that high-velocity outflows associated with axisymmetric geometries may be a general phenomenon for stars in the post-AGB phase of evolution. Similar bipolar outflows may also be detected in the hot post-AGB stars, IRAS13266-5551 (CPD-55 5588) and IRAS17311-4924 (Hen3-1428).

We estimated heliocentric radial velocities (V_r) of +67.55 kms^{-1} (V_{LSR} = 62.79 kms^{-1}) and +26.09 kms^{-1} (V_{LSR} = 27.20 kms^{-1}) for IRAS13266-5551 (CPD-55 5588) and IRAS17311-4924 (Hen3-1428) respectively.

Preliminary estimates of the CNO abundances in IRAS13266-5551 (CPD-55 5588) indicate that these elements are overabundant with [C/Fe]=+0.55, [N/Fe]=+1.24 and [O/Fe]=+0.46 suggesting that the products of Helium burning have been brought to the surface as a result of third dredge-up on the AGB. A comparison with average CNO abundances for mainsequence B-stars from the Ori OB1 association (Table 5.5; Kilian, 1992) also indicates that IRAS13266-5551 (CPD-55 5588) is an evolved star and has gone through the dredge-up episodes during its evolution. We could not estimate the atmospheric parameters and chemical abundances for IRAS17311-4924 (Hen3-1428).

McCausland et al. (1992) and Conlon et al. (1993c) derived the chemical composition of several high galactic latitude hot post-AGB stars. In addition to being metal-poor, these stars showed severe carbon deficiency. Similar carbon depletions were also reported in other hot post-AGB stars at high galactic latitudes eg. LSII+34°26 (García-Lario et al., 1997b), PG1323-086 and PG1704+222 (Moehler and Heber, 1998) and SAO85766 (Parthasarathy et al., 2000b). However, the relatively large number of carbon lines in IRAS13266-5551 (CPD-55 5588) and IRAS17311-4924 (Hen3-1428) suggests that these stars may be carbon-rich similar to the hot post-AGB star IRAS01005+7910 (Klochkova et al., 2002). A better and more detailed abun-

dance analysis of these stars is required.

Finally, from our optical spectra we conclulde that IRAS13266-5551 (CPD-55 5588) and IRAS17311-4924 (Hen3-1428) are most likely in the post-AGB phase of evolution. These stars are unlikely to be luminous blue variables (LBVs). Their spectra are very similar to the hot post-AGB stars IRAS18062+2410 (SAO85766; Parthasarathy et al., 2000b) and IRAS01005+7910 (Klochkova et al., 2002). LBVs are usually found in the galactic plane and are often associated with star forming regions. IRAS13266-5551 (CPD-55 5588) and IRAS17311-4924 (Hen3-1428) on the other hand, are at high galactic latitudes and are not associated with any star forming region. Further, LBVs are characterised by large amplitude variations. In contrast, hot post-AGB stars such as IRAS18062+2410 (SAO85766) were observed to have small amplitude, irregular rapid light variations in the optical (Arkhipova, 1999, 2000).

Acknowledgements : Based on observations made with the Victor M. Blanco 4m telescope of the Cerro Tololo Inter-American Observatory (CTIO), Chile.
We would like to thank John Lester at the University of Toronto, Canada for having kindly provided the Unix version of the WIDTH9 program.

Appendix A: High resolution spectrum of IRAS 13266-5551 (CPD-55 5588)

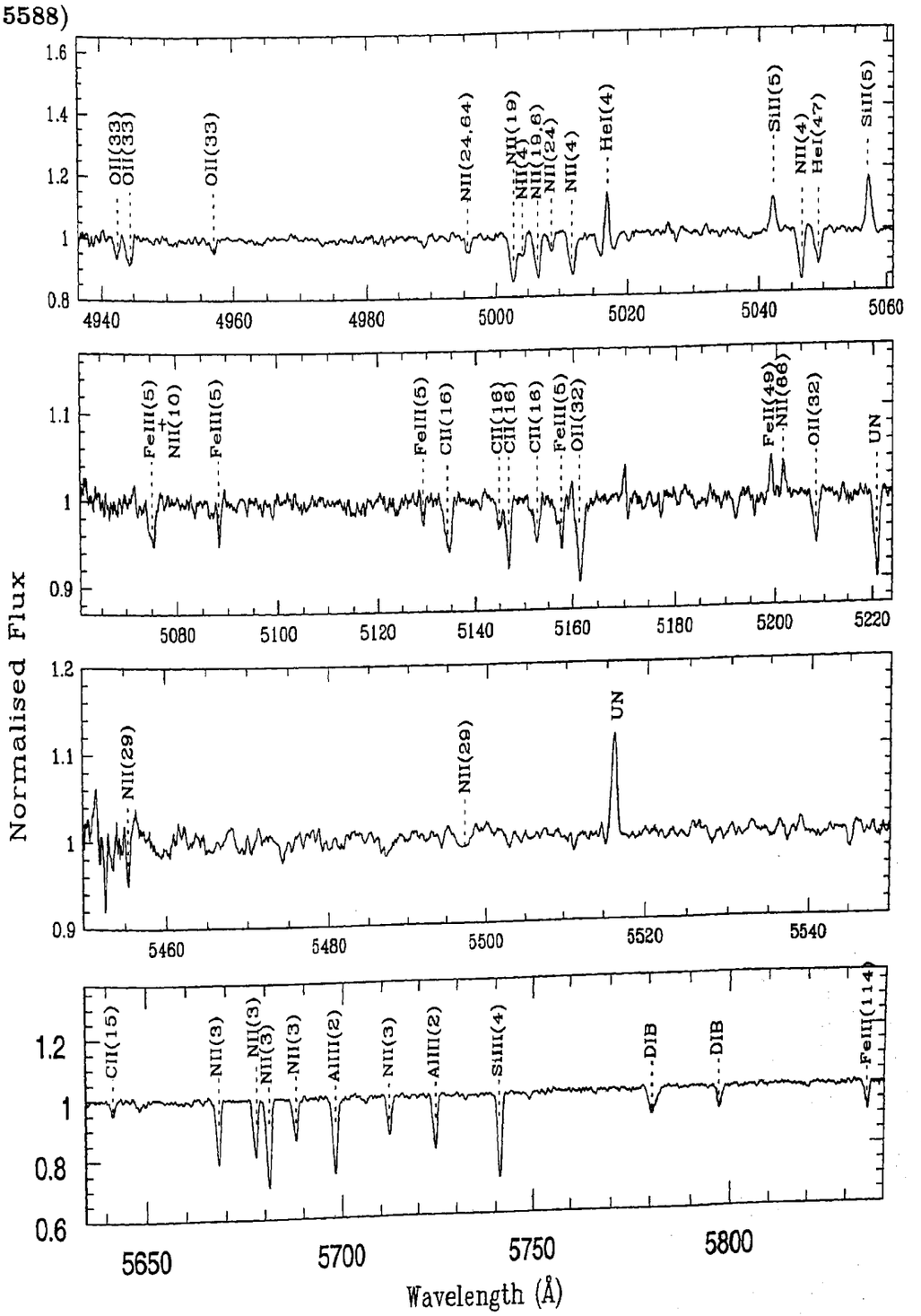

Figure A: Optical spectrum of IRAS13266-5551 (CPD-55 5588)

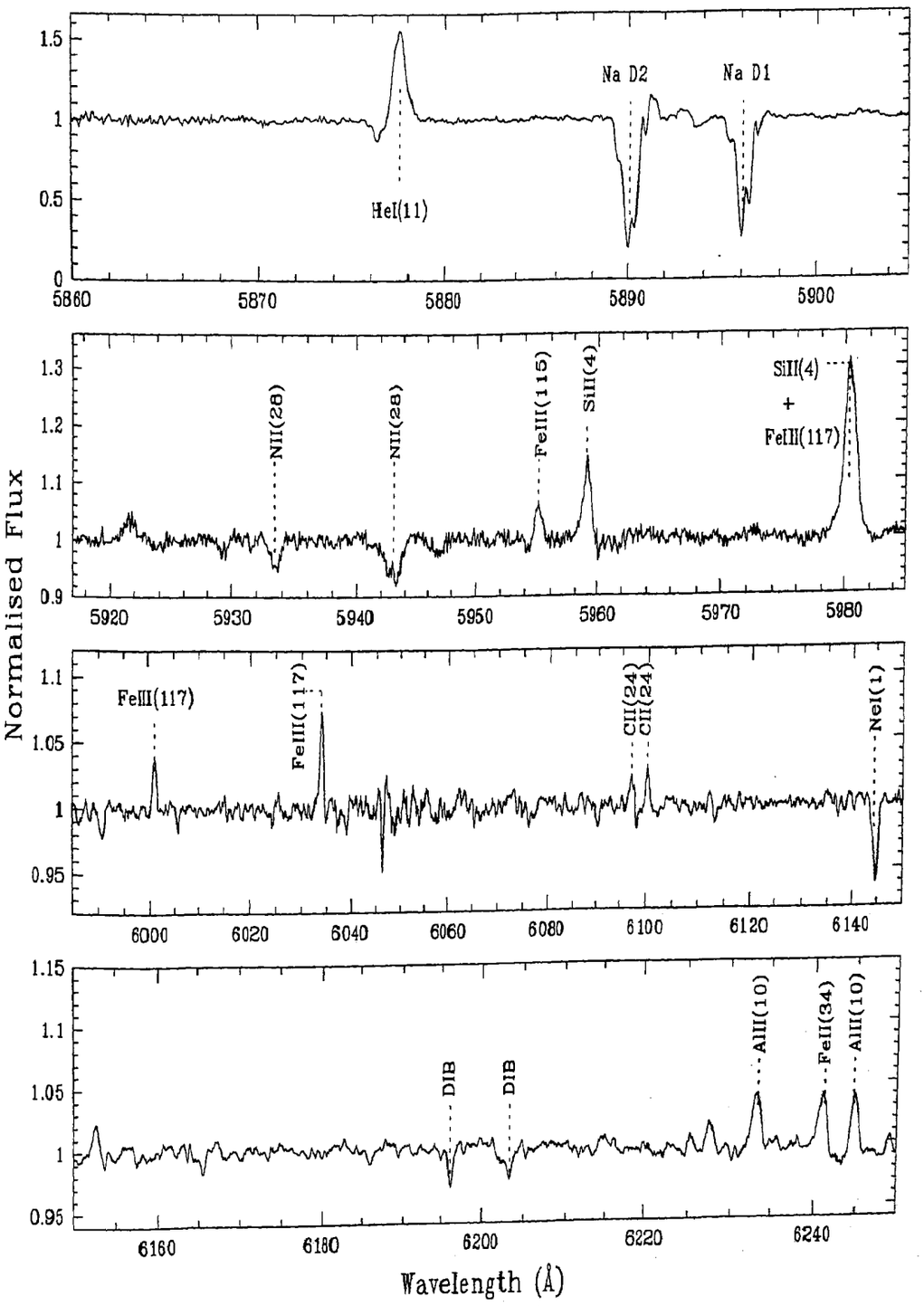

Figure A: Optical spectrum of IRAS13266-5551 (CPD-55 5588) contd...

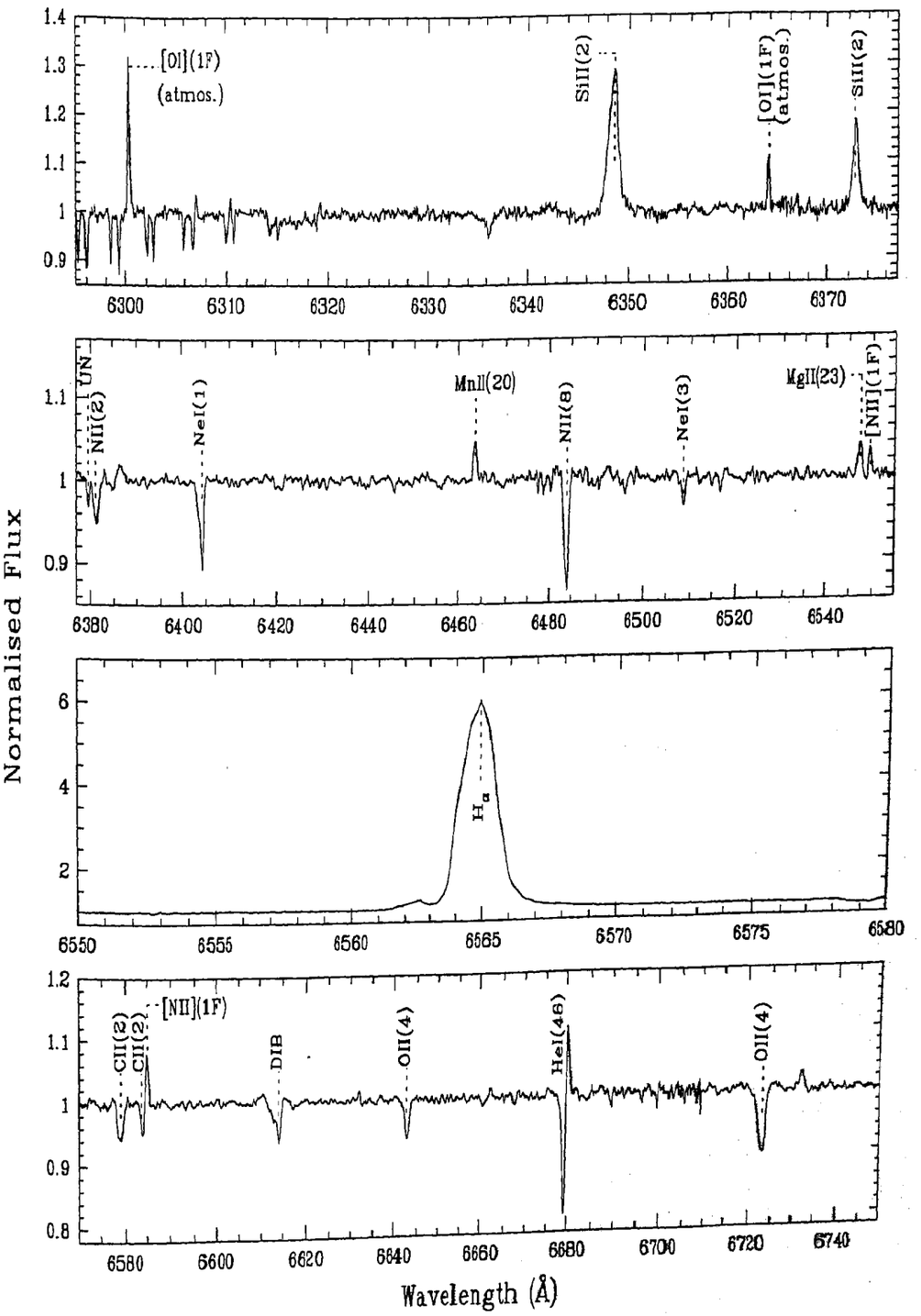

Figure A: Optical spectrum of IRAS13266-5551 (CPD-55 5588) contd...

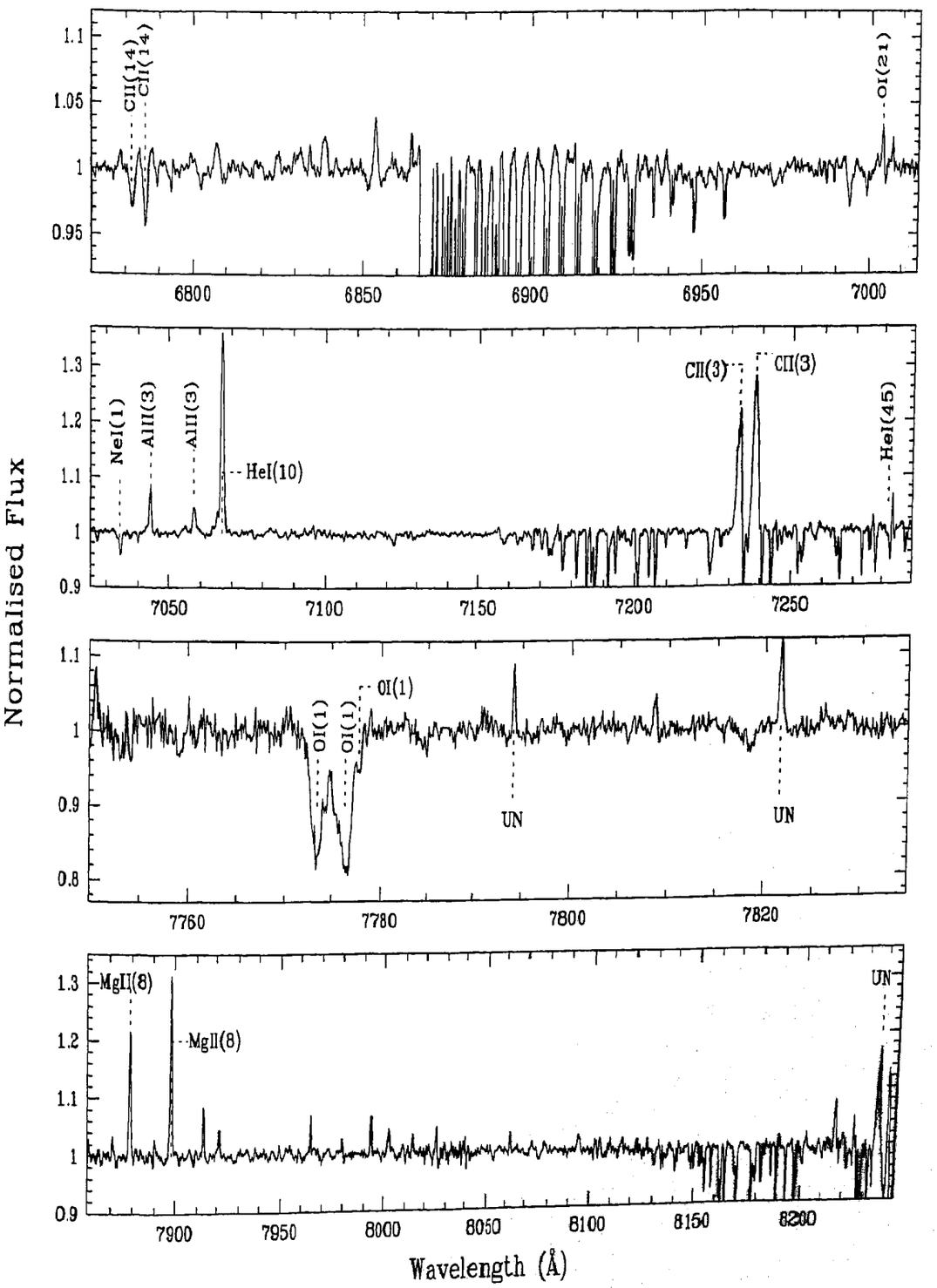

Figure A: Optical spectrum of IRAS13266-5551 (CPD-55 5588) contd...

Appendix B: High resolution spectrum of IRAS17311-4924 (Hen3-1428)

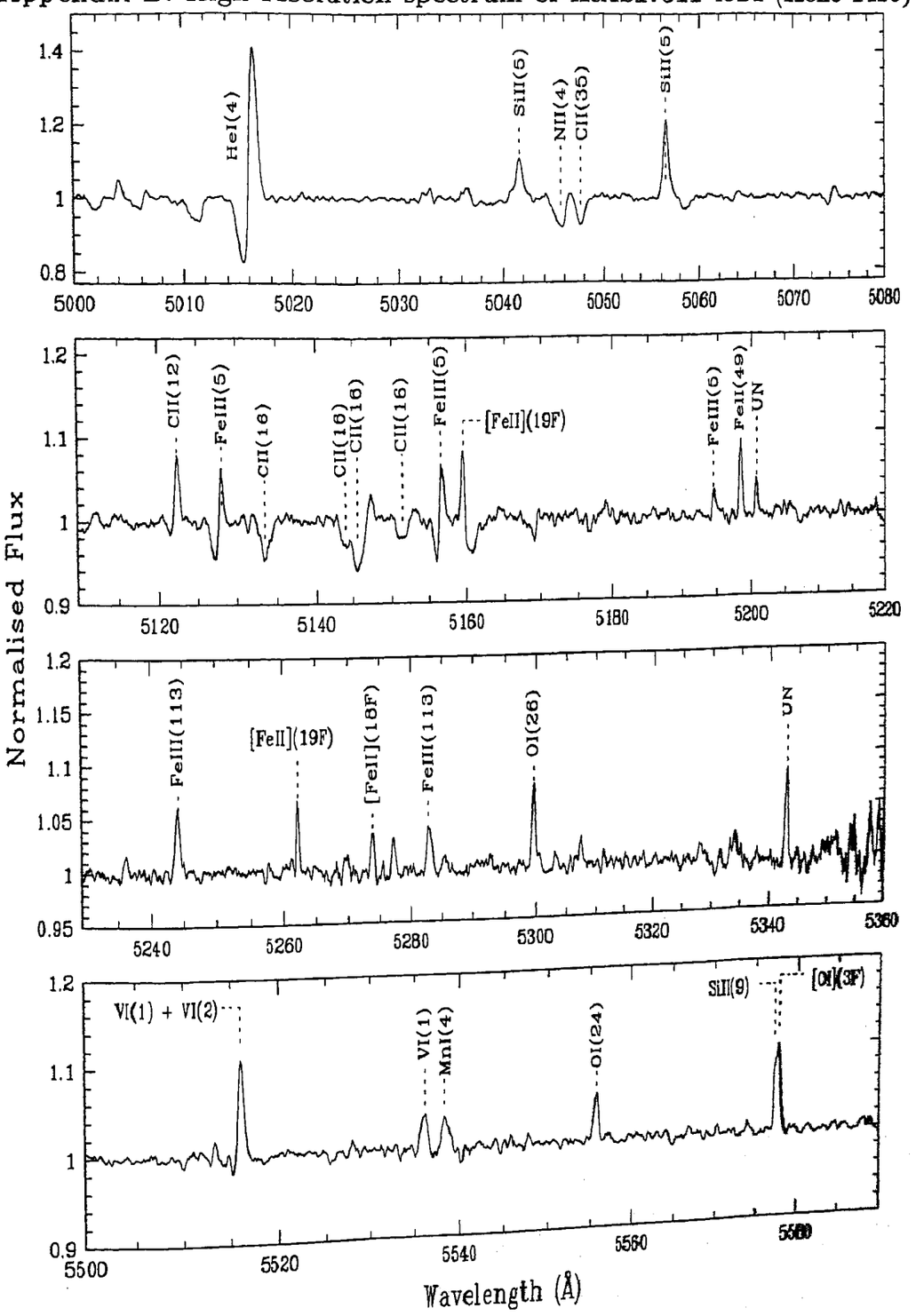

Figure B: Optical spectrum of IRAS17311-4924 (Hen3-1428)

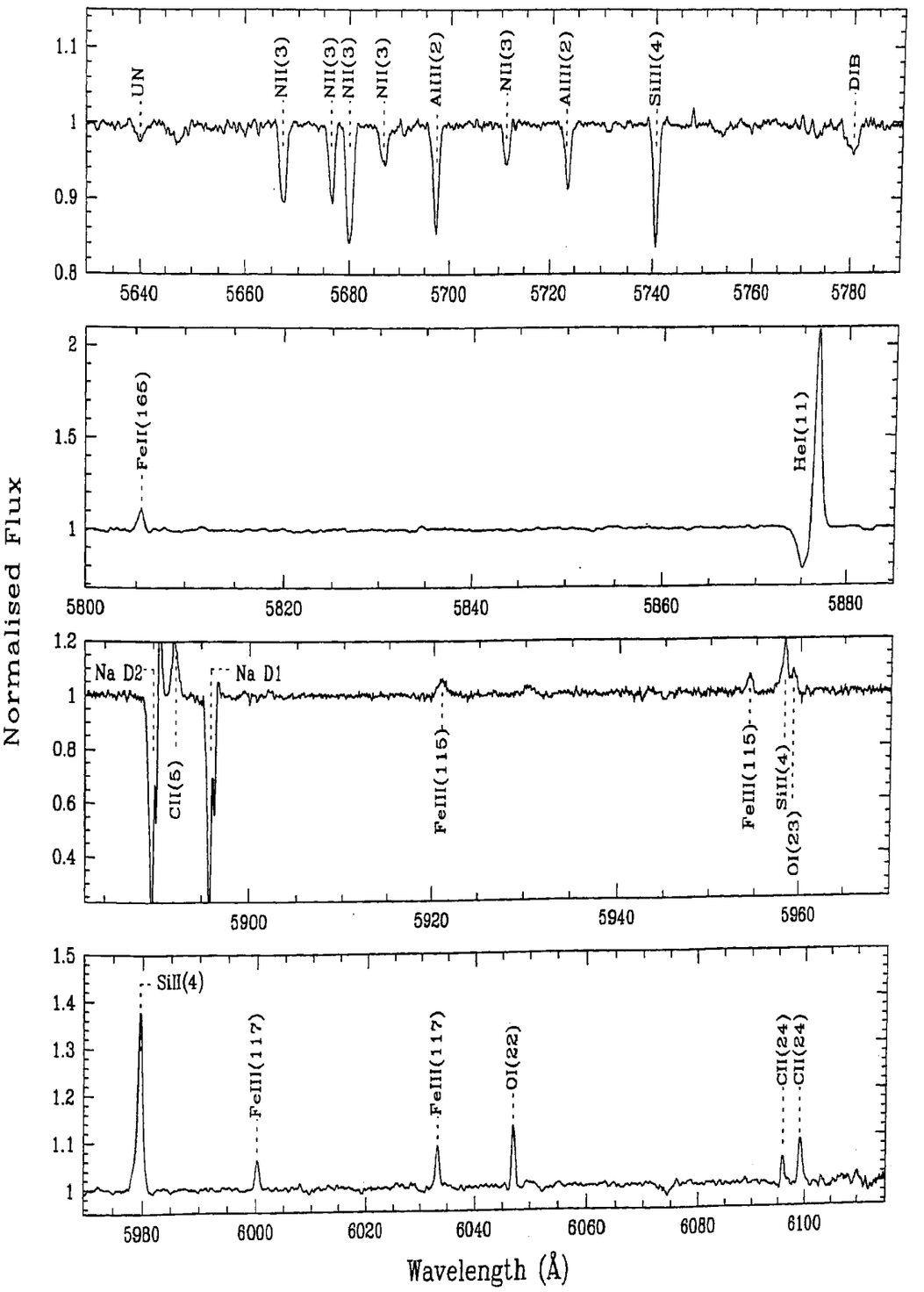

Figure B: Optical spectrum of IRAS17311-4924 (Hen3-1428) contd...

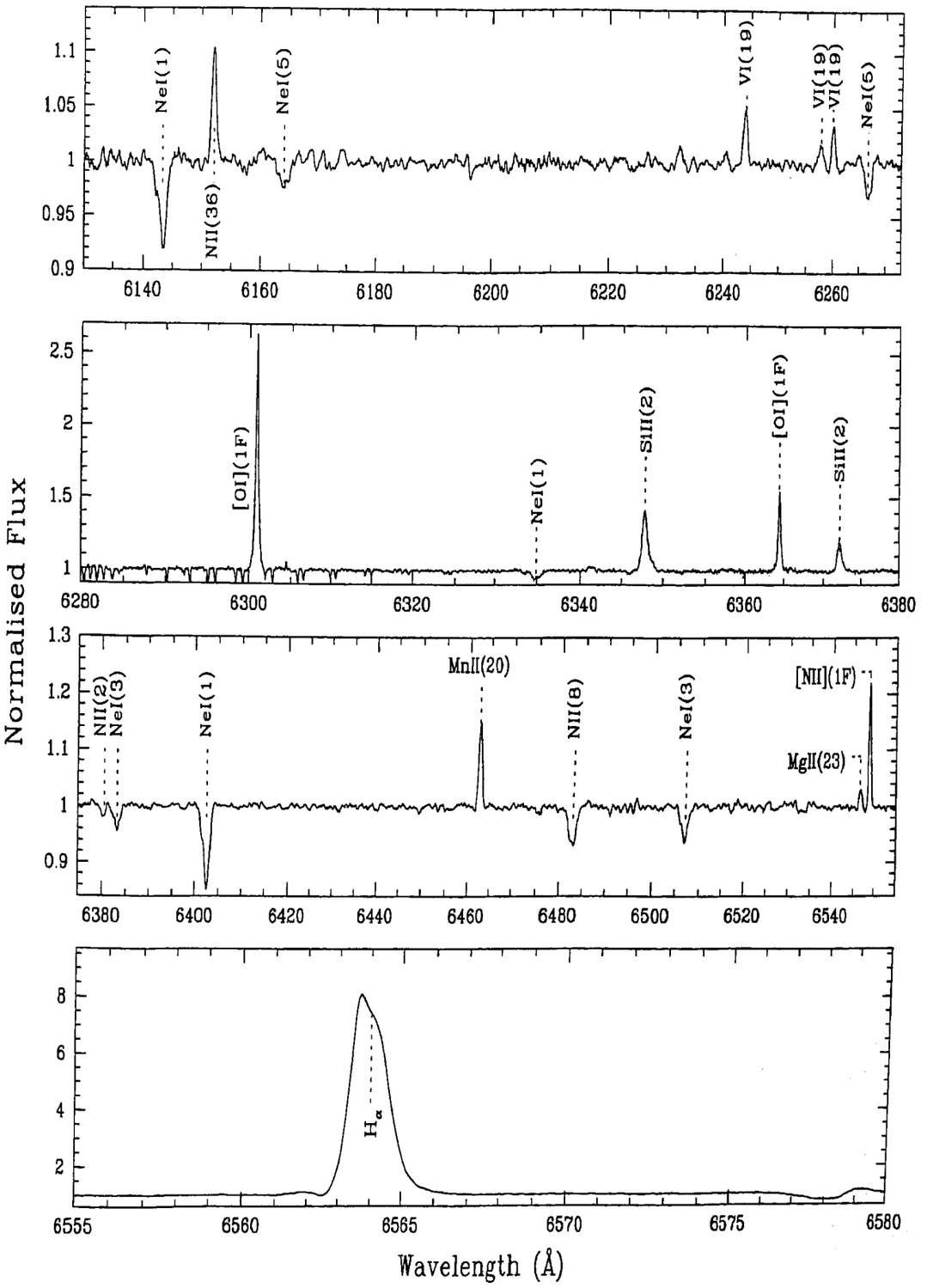

Figure B: Optical spectrum of IRAS17311-4924 (Hen3-1428) contd...

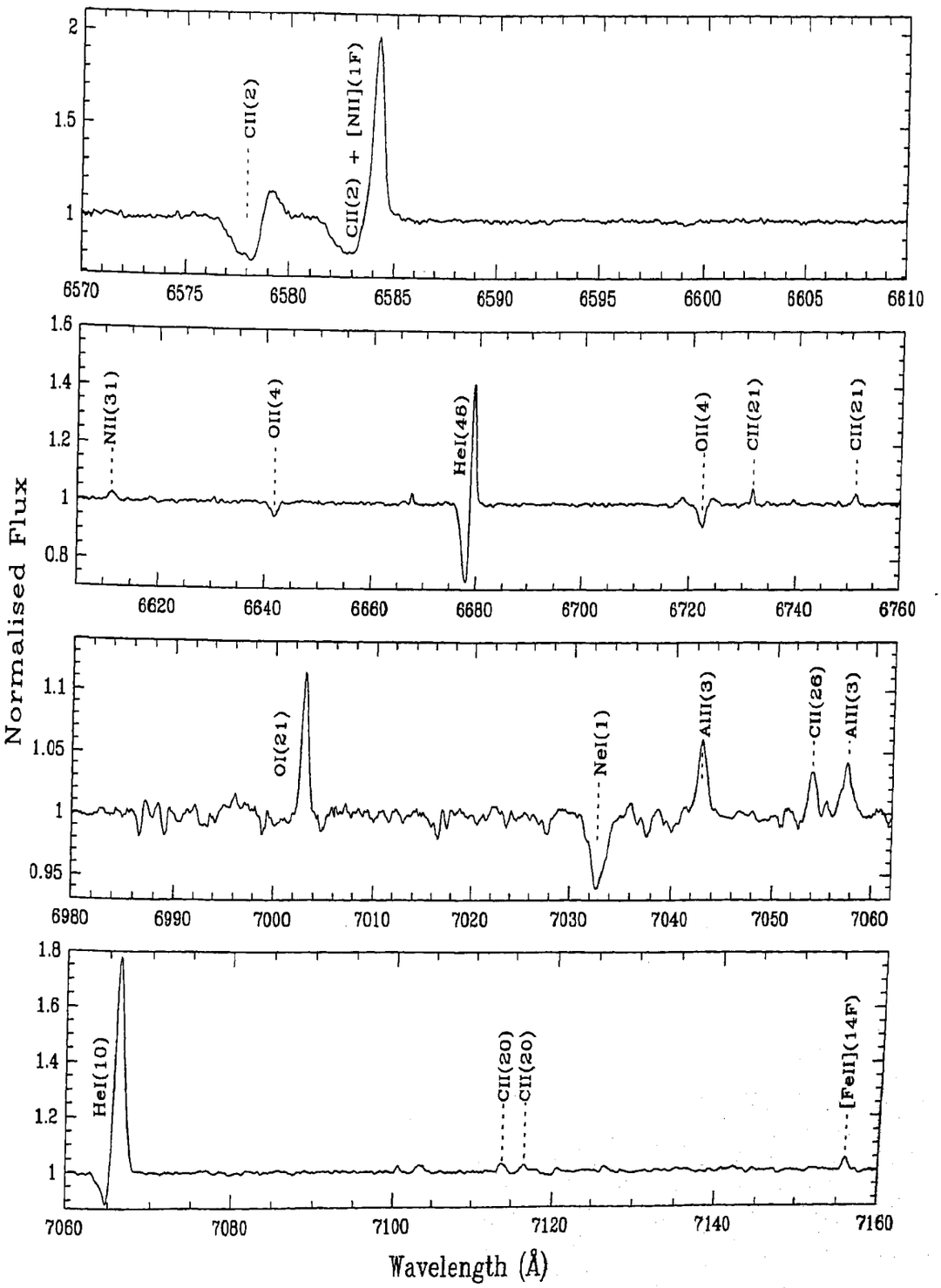

Figure B: Optical spectrum of IRAS17311-4924 (Hen3-1428) contd...

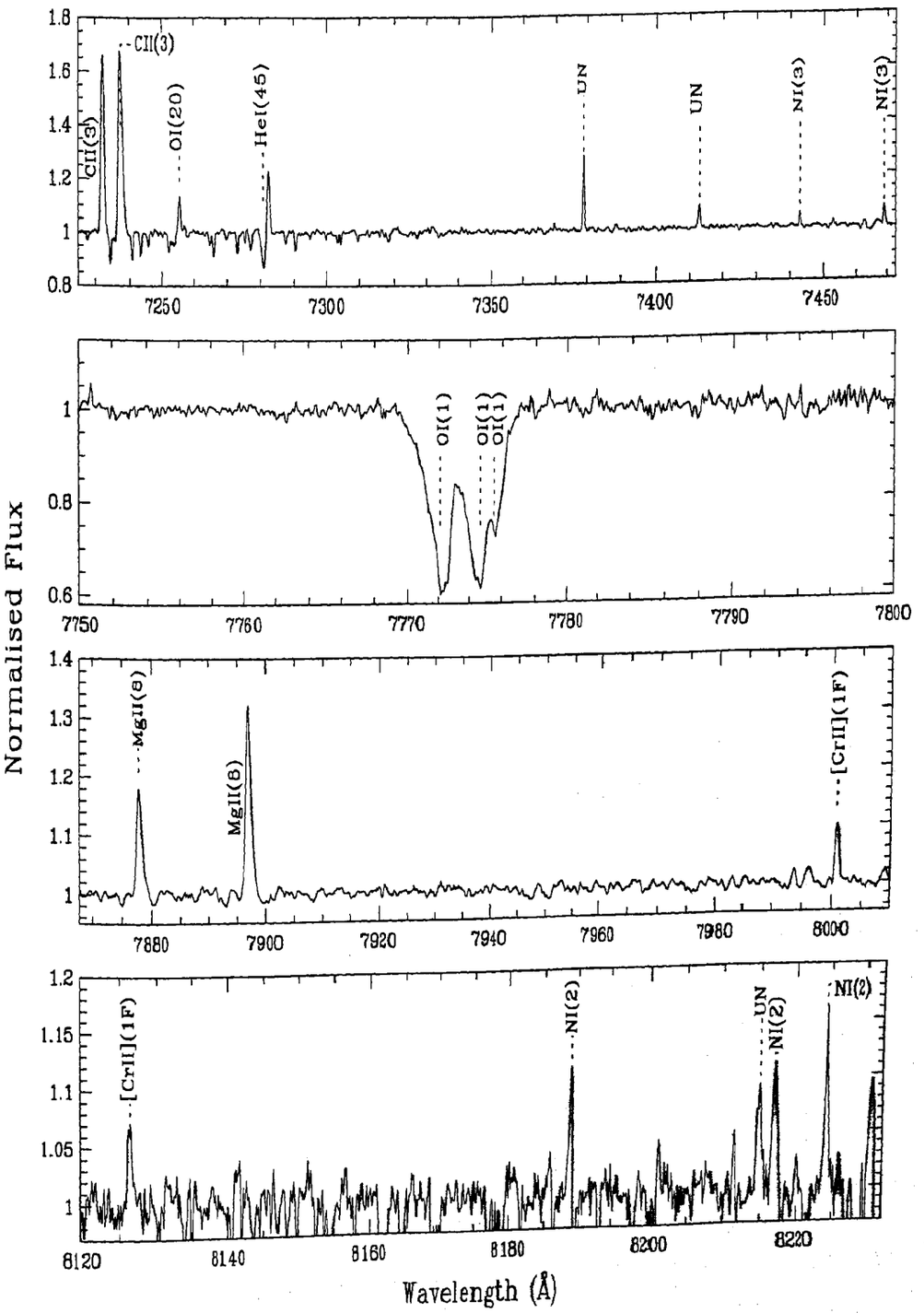

Figure B: Optical spectrum of IRAS17311-4924 (Hen3-1428) contd...

Chapter 6

UV(IUE) spectra of the central stars of high latitude planetary nebulae Hb7 and Sp3

Abstract

We present an analysis of the UV (IUE) spectra of the central stars of Hb7 and Sp3. Comparison with the IUE spectrum of the standard star HD 93205 leads to a spectral classification of O3V for these stars, with an effective temperature of 50,000 K. From the P-Cygni profiles of CIV (1550Å), we derive stellar wind velocities and mass loss rates of -1317 kms$^{-1}\pm$ 300 kms^{-1} and 2.9X10^{-8}M$_{\odot}$ yr^{-1} and -1603 kms$^{-1}\pm$400 kms^{-1} and 7X10^{-9}M$_{\odot}$ yr^{-1} for Hb7 and Sp3 respectively. From all the available data, we reconstruct the spectral energy distribution of Hb7 and Sp3.

6.1 Introduction

The central stars of planetary nebulae (CSPNe) are in general very hot objects and their continuum flux is more easily detectable in the UV than in the optical. The detection of fast winds in CSPNe from UV observations may be considered as one of

the important discoveries of the IUE satellite (Heap 1986, Patriarchi and Perinotto 1991). NV (1240 Å) and CIV (1550 Å) resonance line doublets are the most dominant lines formed in the winds of hot stars. A study of the stellar wind profiles of these lines is important to determine the terminal wind velocities and hence the post-AGB mass-loss rate.

We have carried out a program to study the wind profiles of several high galactic latitude planetary nebulae. A monitoring of the NV and CIV wind profiles in Hen 1357 (=SAO 244567) , showed wind variability in this young PN (Parthasarathy et al. 1993c, 1995) which may be a signature of episodic mass loss in post-AGB stars. In this chapter we present an analysis of the UV (IUE) low resolution spectra of the high galactic latitude PNe Hb7 (PN G003.9−14.9 = IRAS 18523−3219 ; l = 3.97, b = −14.9) and Sp3 (PN G342.5−14.3 = IRAS 18033−5101; l = 342.51, b = −14.32). The photometric colours and optical spectra of these two PNe had indicated that they contain hot central stars (Acker et al. 1992, Aller 1976). We also present the JHK photometry of Hb7 from the 2MASS Point Source Catalog.

6.2 Observations

Low resolution UV spectra of Hb7 and Sp3 were obtained on September 29, 1994 with the SWP camera onboard the IUE satellite. The SWP52257LL image of Hb7 (80 min exposure) and the SWP52256LL image of Sp3 (30 min exposure) were obtained by centering the central stars in the 10″X 23″aperture. The spectra have been re-extracted from the IUE Final Archive at VILSPA which were re-processed using the IUE NEWSIPS pipeline which applies the SWET extraction method as well as the latest flux calibration and close-out camera sensitivity corrections. Line-by-line images have been inspected for spurious features.

6.3 Analysis

The spectra of Hb7 and Sp3 from 1150Å to 1950Å in absolute flux units are shown in Fig. 5.1 a and b. The spectra were dereddened by using E(B−V) = 0.19 for Hb7 (from c(Hβ) = 0.28, Tylenda et al. 1989), and E(B−V) = 0.159 for Sp3 (from HST data, Ciardullo et al. 1999). The dereddened spectra of Hb7 and Sp3 were compared with the dereddened IUE spectra of standard stars (Heck et al. 1984). For comparison, the three spectra were normalised at λ 1601.53Å . Savage et al.(1985) quote a value of E(B−V) = 0.37 for the standard O3 V star, HD93205. Using the 2200Å feature in the UV, we found E(B−V) = 0.34 for this star. Hb7 and Sp3 show good agreement with the UV continuum and spectral features of HD93205 (see Fig. 5.1). Therefore, we adopt the same effective temperature of 50,000 K for the nuclei of Hb7 and Sp3.

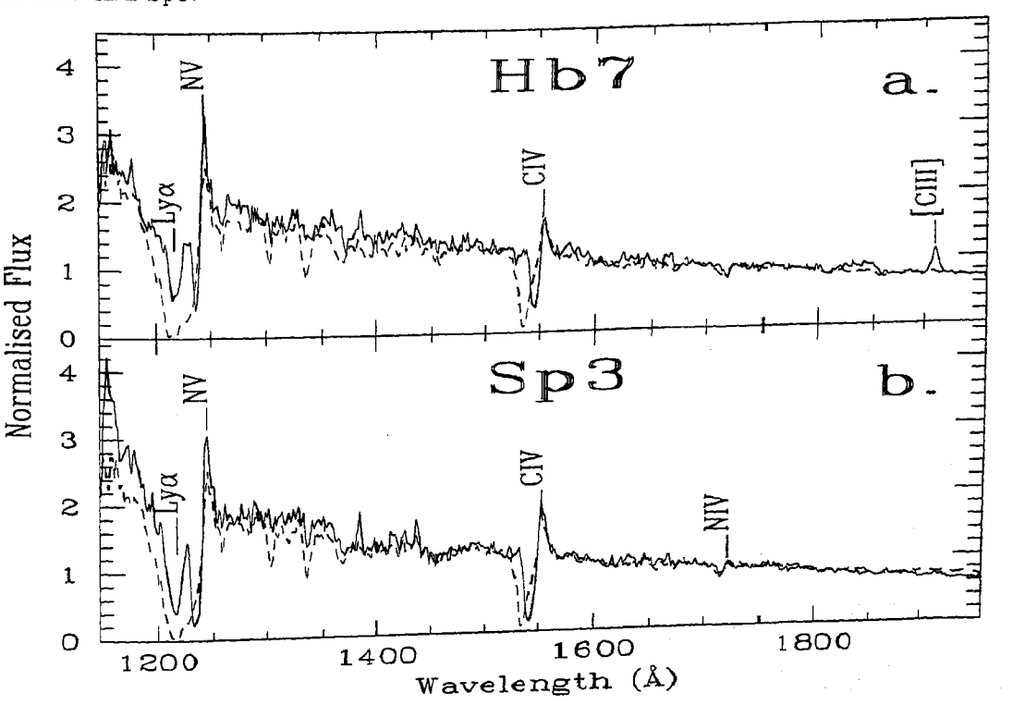

Figure 6.1: The dereddened spectra of Hb7 (**a**), E(B−V)=0.19 and Sp3 (**b**), E(B−V)=0.159 are plotted alongwith the dereddened SWP spectra of a standard O3 -dwarf star(HD93205, E(B−V)=0.34) from the standard star atlas by Heck et al.(1984). The standard star spectrum is represented by a dotted line.

6.3.1 Terminal wind velocities

Using the violet absorption edge in the high resolution UV spectra of HD 93205, Prinja et al. (1990) calculated a terminal wind velocity (v_∞) of -3370 kms^{-1} for this star. They estimated a measurement error of less than 100 kms^{-1} in the determination of this Doppler velocity.

The determination of terminal wind velocity from Doppler shifts in low-dispersion spectra is complicated by the fact that the absorption troughs of strong (saturated) stellar wind lines do not exhibit extended regions of zero residual intensity. In the low resolution spectra of Hb7 and Sp3, the violet edge of NV is contaminated by Lyman α absorption. By measuring differential shifts of the CIV absorption profiles of the two stars with respect to HD 93205, we found Doppler velocities of -1435 kms^{-1} for Hb7 and -1628 kms^{-1} for Sp3. These values may be compared with velocities calculated following the analysis of Prinja(1994).

The empirical relation provided by Prinja (1994) uses the difference between the position of the emission peak and the absorption minimum for the CIV line i.e. $v_\infty = a_1 + a_2(\Delta\lambda) + a_3(\Delta\lambda)^2$ where, $a_1 = -883\pm 48$, $a_2 = 259\pm 9$, $a_3 = -3\pm 2$ and $\Delta\lambda = \lambda^{\rm Emis}_{\rm peak} - \lambda^{\rm Abs}_{\rm min}$, ($\lambda$ in Å and v_∞ in kms^{-1}). Using this relation, we found $v_\infty = -1317$ kms$^{-1}\pm$ 316 kms^{-1} for Hb7 and $v_\infty = -1603$ kms$^{-1}\pm$ 389 kms^{-1} for Sp3. Finally, we adopt a terminal velocity of -1317 kms$^{-1}\pm$ 300 kms^{-1} for Hb7 and of -1603 kms$^{-1}\pm$ 400 kms^{-1} for Sp3.

6.3.2 Stellar temperatures and core-masses

Samland et al. (1992) had estimated the temperature of the central star of Hb7 from photoionization model to be 56,000K. For the central star of Sp3, Preite-Martinez et al. (1991) had estimated the energy-balance temperature to be 39,400K. For an O3 star, the effective temperature ($T_{\rm eff}$) is estimated to be 50,000K (Lang 1992). We adopt the same value of 50,000 K (log $T_{\rm eff} = 4.7$) for the two stars. Pauldrach et al. (1988) analysed the relation between the effective temperature, mass of the nuclei, the terminal velocity and mass-loss rate (see their fig. 10 and 6a). From these

relations, we can deduce a core-mass of 0.644 and 0.565 $M_{\odot}$ and a mass-loss rate of 2.9×10^{-8} $M_{\odot}$ yr.$^{-1}$ and 7×10^{-9} $M_{\odot}$yr.$^{-1}$ for Hb7 and Sp3 respectively.

Table 1: Photometric data of Hb7 and Sp3

	B	V	I	J	H	K
Hb7	13.76[a] (Δm<0.10)	13.97[a] (Δm<0.10)	–	12.768[c] ±0.040	12.866[c] ±0.047	12.251[c] ±0.034
Sp3	12.45[b] (0.10< Δm<0.25)	13.2[d] (Δm<0.05)	13.39[d] (Δm<0.05)	–	–	–

[a]Tylenda et al., 1989; [b]Tylenda et al. 1991; [c]2MASS Point Source Catalog; [d]Ciardullo et al., 1999

6.3.3 Spectral Energy Distributions (SEDs)

The IUE spectra of Hb7 and Sp3 were combined with the available BVI photometry, JHK photometry (Hb7) from the 2MASS Point Source Catalog and IRAS photometry at 12, 25, 60 and 100 μm to reconstruct the overall spectral energy distribution (Fig. 5.2 a and b). The UV data of both stars shows good agreement with a blackbody distribution at 50,000K. The IRAS fluxes do not seem to obey a single black body temperature. By fitting mean blackbody curves to the IRAS fluxes for Hb7 and Sp3, we estimated cold dust temperatures of 130K and 100K respectively.

The JHK flux distribution, for Hb7, shows no indication of the presence of warm dust around the central star. Warm dust is generally attributed to emission from dust grains formed in the outflow close to the central star as a result of on-going post-AGB mass loss. The absence of warm dust may be attributed to photodissociation and diffusion of the dust grains formed close to the hot central star.

Ciardullo et al. (1999) imaged Sp3 with the Wide Field Planetary Camera 2 onboard HST. They found the central star to be a binary with a separation of 0.3″. They found V = 13.20, V−I = −0.19, and E(B−V) = 0.159 for the central star and V=16.86 and V−I = 0.83 for the companion. They considered it as a probable physical pair. The binary nature of the nuclei of Sp3, may explain the too bright

value of the magnitude calculated by Tylenda et al.(1991; B = 12.45, V = 12.51). The V−I colour of the companion is similar to that of an F star. The B magnitude by Tylenda et al. (1991) has been corrected for the contribution from a main sequence F type star and plotted in Fig. 5.2b. In the IUE SWP spectrum of Sp3 we do not find any evidence for the companion star spectrum. Since the F-type companion is several magnitudes fainter, its effect on the continuum flux of the central star in the SWP spectrum appears to be insignificant.

Assuming a temperature of 50,000K for the central stars, the integrated flux in the UV (1150Å to 1950Å) is 1.34×10^{-9} erg s^{-1} cm^{-2} for Hb7 and 2.49×10^{-9}erg s^{-1} cm^{-2} for Sp3. The integrated far infrared fluxes (12μ to 100μ) for Hb7 and Sp3 with blackbody temperatures of 130K and 100K respectively are 0.59×10^{-9} erg s^{-1} cm^{-2} 0.45×10^{-9}erg s^{-1} cm^{-2}. Thus, almost as much energy is radiated in the infrared as is seen coming from the central star(s).

In Table 5.1 we have listed the BVI, JHK magnitudes of Hb7 and Sp3 adopted in this chapter. The JHK magnitudes for Hb7 were obtained from the 2MASS Point Source Catalog within a search radius of 6 ″. The K band image of Hb7 from the 2MASS Catalog is shown in Fig. 5.3. The NICMOS arrays mounted on the 2MASS telescopes provide a resolution of 2″per pixel. Hb7 is not resolved at this resolution and does not appear as an extended source in the 2MASS JHK images.

6.3.4 Dynamical ages of the nebulae

For Hb7, all distance estimates in literature have been obtained assuming a nebular diameter of 4″ (Vorontsov-Velyaminov 1962). However, Vorontsov-Velyaminov's estimate of the nebular diameter was based on low resolution photographic plates and may be wrong. Recently based on CCD images, Gorny et al. (1999) estimated an angular size of 13″× 12″ in H_α. We found this to be consistent with the nebular diameter estimated from the 2MASS images. Since distance estimates for Hb7 based on the wrong angular diameter of 4″cannot be used, we have used the relation between core-mass and quiescent luminosity maximum (L_Q) for AGB stars (Wood and Zarro 1981) to derive the distance. Using L_Q for the luminosity of the star ($8828L_\odot$ for Hb7)

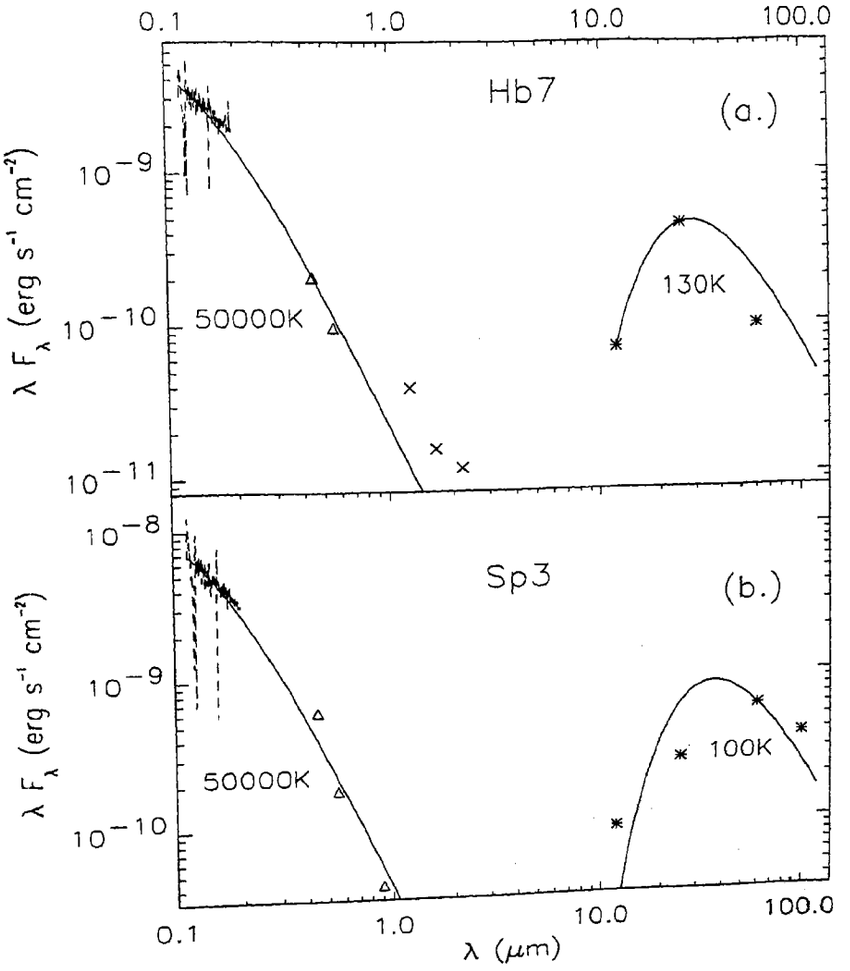

Figure 6.2: Energy distribution of Hb7 (a) and Sp3 (b) from the UV to the far infrared is shown. The data is corrected for interstellar reddening using E(B−V)=0.19 for Hb7 and E(B−V)=0.159 for Sp3. IUE data (dashed line) is plotted alongwith BVI (open triangles), JHK (crosses) and IRAS photometry (asterisk marks).

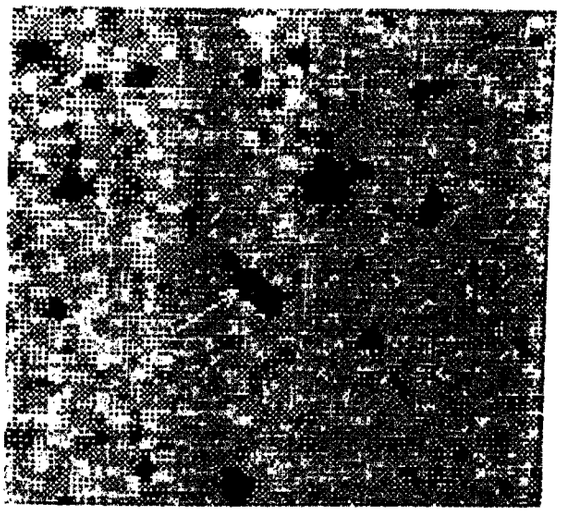

Figure 6.3: 2MASS image of Hb7 in K band

and $M_{bol}(Sun)(= 4.75)$ we found $M_{bol}(Hb7)$ to be -5.1. Applying the bolometric correction and using the formula for the distance modulus we obtained a distance of 5.5 kpc.

Gussie and Taylor (1994) found two components in the expansion velocity distribution of a large sample of PNe. Nebulae with the low-velocity component (12.5 kms^{-1}) were found to be smaller in linear extent than high-expansion velocity nebulae (27.5 kms^{-1}). Assuming an expansion velocity of 12.5 kms^{-1}, angular diameter of 13″ and distance of 5.5 kpc, we obtained a dynamical age of 13418 years for Hb7.

Using Daub's (1982) formalism and an angular radius of 17.8″ (Acker et al 1992), Cahn et al. (1992) obtained a distance of 1.9 ± 0.3 kpc for Sp3. The angular diameter and expansion velocity of Sp3 is 35.5″ and 22 kms^{-1} respectively (Acker et al. 1992). At a distance of 1.9 kpc, we found the age of the nebula to be 7278 years.

The theoretical evolutionary tracks of Blöcker and Schönberner (1990), predict an age of 3000 years for PNe with $\log(T_{eff}/K)$ of 4.7 and core mass of $0.605M_{\odot}$, along the horizontal part of the evolutionary track on the HR-diagram.

6.4 Discussion and conclusions

Our analysis of the UV (IUE) spectra reveals that the central stars of Hb7 and Sp3 are O3 -dwarfs with effective temperatures of 50,000K, core-mass of 0.644 $M_\odot$ and 0.565 $M_\odot$ and mass loss rates of 2.9×10^{-8} $M_\odot$ yr.$^{-1}$ and 7×10^{-9} $M_\odot$ yr.$^{-1}$ respectively. The IRAS fluxes of these objects revealed a cold dust component at 130K for Hb7 and 100K for Sp3. The cold dust component may be interpreted as thermal emission from the dust present in the circumstellar envelope of these stars, a remnant of the previous strong mass loss AGB phase. We estimated dynamical ages of 13.4 X 10^3 years and 7.3 X 10^3 years for Hb7 and Sp3 respectively.

Cerruti-Sola and Perinotto (1985) investigated the frequency of occurence of stellar winds in CSPNe. They found that it depends on the stellar gravity in the sense that CSPNe with a gravity smaller than log g = 5.2 (cgs) almost always have a wind while at higher gravities the presence of wind becomes less and less frequent. The presence of wind in the CSPNe Hb7 and Sp3 indicates that their surface gravities log g < 5.2. Pauldrach et al. (1988) have shown that the presence of a fast wind in a CSPN depends not only on the stellar gravity but also on the luminosity. That is the more a CSPN departs from the Eddington luminosity, the less frequent is the occurence of the wind.

Acknowledgements : Based on observations obtained with the International Ultraviolet Explorer (IUE), retrieved from the IUE Final Archive at VILSPA, Madrid, Spain.

Chapter 7

Conclusions

In this thesis we have studied the observational properties of hot post-AGB stars in the UV, optical and near and far-infrared.

In chapter 2 of the thesis we have analysed the U,B,V,R,I and IRAS data of a small sample of hot post-AGB candidates. Our narrow band H_α images revealed the bipolar morphology of the low excitation PN IRAS17395-0841 (SS 318) with an angular extent of 2.8″. Using our photometric data in combination with the near- and far-infrared data from 2MASS, from the MSX catalog and from the IRAS catalog, we reconstructed their spectral energy distributions (SEDs). The SED of IRAS17423-1755 (Hen3-1475), IRAS18313-1738 (MWC 939) and IRAS19127+1717 (SS 438) showed a warm dust component indicating ongoing post-AGB mass loss. Based on low resolution spectroscopy, we identified two new high galactic latitude hot post-AGB candidates, LSE 163 and LSE 45.

In chapter 3 of the thesis we have analysed the UV(IUE) spectra (1150Å to 3200Å) of 15 hot post-AGB candidates. It was found that 10 hot post-AGB stars were partially obscured due to the presence of circumstellar dust shells. We modelled the circumstellar extinction law in these cases and found it to be linear in λ^{-1}. Linear extinction would arise from dust grains which are small compared to the wavelength of light. Based on this, from the UV spectra, we inferred an upper limit of $\approx$ 200 Å for the radii of the small grains. Emissions due to polycyclic aromatic hydrocarbon

grains (PAH's) are detected in the infrared spectrum of several post-AGB stars/proto-planetary nebulae (PPNe). In particular PAH emission was detected in the post-AGB star, HR4049 which also has a large UV deficiency proportional to λ^{-1}. Waters et al. (1989) speculate that PAH's which survive the strong UV radiation field in the vicinity of hot stars like HR4049 (B9.5Ib-II) may be formed as a result of destruction of larger grains. Large size grains ($\sim$ 200Å) which are responsible for the linear extinction law in the UV (IUE) spectra of 10 hot post-AGB stars may get destroyed, perhaps in shocks when the higher velocity wind from the hot central star collides with remnant material from earlier mass loss phases, giving rise to smaller grains which may be responsbile for PAH emission. Our hot post-AGB stars were placed on the log g – log T_{eff} plot showing the post-AGB evolutionary tracks of Schönberner (1983, 1987). From their positions on the log g – log T_{eff} diagram, we infer a range of core-masses for these stars (0.546 $M_{\odot}$ to 0.644 $M_{\odot}$). Stars with large core mass would evolve more rapidly to the PN stage. Terminal wind velocities, estimated from the CIV (1550Å) and NV (1240Å) resonance lines indicated ongoing post-AGB mass loss in some of these stars.

In chapter 4 of the thesis we have used a radiative transfer code (DUSTY) to model the circumstellar dust shells of 15 hot post-AGB stars. We estimated the dust temperatures, mass loss rates, expansion velocites, angular radii of the inner boundary of the dust envelopes, dynamical ages from the tip of the AGB and the distances to these stars. From the grain types (silicates, graphites, amorphous carbon and/or silicon carbide) used to obtain model fits to the SEDs of these stars, we infer the chemical composition of the circumstellar dust shells. We also studied the ISO spectra of 7 hot post-AGB stars, IRAS14331-6435 (Hen3-1013), IRAS16206-5956 (SAO243756), IRAS17311-4924 (Hen3-1428), IRAS17423-1755 (Hen3-1475), IRAS18062+2410 (SAO85766), IRAS22023+5249 (LSIII +5224) and IRAS22495+5134 (LSIII +5142). Amorphous and crystalline silicate features, PAH and SiC emission were identified in the ISO spectra. PAH emission at 7.7μ, the "26μ" and "main 30μ" features and 11.5μ SiC emission in IRAS17311-4924 (Hen3-1428) indicate carbon-rich circumstellar dust which suggests that the central star may be carbon-rich. However, the 21μ emission feature detected in several cooler carbon-rich PPNe is not present in the ISO

spectrum of this star.

In chapter 5 of the thesis we have analysed the high resolution optical spectra from 4900Å to 8250Å of the hot post-AGB stars, IRAS13266-5551 (CPD-55 5588) and IRAS17311-4924 (Hen3-1428). Absorption lines of C II, N II, O II, Al III, Si III and Fe III and emission lines of H I, He I, C II, N I, [N II], O I, [O I], Mg II, Al II, Si II, V I, Mn II, Fe II, Fe III, [Fe II] and [Cr II] were identified. The complete linelists are presented. The presence of He I lines and the absence of He II lines indicates 18000K $\leq T_{eff} \leq$ 25000K for the two stars. Atmospheric parameters (T_{eff} = 23000K, log g = 3.0 and ξ_t = 10 kms^{-1}) were estimated for IRAS13266-5551 (CPD-55 5588) under the LTE approximation. Preliminary estimates of the CNO abundances were also obtained for this star. Heliocentric radial velocities of 67.55 $\pm$ 1.26 kms^{-1} and 26.09 $\pm$ 1.88 kms^{-1} were derived for IRAS13266-5551 (CPD-55 5588) and IRAS17311-4924 (Hen3-1428). The high galactic latitude and large radial velocity of IRAS13266-5551 (CPD-55 5588) indicate that it is a high velocity star belonging to the old disk population.

In chapter 6 of the thesis we have analysed the UV(IUE) spectra of two high galactic latitude planetary nebulae (PNe), IRAS18523-3219 (Hb7) and IRAS18033-5101 (Sp3). The CIV (1550Å) and NV (1240Å) resonance lines showed P-Cygni profiles indicating stellar wind and post-AGB mass loss. We derived stellar wind velocities and mass loss rates of -1317 kms$^{-1}\pm$ 300 kms^{-1} and 2.9X10^{-8}M$_\odot$ yr^{-1} and -1603 kms$^{-1}\pm$400 kms^{-1} and 7X10^{-9}M$_\odot$ yr^{-1} for Hb7 and Sp3 respectively. Based on their UV(IUE) spectra, Hb7 and Sp3 were classified as O3-dwarfs with core masses of 0.644 M$_\odot$ and 0.565 M$_\odot$ respectively. From the available optical, near- and far-infrared data we reconstructed the SEDs of these two stars.

From modelling of the far-infrared (IRAS) fluxes of the hot post-AGB stars using the DUSTY code, we derived mass loss rates of $10^{-6} - 10^{-5}$M$_\odot$yr^{-1} and expansion velocities ranging from $\sim 6 - 30$ kms^{-1}. The derived dynamical ages range from a few hundred to a few thousand years and are consistent with the evolutionary models of Schönberner & Blöcker (1993). The angular radii of the inner boundary of the circumstellar dust shells, derived from our models, indicate that many of the

nebulae should be resolvable in the mid-infrared. Mid-IR imaging would therefore serve as an important test of our models and the predicted values. The circumstellar extinction law in these stars indicates that the circumstellar grains may have radii of upto $\sim$ 200Å . Hot post-AGB stars such as IRAS16206-5956 (SAO243756) and IRAS18062+2410 (SAO85766) were found to be variable in the UV and optical. The variability may be attributed to a dusty disk in motion around the central stars and/or to stellar pulsations. Long and short term monitoring of these stars is important to understand the observed variability. The presence of warm dust (in addition to the cold circumstellar dust) in some of these stars and the H_α P-Cygni profiles indicate ongoing post-AGB mass loss. From the CIV (1550Å) and NV (1240Å) lines in the UV(IUE) spectra, we derived stellar wind velocities in the range -1066 kms^{-1} to -3978 kms^{-1}. The fast stellar wind interacts with the cooler circumstellar dust (a remnant of mass loss on the AGB phase of the stars) to shape the morphology of the PPNe and PNe, as described by the "interacting stellar wind model" of Kwok et al. (1978). Most hot post-AGB stars show H_α in emission and sometimes [NII] and [SII]. High resolution imaging of these stars in H_α, [NII], [SII] and the continuum filters with the Wide Field Planetary Camera 2 (WFPC2) on board the HST would resolve the nebulae and help in understanding the influence of the fast stellar wind on the morphology and shaping of PNe. NLTE analysis of the high resolution spectra of these stars in the blue region is important to derive accurate atmospheric parameters and chemical compositions.

Bibliography

Acker, A., Ochsenbein, F., Stenholm, B., Tylenda, R., Marcout, J., Schohn, C., 1992, Strasbourg-ESO Catalogue of Galactic Planetary Nebulae

Allen, D.A., Swings,J.P., 1976, A&A 47, 293

Aller, L.H., 1976, PASP, 88, 574

Anders, E., Grevesse, N., 1989, Geochim. Cosmochim. Acta 53, 197

Arkhipova, V. P., Ikonnikova, N. P., Noskova, R. I., Sokol, G. V., Esipov, V. F., Klochkova, V. G., 1999, AstL, 25, 25

Arkhipova, V. P., Ikonnikova, N. P., Noskova, R. I., Sokol, G. V., 2000, AstL, 26, 609

Arkhipova, V.P., Klochkova, V.G., Sokol, G.V., 2001a, AstL, 27, 99

Arkhipova, V.P., Ikonnikova, N.P., Noskova, R.I., et al., 2001b, AstL, 27, 719

Arkhipova, V. P., Ikonnikova, N. P., Noskova, R. I., Komissarova, G. V., 2002, AstL, 28, 257

Auer, L.H., Mihalas, D., 1973, ApJ, 184, 151

Beaulieu,S.F., Dopita,M.A., Freeman,K.C., 1999, AJ 515, 610

Bedijn,P.J., 1987, A&A 186, 136

Beintema, D.A., van den Ancker, M.E., Molster, F.J. et al., 1996, 315, L369

Blöcker,T.,1995,A&A 299,755

Bobrowsky, M., Zijlstra, A.A., Grebel, E.K. et al., 1995, ApJ 446, L89

Bobrowsky, M., Sahu, K.C., Parthasarathy, M., García-Lario, P. 1998, Nature 392, 469

Bogdanov, M.B., 2000, ARep., 44, 685

Bogdanov, M.B., 2002, AstL, 28, 617

Boothroyd, A.I., Sackmann, I., -J., Ahern, S.C., 1993, ApJ, 416. 762

Borkowski, K.J., Blondin, J.M., & Harrington, J.P., 1997, ApJ 482, L97

Borkowski, K.J., Harrington, J.P., 2001, ApJ 550, 778

Blöcker, T., Schönberner, D., 1990, A&A, 240, L11

Blöcker, T.,1995,A&A 299,755

Buss, R. H. Jr., Lamers, H.J.G.L.M., Snow, T.P., Jr., 1989, ApJ, 347, 977

Cahn, J.H., Kaler, J.B. and Stanghellini, L., 1992, A&AS, 94, 399

Cameron, A.G.W., Fowler, W.A., 1971, ApJ, 164, 111

Castella, A., Barbero, J., 1983, presentation at *IUE Three-Agency Meeting*, March

Cernicharo, J., Gottlieb, C.A., Guélin, M., et al., 1989, ApJ, 341, L25

Cernicharo, J., Yamamura, I., González-Alfonso, E., et al., 1999, ApJ, 526, L41

Cerruti-Sola, M., Perinotto, M., 1985, ApJ, 291, 237

Chu, Y., Manchado, A., Jacoby, G.H., Kwitter, K.B., 1991, ApJ, 376, 150

Ciardullo, R., Bond, H. E., Sipior, M. S., Fullton, L. K., Zhang, C. Y., Schaefer, K.G., 1999, ApJ, 118, 488

Clegg, P.E., Ade, P.A.R., Armand, C., et al., 1996, A&A, 315, L38

Cohen, M., Walker, R.G., Witteborn, F.C., 1992, AJ 104, 2030

Conlon, E.S., Dufton, P.L., Keenan, F.P., McCausland, R.J.H., Little, J.E., 1993a, A&A, 272, 243

Conlon, E.S., Dufton, P.L., McCausland, R.J.H., Keenan, F.P., 1993b, ApJ, 408, 593

Conlon, E.S., McCausland, R.J.H., Dufton, P.L., Keenan, F.P., 1993c, in *Luminous High-Latitude Stars*, ASP Conf. Ser. 45, 146, Sasselov, D.D. (ed.)

Conti, P.S., Frost, S.A., 1977, ApJ, 212, 728

Corradi R.L.M., Schönberner D., Steffen M., Perinotto M., 2000, A&A, 354, 1071

Cox, P., 1993, ASP Conf. Series, 41, p. 163, Sun Kwok (ed.)

Daub, C.T., 1982, ApJ, 260, 612

de Graauw, Th., Haser, L.N., Beintema, D.A., et al., 1996, A&A, 315, L49

de Winter, D., van den Ancker, M.E., Maira, A. et al., 2001, A&A, 380, 609

Downes R.A., Keyes C.H. 1988, AJ, 96, 777

Draine, B.T. & Lee, H.M. 1984, ApJ 285, 89

Drilling, J.S., Bergeron, L.E., 1995, PASP 107, 846

Ebbets, D., 1982, ApJS, 48, 399

Faraggiana, R., Gerbaldi, M., van't Veer, C., Floquet, M., 1988, A&A, 201, 259

Feibelman, W. A., 1995, ApJ, 443, 245

Forrest, W.J., McCarthy, J.F., Houck, J.R., 1979, ApJ, 233, 611

Forrest, W.J., Houck, J.R., McCarthy, J.F., 1981, ApJ, 248, 195

Fouque, P., Le Bertre, T., Epchtein, N., et al., 1992, A&AS, 93, 151

Frank, A., 1994, AJ, 107, 261

Garcia-Lario, P., Manchado, A., Pych, W., Pottasch, S.R., 1997a, A&AS 126, 479

García-Lario, P., Parthasarathy, M., de Martino, D., et al. 1997b, A&A, 326, 1103

Gauba, G., Parthasarathy, M., Nakada, Y., Fujii, T., 2001, A&A, 373, 572

Gauba, G., Parthasarathy, M., Kumar, B., Yadav, R.K.S., Sagar, R., 2003a, A&A, 404, 305

Gauba, G. and Parthasarathy, M. , 2003b, A&A (in press)

Gauba, G., Parthasarathy, M., 2003c, submitted to A&A

Goebel, J.H., Moseley, S.H., 1985, ApJ, 290, L35

Górny, S.K., Schwarz, H.E., Corradi, R.L.M., Van Winckel, H., 1999, A&A, 136, 145

Groenewegen, M.A.T., de Jong, T., Geballe, T.R., 1994, A&A, 287, 163

Gussie, G.T., Taylor, A.R. 1994, PASP, 106, 500

Habing, H.J., Blommaert, J.A.D.L., 1993, in IAU Symp. 155, p. 243, Acker, A. and Weinberger, R. (eds.)

Handler,G., 1999, A&AS, 135, 493

Hanner, M.S. 1988, NASA Conf. Pub. 3004, 22

Heap, S.R., 1986, in Eight Years of IUE, ESA SP-263, p.291

Heck, A., Egret, D., Jaschek, M., Jaschek, C., 1984, IUE Low-Dispersion Spectra Reference Atlas - Part 1. Normal Stars, ESA SP - 1052

Henize, K.G., 1976, ApJS 30, 491

Herbig, G.H., 1993, ApJ, 407, 142

Hog, E., Fabricius, C., Makarov, V.V., et al., 2000, A&A 355, L27

Hony, S., Waters, L.B.F.M., Tielens, A.G.G.M., 2002, A&A, 390, 533

Hony, S., Tielens, A.G.G.M., Waters, L.B.F.M., de Koter, A., 2003, A&A, 402, 211

Hoogzaad, S.N., Molster, F.J., Dominik, C. et al., 2002, A&A, 389, 547

Hrivnak, B.J., Kwok, S., Volk, K.M. 1989, ApJ 346, 265

Hrivnak, B.J., Volk, K., Kwok, S., 2000, ApJ, 535, 275

Hubeny I., Stefl S., Harmanec P., 1985, Bull. Astron. Inst. Czechosl. 36, 214

Humphreys, R.M., 1975, A&AS, 19, 243

Iben, I.,Jr., Renzini, A., 1983, ARA&A 21, 271

Iben, I., Jr., 1985, QJRAS, 26, 1

Ivezić, Z., Nenkova, M., Elitzur, M., 1999, *User Manual for DUSTY*, University of Kentucky Internal Report

Jacoby, G.H., Hunter, D.A., Christian, C.A., 1984, ApJS 56, 257

Jørgensen, U.G., Hron, J., Loidl, R., 2000, A&A, 356, 253

Jourdain de Muizon, N., Cox, P., Lequeux, J., 1990, A&A, 83, 337

Jura, M., 1986, ApJ, 303, 327

Kaler,J.B., 1983, ApJ, 264, 594

Kazarovets, E.V., Samus, N.N., Durlevich, O. V., 2000, IBVS.4870, 1K

Kessler, M.F., Steinz, J.A., Anderegg, M.E., et al. 1996, A&A 315, L27

Kilian, J., 1992, A&A, 262, 171

Kilkenny, D., Pauls, L., 1990, MNRAS, 244, 133

Klein, R.I., Castor, J.I., 1978, ApJ, 220, 902

Klochkova, V.G., Yushkin, M.V., Miroshnichenko, A.S. et al., 2002, A&A, 392, 143

Klutz, M., Swings, J.P., 1977, A&A 56, 143

Kozok, J.R., 1985a, A&AS, 61, 387

Kozok, J.R., 1985b, A&AS, 62, 7

Kurucz, R.L., 1994, Solar Abundance Model Atmospheres, Kurucz CDROM No. 19, Smithsonian Astrophysical Observatory

Kwok, S., Purton, C.R., Fitzgerald, P.M., 1978, ApJ, 219, L125

Kwok, S., 1987, in *Late Stages of Stellar Evolution*, p. 321, Kwok, S. and Pottasch, S.R. (eds.), D. Reidel Publishing Company

Kwok, S., 1993, ARA&A, 31, 63

Kwok, S., Volk, K., Bidelman, W.P., 1997, ApJS, 112, 557

Kwok, S., 2001, p. 3 in *Post-AGB Objects as a Phase of Stellar Evolution*, ApSS, Vol. 265, Ed. Szczerba, R. and Górny, S.K., Kluwer Academic Publishers, Boston/Dordrecht/London

Kwok,S., Su, K.Y.L, Stoesz, J.A., 2001, p. 115 in *Post-AGB Objects as a Phase of Stellar Evolution*, ApSS, Vol. 265, Ed. Szczerba, R. and Górny, S.K., Kluwer Academic Publishers, Boston/Dordrecht/London

Kwok, S., Volk, K., Hrivnak, B.J., 2002, ApJ, 573, 720

Lamers, H.J.G.L.M., Waters, L.B.F.M. et al. 1986, A&A 154, L20

Landolt,A.U., 1992, AJ 104, 340

Lang,K.R., 1992, Astrophysical Data : Planets and Stars, Springer-Verlag

Lattanzio, J., Forestini, M., 1999, IAU Symp. 191, p. 31, Le Bertre, T., Lébre, A., Waelkens, C. (eds.)

Lawrence, G., Jones, T.J., Gehrz, R.D., 1990, AJ, 99, 1232

Leitherer, C., 1988, ApJ, 326, 356

Likkel,L., 1989, ApJ 344, 350

Likkel,L., Forveille,T., Omont,A., Morris,M., 1991, A&A 246, 153

Loup C., Forveille T., Nyman L.A., Omont A., 1990, A&A 227, L29

Loup,C., Forveille,T., Omont, A., Paul, J.F., 1993, A&AS, 99, 291

Marten, H., Gesicki, K., Szczerba, R., 1993, in IAU Symp. 155, p. 315, Acker, A. and Weinberger, R. (eds.)

Massey,P., Davis,L.E., 1992, *A User's Guide to Stellar CCD Photometry with IRAF*

Mathis, J.S., Rumpl, W., Nordsieck, K.H., 1977, ApJ 17, 25

McCausland, R.J.H., Conlon, E.S., Dufton, P.L., Keenan, F.P., 1992, ApJ, 394, 298

Meixner, M., Skinner, C.J., Graham, J.R., et al., 1997, ApJ, 482, 897

Merrill, K.M., Stein, W.A., 1976, PASP, 88, 285

Miroshnichenko, A.S., Fremat, I., Houziaux, L., et al., 1998, A&AS, 131, 469

Moehler,S. and Heber,U., 1998, A&A 335, 985

Monet, D., Bird, A., Canzian, B., et al., 1998, USNO-A V2.0, *A Catalog of Astrometric Standards*

Monier, R., Parthasarathy, M., 1999, A&A, 341, 117

Mooney, C.J., Rolleston, W.R.J., Keenan, F.P., Dufton, P.L. et al., 2002, MNRAS, 337, 851

Moore, C.E., 1945, *A multiplet table of astrophysical interest*

Mowlavi, N., Meynet, G., 2000, A&A, 361, 959

Napiwotzki, R., Heber, U., Köppen, J., 1994, A&A, 292, 239

Nichols, J.S., Garhart, M.P., De La Peña, M.D., Levay, K., 1994, NASA *IUE Newsletter* No. 53

Nichols, J.S., Linsky, J.L., 1996, AJ, 111, 517

Noguchi, K., Maihara, T., Okuda, H., et al., 1977, PASJ, 29, 511

Nyman, L.A., Booth, R.S., Carlstrom, U. et al., 1992, A&AS, 93, 121

Olofsson, H., Carlstrom, U., Eriksson, K., Gustafsson, B., Willson, L.A., 1990, A&A, 230, L13

Omont, A., Forveille, T., Moseley, S.H., 1990, ApJ, 355, L27

Omont, A., Moseley, S.H., Cox, P., et al., 1995, ApJ, 454, 819

Ossenkopf, V., Henning, Th. & Mathis, J.S. 1992, A&A 261, 567

Oudmaijer, R.D., 1996, A&A, 306, 823

Parthasarathy, M., Pottasch, S.R., 1986, A&A 154, L16

Parthasarathy, M., Pottasch, S.R., 1989, A&A 225, 521

Parthasarathy, M., García-Lario, P., Pottasch, S.R, 1992, A&A, 264, 159

Parthasarathy, M., 1993a, in *Luminous High-Latitude Stars*, ASP Conf. Ser. 45, 173, Sasselov D.D(ed.)

Parthasarathy, M., 1993b, ApJ 414, L109

Parthasarathy, M., Garcia-Lario, P., Pottasch, S.R., Manchado, A., et al., 1993c, A&A, 267, L19

Parthasarathy, M., 1994, in *The MK Process at 50 Years*, ASP Conf. Ser. 60, 261

Parthasarathy, M., Garcia-Lario, P., de Martino, D., et al., 1995, A&A, 300, L25

Parthasarathy, M., 1999, in IAU Symp. 191, 475, Le Bertre, T., Lébre, A. and Waelkens, C. (eds.)

Parthasarathy, M., Vijapurkar, J., Drilling, J.S., 2000a, A&AS 145, 269

Parthasarathy, M., García-Lario, P., Sivarani, T. et al., 2000b, A&A 357, 241

Parthasarathy, M., García-Lario, P., Gauba, G. et al., 2001a, A&A 376, 941

Parthasarathy, M., Gauba, G., T. Fujii, Y. Nakada, 2001b, p. 29 in *Post-AGB Objects as a Phase of Stellar Evolution*, ApSS, Vol. 265, Ed. Szczerba, R. and Górny, S.K., Kluwer Academic Publishers, Boston/Dordrecht/London

Patriarchi, P., Perinotto, M., 1991, A&AS, 91, 325

Pauldrach, A., Puls, J., Kudritzki, R. P., Mendez, R. H., Heap, S. R., 1988, A&A, 207, 123

Pègouriè, B. 1988, A&A 194, 335

Perinotto, M., Benvenuti, P., and Cerruti-Sola, M., 1982, A&A, 108, 314

Pottasch, S.R., Bignell, C., Olling, R., Zijlstra,A.A., 1988a, A&A 205, 248

Pottasch, S.R., Parthasarathy, M. 1988b, A&A 192, 182

Pottasch, S.R., 1992, A&ARV, 4, 215

Preite-Martinez, A., A&AS 1988, 76, 317

Preite-Martinez, A., Acker, A., Köppen, J., Stenholm, B., 1991, A&AS,88, 12 121

Prinja, R. K., Barlow, M. J., Howarth, I. D., 1990, ApJ, 361, 607

Prinja, R. K., 1994, A&A, 289, 221

Reddy, B.E., Parthasarathy, M., Gonzalez, G., Bakker, E.J., 1997, A&A, 328, 331

Reed, B.C., 1998, ApJS 115, 271

Ridgway, S.T., Carbon D.F., Hall, D.N., 1978, ApJ, 225, 138

Rieke, G.H., Lebofsky, M.J., 1985, ApJ, 288, 618

Riera, A., García-Lario, P., Manchado, A., et al., 1995, A&A 302,137

Ryans, R.S.I., Dufton, P.L., Mooney, C.J., et al., 2003, A&A, 401, 1119

Samland, M., Köppen, J., Acker, A., Stenholm, B., 1992, A&A, 264, 184

Sanchez Contreras, C., Sahai, R., 2001, ApJ 553, L173

Savage, B. D., Massa, D., Meade, M., Wesselius, P. R., 1985, ApJS, 59, 397

Schaeidt, S.G., Morris, P.W., Salama, A., et al., 1996, A&A, 315, L55

Schild, R.E., Garrison, R.F., Hiltner, W.A., 1983, AJ, 88, 67

Schlegel,D.J., Finkbeiner,D.P., Davis,M, 1998, ApJ 500, 525

Schmidt-Kaler, Th., 1982, in Landolt-Börnstein: Numerical Data and Functional Relationships in Science and Technology, vol. 2b, ed. K. Schaifers & H. H. Voigt (Springer-Verlag, Berlin)

Schönberner, D., 1983, ApJ 272, 708

Schönberner, D., 1986, A&A, 169, 189

Schönberner, D., 1987, in *Late Stages of Stellar Evolution*, eds. S. Kwok, S.R. Pottasch, Reidel, Dordrecht, p. 341

Schönberner, D., Blöcker, T., 1993,in *Luminous High-Latitude Stars*, ASP Conf. Ser. 45, 337, Sasselov, D.D.(ed.)

Schwarz, H.E., Corradi, R.L.M., Melnick, J., 1992, A&AS, 96, 2

Seaton M.J., 1979, MNRAS, 187, 73

Siebenmorgen, R., Zijlstra, A.A., Krügel, E., 1994, MNRAS, 271, 449

Sivarani, T., Parthasarathy, M., García-Lario, P., et al., 1999, A&AS, 137, 505

Spitzer, L., 1978, *Physical Processes in the Interstellar Medium* (New York: Wiley), p. 151

Stephenson, C.B., 1986, ApJ, 300, 779

Stephenson, C.B., Sanduleak, N., 1971, *Publ. Warner & Swasey Obs., 1, part no. 1, 1*

Su,K.Y.L., Hrivnak, B.J., Kwok, S., 2001, AJ, 122, 1525

Swinyard, B.M., Clegg, P.E., Ade, P.A.R., et al., 1996, A&A, 315, L43

Swinyard, B.M., Burgdorf, M.J., Clegg, P.E., et al., 1998, Proc. SPIE, Vol. 3354, p.888

Szczerba, R., Henning, Th., Volk, K., Kwok, S., Cox, P., 1999, A&A, 345, L39

Szczerba, R., Górny, S.K., Zalfresso-Jundzillo, M., 2001, p. 13 in *Post-AGB Objects as a Phase of Stellar Evolution*, ApSS, Vol. 265, Ed. Szczerba, R. and Górny, S.K., Kluwer Academic Publishers, Boston/Dordrecht/London

Te Lintel Hekkert, P., Chapman, J.M., Zijlstra, A.A., 1992, ApJ, 390, L23

Thé,P.S., de Winter, D., Perez, M.R., 1994, A&AS, 104, 315

Thompson G.E., Nandy K., Jamar C., et al. 1978, Catalogue of stellar ultraviolet fluxes, SERC

Tielens, A.G.G.M., 1983, ApJ, 271, 702

Trams, N.R, van der Veen, W.E.C.J., Waelkens, C. et al., 1990, A&A, 233, 153

Treffers, R.R., Cohen, M., 1984, ApJ, 188, 545

Tylenda, R., Acker, A., Gleizes F., Stenholm B., 1989, A&AS, 77, 39

Tylenda, R., Acker, A., Stenholm, B., Gleizes, F., Raytchev, B., 1991, A&AS, 89, 77

Tylenda, R., Acker, A., Stenholm, B., Köppen, J., 1992, A&AS, 95, 337

Tylenda, R., and Stasińska, G. 1994, A&A, 288, 897

van der Veen, W.E.C.J, Habing, H.J., 1988, A&A 194, 125

Van Winckel, H., Reyniers, M., 2000, A&A, 354, 135

Vassiliadis, E., Wood, P. R., 1994, ApJS, 92, 125

Vijapurkar, J.,Drilling,J.S., Parthasarathy,M., 1997, AJ 114, 1573

Vijapurkar, J., Parthasarathy,M., Drilling,J.S., 1998, BASI 26, 497

Volk,K., Cohen,M., 1989, AJ 98, 1918

Volk, K.M., Kwok, S., 1989, ApJ, 342, 345

Volk, K., Xiong, G.Z., Kwok, S., 2000, ApJ, 530, 408

Volk, K., Kwok, S., Hrivnak, B.J., 2002, ApJ, 567, 412

Vorontsov-Velyaminov, B. A., 1962, *Soobse. Astr. Inst. Sternbergra*, No. 118, 3

Wackerling,L.R., 1970, *Mem. Roy. Astron. Soc.*, 73, 153

Waters,L.B.F.M., Lamers,H.J.G.L.M., Snow, T.P. et al., 1989, A&A, 211, 208

Waters, L.B.F.M., Molster, F.J., de Jong, T. et al., 1996, A&A, 315, L361

Waters, L.B.F.M., Beintema, D.A., Zijlstra, A.A., et al., 1998, A&A, 331, L61

Waters, L.B.F.M., Molster, F.J., 1999, IAU Symp. 191, p. 209, T. Le Bertre, A. Lébre and C. Waelkens (eds.)

Whitelock,P.A., Menzies,J.W., 1986, MNRAS 223, 497

Whittet, D.C.B., 2003, p. 226, *Dust in the Galactic Environment, Second Edition*, Institute of Physics Publishing

Wood,P. R., Zarro, D. M., 1981, ApJ 247, 247

Zijlstra,A.,A., Loup,C., Waters,L.B.F.M., de Jong,T., 1992, A&A, 265, L5